Linear and Nonlinear Dynamics of a Turbine Blade in Presence of an Underplatform Damper with Friction

BY

STEFANO MICHELIS
Laurea, Politenico di Torino, Torino, Italy, 2012

THESIS

Submitted as partial fulfillments of the requirements
for degree of Master of Science in Mechanical Engineering
in the Graduate College of the
University of Illinois at Chicago, 2014

Chicago, Illinois

Defense Committee:

Ahmed A. Shabana, Chair and Advisor
Craig Foster
Teresa Maria Berruti, Politenico di Torino

This thesis is dedicated to my parents who have always been a reference in my life supporting all my choices like my fantastic experience abroad. I would like also to express an heartfelt thanks to Camilla who encourages me and lies with me every day patiently and always remembers me that everyday life is not made only by university commitments, to Ennio, Mario and Matteo who make amusing all my days in Turin, to my colleagues Enrico e Federico with whom I shared my amazing stay in Chicago not only as classmates but as trusted friends, to my hometown buddies Andrea, Federico and Stefano on whom I can rely on however I seldom meet them and last but not least to all my friends in the student college with whom I spend my university life.

TABLE OF CONTENTS

CHAPTER **PAGE**

1. **INTRODUCTION**.....1

1.1. The finite element method..... 1

1.2. Overview of the physical model and statement of the problem..... 4

2. **LINEAR DYNAMICS OF THE BLADE**.....7

2.1. Multibody systems.....8

2.1.1. Reference frames..... 9

2.1.2. Rigid body mechanics..... 11

2.1.3. Deformable body mechanics..... 14

2.1.3.1. Floating frame of reference formulation..... 16

2.1.3.2. Mass matrix.....18

2.1.3.3. Stiffness matrix.....22

2.1.3.4. Equations of motion.....24

2.1.4. Turbine blade model.....26

2.1.4.1. Planar analysis.....29

2.1.4.1.1. Four nodes rectangular element..... 31

2.1.4.1.1.1. 2D Plate element validation.....35

2.1.4.1.2. Three nodes triangular element..... 39

2.1.4.1.2.1. Triangular element validation..... 45

2.1.4.1.3. Discretization with 2D plates element..... 48

TABLE OF CONTENTS (CONTINUED)

CHAPTER **PAGE**

2.1.4.1.4. Discretization with triangular elements……..55

2.1.4.2. 3D Analysis…… 62

2.1.4.2.1. Discretization with 8 nodes hexahedral…… 65

3. **DYNAMICS OF THE BLADE IN NON-LINEAR CONDITIONS**.....70

3.1. Modal analysis of the whole system……71

3.2. Influence of the contact parameters……..78

3.3. Forced response in frequency domain…….. 87

3.3.1. Linear forced response…… 89

3.3.1.1. Linear forced response in ansys…… 90

3.3.1.2. Linear forced response in matlab…….. 95

3.3.1.2.1. Component mode synthesis: the Craig Bampton method……..96

3.3.1.2.2. Matlab results…….. 100

3.3.1.3. Linear forced response comparison…….. 103

3.3.2. Non-linear forced response…….. 108

3.3.2.1. State of the art……..110

3.3.2.1.1. Variability in the dynamics of semi-cylindrical friction dampers…… 111

3.3.2.1.2. A refined approach for modeling friction dampers for turbine blades. .116

3.3.2.1.3. Identification of the damping coefficient……120

3.3.2.1.4. Coupling between turbine blades and friction dampers……123

3.3.2.2. Underplatform damper…… 128

TABLE OF CONTENTS (CONTINUED)

CHAPTER **PAGE**

3.3.2.3. Finite element model……131

3.3.2.4. Balance equations and harmonic balance method……134

3.3.2.5. Contact model……138

3.3.2.6. Model reduction and numerical solution……142

3.3.2.7. Non-linear response of the system……147

3.4. Forced response in time domain……156

3.4.1. Linear forced response……157

3.4.2. Non linear forced response……164

3.4.2.1. Contact model……167

3.4.2.2. Numerical solution……170

4. **CONCLUSIONS**……182

APPENDICES……186

APPENDIX A: 2D RECTANGULAR ELEMENT MATLAB SCRIPT……187

APPENDIX B: 2D TRIANGULAR ELEMENT MATLAB SCRIPT……189

CITED LITERATURE……191

VITA……194

LIST OF TABLES

TABLE		PAGE
I	BEAM CHARACTERISTICS	36
II	NODAL SOLUTION: COMPARISON BETWEEN ANSYS AND SAMS NODAL DISPLACEMENTS	37
III	BEAM CHARACTERISTICS	46
IV	COMPARISON BETWEEN ANSYS AND SAMS/2000 RESULTS	47
V	MATERIAL PROPERTIES OF THE BLADE	72
VI	NATURAL FREQUENCIES OF THE GLUED SYSTEM WITHOUT DAMPER	74
VII	LINEAR FORCED RESPONSE INPUT PARAMETERS	92
VIII	INPUT PARAMETERS, MATLAB CODE FOR LINEAR FORCED RESPONSE	101
IX	FREQUENCY COMPARISON: LINEAR RESPONSE IN MATLAB VS MODAL ANALYSIS IN ANSYS	107
X	CONTACT CONDITIONS	139
XI	IP AND OOP PEAKS IN THE NON LINEAR FORCED RESPONSE, RIGHT TIP TL2.	152
XII	CONTACT STATUS	168

LIST OF FIGURES

FIGURE **PAGE**

1.1 Blades model…….. 4

1.2 FEM model of the physical system…….. 6

2.1 Global and local reference frames. Reprinted from Shabana, Ahmed A., *Dynamics of Multibody Systems*. Chicago: Cambridge University Press 2005, 2005: 17…….. 10

2.2 Turbine Blade Geometry…….. 27

2.3 Blade model built in SAMS/2000 environment (reproduction in SolidWorks). ……28

2.4 Rectangular element domain. Reprinted from Moharos István, Oldal István, Szekrényes András. *Finite element methode*. Budapest: Typotex Publishing House, 2012…….. 32

2.5 Constrained beam, validation model for 2D plate in Ansys…….. 35

2.6 Nodal solution with Ansys…….. 37

2.7 Linear Triangular element. Reprinted from Moharos István, Oldal István, Szekrényes András. *Finite element methode*. Budapest: Typotex Publishing House, 2012…….. 39

2.8 Triangular element interpolating functions…….. 40

2.9 Beam discretization with triangular elements…….. 45

2.10 Nodal displacement of the beam along the y-axis…….. 46

2.11 Planar model…….. 48

2.12 Plane182 Ansys Element. Reprinted from Ansys 14.0 Help (2011), *Plane182 element*…….. 49

2.13 Blade discretization with 2D plates…….. 50

LIST OF FIGURES (CONTINUED)

FIGURE		PAGE
2.14	Nodes location, Ansys……	51
2.15	Nodal displacement node 165, middle of the airfoil, Matlab……	52
2.16	Nodal displacement node 10, top of the airfoil, Matlab……	53
2.17	Nodal displacement node 165, top of the airfoil, Matlab…… ..	53
2.18	Nodal displacement node 10, top of the airfoil, Matlab……	54
2.19	Example of Presams file: deformable body model, node list…… ..	55
2.20	Example of Presams file: deformable body model, element connectivity. .	56
2.21	Example of Presams file: deformable body model, element properties.	56
2.22	Blade discretization with 2D triangular elements…… ..	57
2.23	Node location, Ansys…… .58	
2.24	Comparison nodal displacement with 2D plate and 2D triangle discretization, top of the airfoil…… ..	59
2.25	Comparison nodal displacement with 2D plate and 2D triangle discretization, middle airfoil……	59
2.26	Comparison nodal displacement with 2D plate and 2D triangle discretization, top of the airfoil…… ..	60
2.27	Comparison nodal displacement with 2D plate and 2D triangle discretization, middle of the airfoil…… ..	61
2.28	8 nodes Hexahedral element……	63
2.29	Solid45 Ansys Element. Reprinted from Ansys 14.0 Help (2011), *Solid45 element*……	65
2.30	3D Solid Model: mesh generation in Ansys……	66
2.31	Example of Presams file: deformable 3D body model, node list……	67

LIST OF FIGURES (CONTINUED)

FIGURE **PAGE**

2.32 Example of Presams file: deformable 3D body model, element connectivity…… 67

2.33 Example of Presams file: deformable 3D body model, element properties.67

2.34 Nodes position 3D model…… 68

2.35 Nodal displacement x-axis node 10…….. 69

2.36 Nodal deformation x-axis, node 362…… .. 69

3.1 Solid95 element. Reprinted from Ansys 14.0 Help (2011), *Solid95 element.* .. …… 72

3.2 Solid model discretization in Ansys Environment…….. 73

3.3 First and second modal shapes of the system from Ansys…… 75

3.4 Third and Fourth modal shapes of the system from Ansys……. 76

3.5 Fifth and sixth modal shapes of the system from Ansys……..… .. 76

3.6 Seventh and eighth modal shapes of the system from Ansys…….. 77

3.7 Ninth and tenth modal shapes of the system from Ansys…… .. 77

3.8 Conta174 element. Reprinted from Ansys 14.0 Help (2011), *Conta174 element*…….79

3.9 Targe170 element. Reprinted from Ansys 14.0 Help (2011), *Targe170 element*……..... 80

3.10 Contact Pairs creation in Ansys……..... 81

3.11 Contact due to stresses with 10^{-4} (m) interference, Ansys……. ... 81

3.12 First Frequency: effects of the stiffness and interference……. 82

3.13 Second Frequency: effects of the stiffness and interference…….... 83

3.14 Third Frequency: effects of the stiffness and interference…….... 83

LIST OF FIGURES (CONTINUED)

FIGURE **PAGE**

3.15 Fourth Frequency: effects of the stiffness and interference……..... 84

3.16 Fifth Frequency: effects of the stiffness and interference……..... 84

3.17 Sixth Frequency: effects of the stiffness and interference…….. 85

3.18 Seventh Frequency: effects of the stiffness and interference…… 85

3.19 Eight Frequency: effects of the stiffness and interference……..... 86

3.20 Blades discretization with solid95 elements in Ansys, linear forced response. …….. 91

3.21 System discretization for the linear forced response, Ansys……. 93

3.22 Linear forced response in Ansys, Fe =5 N…….94

3.23 Master degrees of freedoms used in the Craig-Bamptom Method, Ansys. .... …….. 98

3.24 Linear forced response with Matlab code…….. 101

3.25 Linear forced response for Fe ranging from 5 to 300 N, Matlab…….. 102

3.26 Ansys and Matlab results comparioson, right tip TL2 x-axis displacement. .... …….104

3.27 Linear response along x-axis, Matlab……..... 105

3.28 Linear response along z-axis, Matlab…….. 106

3.29 Rotor disc for gas turbine engine. Reprinted Phipps, Anthony B. (Derby, GB), *Rotor disc for gas turbine engine,* 2005…….. 108

3.30 Damper model. Reprinted from [10]…….111

3.31 Contact model. Reprinted from [10]…….112

3.32 Case of study. Reprinted from [10]…….. 112

LIST OF FIGURES (CONTINUED)

FIGURE **PAGE**

3.33 Effect of the damper mass on the IP peaks (left) and OOP peaks (right). Reprinted from [10]..... 113

3.34 Effect of the preloads. Reprinted from [10]..... 114

3.35 Effects of the friction coefficient. Reprinted from [10]..... 114

3.36 Effects of the excitation force. Reprinted from [10].....115

3.37 Blade model. Reprinted from [11]..... .116

3.38 Figure a: effect of the damper mass on the frequency response, the number is the multiplier of the damper mass; Figure b: effect of the excitation force. Reprinted from [11].....118

3.39 Map of the contact status. Reprinted from [11]..... . 119

3.40 Damping ratio comparison between turbine blades and beam cut out of the same blade material. Reprinted from [12]..... 120

3.41 Comparison between free blades and blades modeled with friction elements. Reprinted from [12]..... .. 121

3.42 Damping ratio dependence on blade vibration amplitude and nodal diameters, TC=blades with friction damper, v=free blades. Reprinted from [12]..... 122

3.43 V-shroud profile and experimental results. Reprinted from [12]..... .. 122

3.44 System of Blades with excitation force vector with A-B mistuning. Reprinted from [13]..... .. 123

3.45 Application of the mistuning on blade A. Reprinted from [13]..... 124

3.46 FRF of blades A and B, effect of the centrifugal force and the application of the mistuning. Reprinted from [13]..... .. 125

LIST OF FIGURES (CONTINUED)

FIGURE **PAGE**

3.47 System of two blades plus underplatform damper analyzed by DATAR code. Reprinted from [13]…….. 125

3.48 Performance for mode 1 for different value of EO. Reprinted from [13]. 126

3.49 Frequency response of the system of two blades and Campbell diagrams. Figure a comparison between mode 1-3, Figure b comparison between mode 1 and 2. The red curve represents the blade A, the blue curve blade B. Reprinted from [13]…….. 127

3.50 System of two blades and an underplatform damper, Solidworks……. .. 129

3.51 Zoom, underplatform damper in contact with the blades…….. 129

3.52 Underplatform damper, finite element model in Ansys…….. 130

3.53 FEM of the structure for non linear analysis, Ansys…….. 131

3.54 Underplatform damper, FEM model in Ansys…… 132

3.55 2D contact model for non linear dynamic analysis. Reprinted from Stefano Zucca, Christian M. Firrone, Muzio Gola. *Modeling underplatform dampers for turbine blades: a refined approach in the frequency domain*. Journal of Vibration and Control, 2012: 1-16…….. 139

3.56 Contact between adjacent nodes…….. 141

3.57 Matrix reduction in non linear analysis……143

3.58 Damper discretization, left contact…….. 144

3.59 Damper discretization, right contact…….. 144

3.60 Non-linear analysis, application of the external force vector…….. 148

3.61 Non-linear response of the right tip TL2, IP and OOP…….. .. 149

3.62 FRF right tip TL2, IP and OOP peaks…… .150

LIST OF FIGURES (CONTINUED)

FIGURE		PAGE
3.63	FRF with free response, right tip TL2	151
3.64	IP performance, resonance frequencies vs excitation force	153
3.65	OOP performance, resonance frequencies vs excitation force	153
3.66	IP performance, resonance amplitude vs excitation force	154
3.67	OOP performance, resonance amplitude vs excitation force	155
3.68	Linear forced response in time domain, FEM model	159
3.69	X-axis displacement, right tip	160
3.70	Linear forced response from time integration	161
3.71	Linear forced response comparison	162
3.72	System model	165
3.73	System representation	166
3.74	Non linear response, right tip in time domain	171
3.75	zoom	171
3.76	Hysteresis cycle right contact	173
3.77	Hysteresis cycle left contact 1	173
3.78	Hysteresis cycle left contact 2	174
3.79	Transient and steady state in stick conditions	175
3.80	Non linear forced response comparison in stick conditions for the right tip, Fe=5N	176
3.81	Displacement of the right tip: transient and steady state	177
3.82	Hysteresis cycle for right contact in slip condition	178
3.83	Hysteresis cycle left contact 1, slip condition	178
3.84	Hysteresis cycle left contact 2, lift off	179

LIST OF FIGURES (CONTINUED)

FIGURE		PAGE
3.85	Tangential contact force on the right contact vs time, for 4 cycles……..	180
3.86	Tangential contact force on the left 1 contact vs time, for 4 cycles……....	180
3.87	Tangential contact force on the left 2 contact vs time, for 4 cycles…….	181

SUMMARY

In this thesis, a numerical simulation of the linear behavior of a turbine blade subjected to a rotation with large displacements has been carried out by the use of a specialized code. A finite element formulation of the problem has been considered in order to to develop a realist model and examine the vibration of the blade undergoing a rigid body rotation. In order to achieve this goal, the dynamics of the multibody rotor blade system has been studied by the use of the Floating Frame of Reference Formulation [1] applied to the case of a deformable body, the blade, connected to a rigid body, which represents a rotor rotating at a constant angular velocity.

The second part of the thesis focuses on the non-linear dynamics of a system consisting of two blades with a underplatform damper between them. Turbine blades frequently reach the resonance conditions due to the high speed of rotation in working environment with the consequence of an increased amplitude of vibration which can cause fatigue failure of the structure. The presence of an underplatform damper can help to dissipate a part of the energy at resonance through frictional contact between the blades platform and the damper, increasing the fatigue life of the blades.

1. INTRODUCTION

1.1. The finite element method

Nowadays most engineering problems have become so complex to require very powerful tools in order to solve them, and in many cases the simulation of the physics has become essential. One of the most important theory that can be applied in order to simulate the behavior of a real system without losing in accuracy, is the finite element method, which had been developed in the second half of the 1900'.

A finite element method is a particular kind of method that can be applied to study the behavior of a complex physical system discretizing it into a set of less complex components, called finite elements. The physical behavior of each element is well known and can be expressed by the use of certain shape functions, i.e. functions which enable us to define how the element deforms. Once the dynamics of the single simple component is defined, the overall behavior of the physical system can be obtained by connecting or assembling the collection of all the elements. Many different types of elements are available in literature, with dependence on the accuracy and the complexity of the system which we are dealing with. The subdivision of the physical domain into a set of smaller components has several advantages, including simplification of the problem formulation and an accurate model representation. Once the model is developed, the resulting set of algebraic and differential equations can be solved numerically.

In this thesis, the finite element method is used to investigate the linear and nonlinear dynamics of two turbine blade system. Turbine blades are mechanical components

frequently subjected to fatigue failure due to application of cyclic loads during their functional operation. Due to the frequent shutting down and starting up, turbine blades frequently reach resonance with the consequence of a growth in the amplitude of vibration and in a reduction of their fatigue life.

This is the reason why a complete dynamic analysis of a simple model of turbine blades has been investigated looking into the linear and non-linear behavior of the system. The first part of the thesis analyses the blade's deformation due to the application of a rotation with large displacement by the use of a multibody code. The blade has been fixed on a rigid rotor and brought in rotation at a constant angular velocity in order to simulate what happens on the turbine disk. The model has been studied by the application of the Floating Frame of Reference Formulation according to which the blade is considered as deformable body, discretized into a set of finite elements. The discretization of the model is carried out using different elements in order to show how different finite elements approximations can lead to the same results.

Since the motion of the blade is essentially a rotation about a fixed axis, the first two tests are carried out considering a planar motion of the body by the use of two planar finite elements, a 2D plate and a 2D triangle, implemented in the general purpose multibody system code SAMS/2000. Finally the same simulation is carried out using a 3D model, using solid elements to discretize the system components. This analysis is performed in order to establish a general multibody system procedure that can be used in the future in the analysis of more complex rotor blades systems.

After examining the linear behavior of the blade, the second part of the thesis takes into account the dynamics of the blade in presence of an underplatform damper with friction contact. Many articles about the coupling between turbine blades and friction dampers can be found in literature: turbine blades are usually characterized by a very low

structural damping which is not sufficient to prevent fatigue failure of the blades due to the high amplitude of vibration reached at resonance. This is the main reason why an underplatform damper is often used between the blades in order to dissipate a certain amount of energy through friction. The presence of the damper does not allow only a reduction of the amplitude of vibration but also a slight increase in the resonance frequency. Resonant fatigue is an important failure mechanism that usually arises in turbine blades due to the application of an external force acting at a frequency equal to the natural frequency of the blade. An inadequate damping can lead to an increase of the blade's amplitude of vibration with the consequence high cycle fatigue failure. In this thesis, an asymmetric damper with a cylindrical and a flat contact surfaces will be studied coupled with a set of two dummy blades connected to a fixture.

It is important to point out that a simplified model has been used in this investigation, in order to have an efficient solution and at the same time show a possible applications of the same procedure to more realistic problems.

1.2. Overview of the physical model and statement of the problem

As already mentioned before, this investigation is focused on the development of a simplified model of two turbine blades, fastened on a fixture and detached by an under-platform damper between them. Each blade is characterized by an airfoil, a central body and a root which enables to attach the blade to its fixture. The central part of the blade is rounded in order to allow the space for the damper. The shape of the fixture depends on the measuring tools used to study the whole system and it is designed in order to keep two blades. Finally the underplatform damper is fixed between the two blades in order to influence the dynamics of both, taking into account also the friction contact. Figure 1.1 shows the structure of the physical system previously described.

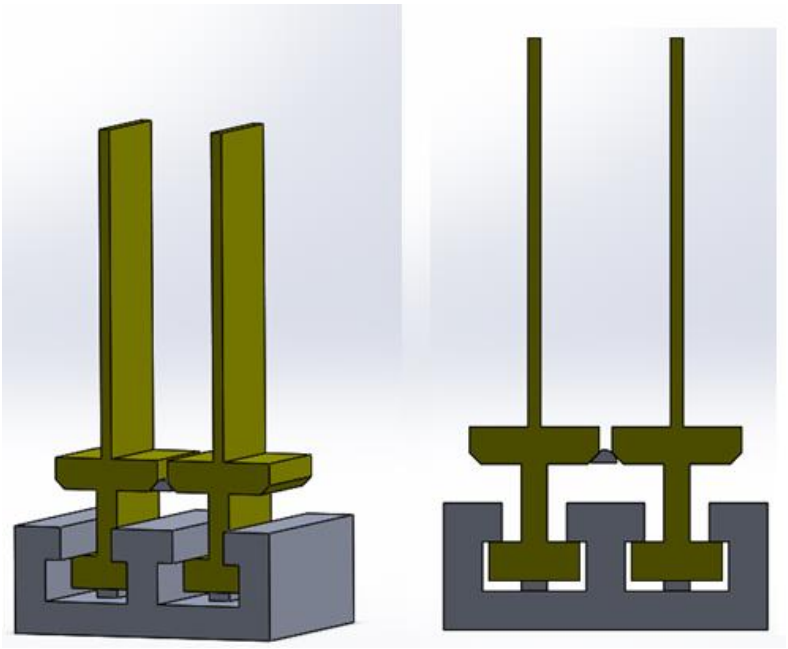

Figure 1.1 Blades model.

In the first part of the thesis, the linear behavior of the blade subjected to a rotation with a large displacement examined by considering the blade as a flexible body connected to a rectangular rotor which rotates about a fixed axis. The rotor is modeled as a rigid body, rotating at a constant angular velocity. The blade is centered on the rotor and connected to it using a rigid joint. Turbine blades usually work in hostile environment, at high temperature and at a very high angular velocity, this is the reason why a numerical simulation of the blade's dynamics can be useful to define how the blade vibrates during rotation subjected to the centrifugal force. The discretization of the model obtained through the finite element Analysis enables to consider the displacement of each node of the body.

The second part of the work, mainly deals with the non-linear dynamics of two-blade system due to the presence of the contact forces induced by the underplatform damper between them. During the blade rotation, the centrifugal force presses the damper against the blades, introducing the non-linearity caused by the friction contact. The presence of the damper not only affects the natural frequencies of the system but also its modal shapes, allowing a reduction of the amplitude of vibration of the blades at resonance. This results of the analysis of the forced response of the blades will be obtained in the frequency and time domain focusing on the advantages of the two approaches. The finite element model and the preliminary calculations will be performed in Ansys, while the numerical simulation of the non-linear dynamics will be evaluated using a special purpose developed Matlab code developed by the author of this thesis.

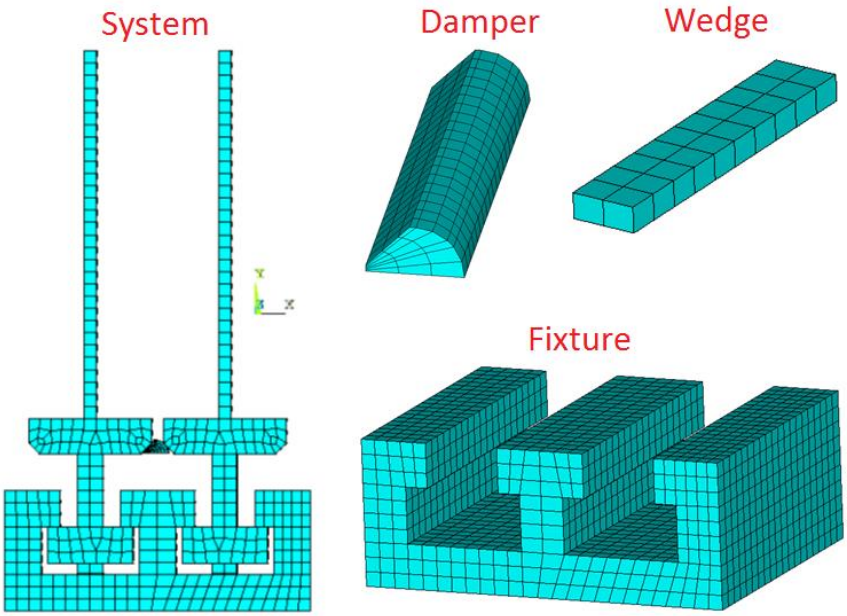

Figure 1.2 FEM model of the physical system.

2. LINEAR DYNAMICS OF THE BLADE

In this first part of the thesis, the numerical simulation of the linear dynamics of the single blade is performed using a general purpose multibody system code called SAMS, a computer simulation program which enables to study complex multibody systems consisting of rigid and deformable bodies.

A discretization of the blade as a deformable body is made in order to evaluate its motion by the application of the Floating Frame of Reference Formulation [1]. Two different 2-dimensional elements have been purposely developed and validated to simulate the rotation of the blade using the SAMS code. For sake of simplicity, since the blade rotates about a fixed axis, its motion can be first approximated as planar motion which justifies the use of the planar finite elements. In addition, another three dimensional simulation with solid elements implemented in the program is performed to obtain a model close to the real system.

2.1. Multibody systems

A considerable amount of mechanical and physical systems are characterized by the presence of interconnected components which undergo large translational and rotational displacements. A multibody system is defined as a set of bodies whose motion is constrained by the presence of different types of joints. A multibody system can be represented by either rigid and/or by deformable bodies. A body is said to be rigid if the relative distance between two arbitrary points on the body remains the same after the application of a translation or a rotation, while it is said to be deformable if the application of a large rotation or translation produces a change in the position of the points inside the body. The rigid body motion can be described by the use of six generalized coordinates, three rotations and three translations, producing a highly non-linear mathematical model.

2.1.1. Reference frames

To describe the dynamics of a multibody system, it is necessary to introduce a set of reference frames in order to evaluate the position of the body and define its kinematics. A frame of reference is a reference system defined by three orthogonal axes intersecting in the origin of the frame.

Generally two different types of reference system are considered in a multibody system, a global reference system which is fixed in space and unique for all the bodies and a local reference system which is associated with a body in the multibody system. It is possible to define with X_1,X_2 and X_3respectively the three axes of the global reference system and with X_1^i,X_2^i and X_3^i the three axes of the local one, where i indicates the body we are dealing with. Finally i_1, i_2 and i_3 and i_1^i, i_2^i and i_3^i represent respectively the unit vectors of the global and the local reference systems. It follows that the position of a generic point in the multibody system, can be easily expressed in terms of both the global and the local coordinates; if u is the vector indicating the position of a generic point in the global reference system, it follows that:

$$u^i = \bar{u}_1^i i_1^i + \bar{u}_2^i i_2^i + \bar{u}_3^i i_3^i \qquad 2.1$$

$$u^i = u_1^i i_1 + u_2^i i_2 + u_3^i i_3 \qquad 2.2$$

Where u^{i} is the generic vector which indicates the position of a point in the global reference system and $\mathrm{u}_1^{\mathrm{i}}$ and $\bar{\mathrm{u}}_1^{\mathrm{i}}$ represents the component of the vector defined in the global and in the local reference systems, respectively.

The orientation of the local reference system with respect to the global one can be expressed through the use of a transformation matrix, which has a definition that depends on the 2D or 3D case.

$$u^i = \mathrm{A}^i \bar{u}^i \qquad 2.3$$

A^i is the transformation matrix that defines the orientation of the coordinate system of body i.

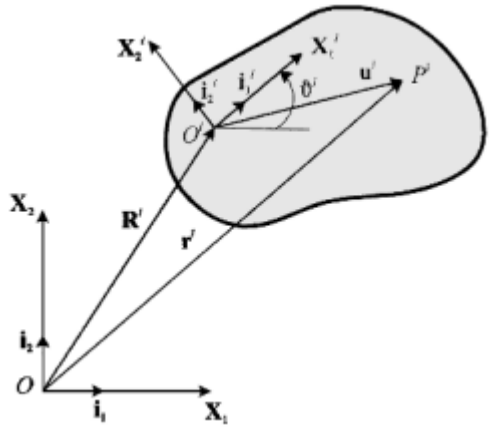

Figure 2.1 Global and local reference frames. Reprinted from Shabana, Ahmed A., *Dynamics of Multi-body Systems*. Chicago: Cambridge University Press 2005, 2005: 17.

2.1.2. Rigid body mechanics

The configuration of a rigid body in space can be defined using six independent coordinates, three translations which define the position of the body reference point and three rotations required to show the body orientation. In the simpler case of a 2D problem, only three coordinates are necessary to define the configuration of the body, two translations and one rotation. The generic position of a point in the space, r^i, can be expressed as the sum of a vector, R^i, which defines the location of the origin of the body reference system with respect to the global system and a second vector which defines the position of the point in the local reference system.

$$r^i = R^i + \mathrm{A}^i \bar{u}^i \qquad 2.4$$

Differentiating equation 2.4 with respect to time, it is possible to obtain the kinematic equations of the rigid body. The angular velocity vector ω is obtained from the differentiation of the transformation matrix and in the simpler case of planar motion it is possible to show that the angular velocity vector is always equal to the product of the angular velocity, $\dot{\theta}$, and the unit vector along the axis of rotation, and the angular velocity vector is the same in the global and local reference systems.

$$\dot{r}^i = \dot{R}^i + \mathrm{A}^i(\bar{\omega}^i \times \bar{u}^i) = \dot{R}^i + \mathrm{A}^i \tilde{\bar{\omega}}^i \bar{u}^i \qquad 2.5$$

or defined in the global reference system:

$$\dot{r}^i = \dot{R}^i + (\omega^i \times u^i) = \dot{R}^i + \tilde{\omega}^i u^i \qquad 2.6$$

Where ω and $\bar{\omega}$ are respectively the angular velocity vectors defined in the global and in the local reference systems. $\tilde{\omega}$ and $\tilde{\bar{\omega}}$ are two skew symmetric matrices associated with the angular velocity vector and they can be used to replace the cross product. In the planar analysis, the angular velocity vector can be defined in the global and local systems as follows:

$$\omega^i = \dot{\theta}\, i_3 \qquad 2.7$$

$$\bar{\omega}^i = \dot{\theta}\, i_3^i \qquad 2.8$$

Differentiating again the velocity equation, one obtains the acceleration equation of the arbitrary point. It is evident that the acceleration is characterized by the presence of a normal component orthogonal to the cross product between the angular velocity vector and the position vector, and a tangential component orthogonal to the position vector u^i. α^i is the angular acceleration vector defined in the global reference system, while the vector with the bar represents the angular velocity defined in the local reference system.

$$\ddot{r}^i = \ddot{R}^i + \mathrm{A}^i(\bar{\alpha}^i \times \bar{u}^i) + \mathrm{A}^i\bar{\omega}^i \times (\bar{\omega}^i \times \bar{u}^i) \quad 2.9$$

$$\ddot{r}^i = \ddot{R}^i + \left(\alpha^i \times u^i\right) + \omega^i \times (\omega^i \times u^i) \quad 2.10$$

The rigid body dynamics represents a useful approximation to define the behavior of a body subjected to translations and rotations with large displacements, and in this work it is used to describe the rotor on which the turbine blade is mounted during the rotation. The blade model is more complex since it is assumed as a deformable body.

2.1.3. Deformable body mechanics

The assumptions used ti formulate the dynamic equations of a rigid body are not valid in the case of a deformable body, which changes its shape when the body is ubjected to external forces. The definition of the reference frames remains the same for both the local and the global references; the only change is due to the fact that the vector which defines the location of the arbitrary point in the deformable body with respect to the origin of the body coordinate system no longer has a constant length.

The vector $\bar{u}^i$ is now obtained by the sum of a constant component, $\bar{u}_0^i$ which defines the position of a generic point P^i inside the deformable body in the undeformed configuration, and a second component $\bar{u}_f^i$ which defines the deformation vector, and varies with dependence on the motion of the body.

$$\bar{u}^i = \bar{u}_0^i + \bar{u}_f^i \qquad 2.11$$

The velocity equations in the case of the deformable body can be directly obtained by differentiating the position equation 2.4 as:

$$\dot{r}^i = \dot{R}^i + \mathrm{A}^i(\bar{\omega}^i \times \bar{u}^i) + \mathrm{A}^i\dot{\bar{u}}_f^i \qquad 2.12$$

In a similar manner, the acceleration equation can be obtained as

$$\ddot{r}^i = \ddot{R}^i + \mathrm{A}^i(\bar{\alpha}^i \times \bar{u}^i) + \mathrm{A}^i\bar{\omega}^i \times (\bar{\omega}^i \times \bar{u}^i) + 2\mathrm{A}^i\left(\bar{\omega}^i \times \dot{\bar{u}}_f^i\right) + \mathrm{A}^i\ddot{\bar{u}}_f^i \qquad 2.13$$

The same equations can be written in terms of the global reference system as previously discussed in the case of the rigid body. The two additional terms in the acceleration equation are related respectively to the Coriolis component of the acceleration and the local component of the acceleration which takes into account the contribution of the deformation. The turbine blades studied in this thesis will be considered as deformable bodies, while the block representing the rotor was assumed to be a rigid body.

2.1.3.1. Floating frame of reference formulation

In the previous subsections, the main equations governing the kinematics of a multi-body system are represented, it is now necessary to introduce how to formulate the equations of motion of deformable bodies subjected to translations and rotations with large displacements using the Floating Frame of Reference formulation [1] in terms of the inertia shape integrals in addition to the vector of the generalized forces and the stiffness and mass matrices. The inertia shape integrals can be defined using the assumed displacement field, represent the coupling between the elastic body deformation and the reference motion. Two different kinds of generalized coordinates, elastic and reference, will be used to define the configuration of the deformable body in space. The first describes the deformation of the body with respect to its reference, while the second defines the orientation and the location of the body reference with respect to the global system.

In the case of a deformable body, it was shown that the position of an arbitrary point can be defined by the vector $\bar{u}^i$, equation 2.11, which has a constant component $\bar{u}_0^i$ and a variable component $\bar{u}_f^i$. The variable component $\bar{u}_f^i$ is obtained by the product of a matrix of shape functions, S^i, i.e. functions which describe the shape assumed by the body during deformation, and a vector of elastic coordinates q_f^i.

$$\bar{u}_f^i = S^i q_f^i \qquad 2.14$$

The number of elastic coordinates can be chosen depending on the system and forces to be examined. This is the case of the turbine blade considered in this thesis which has been discretized in a set of finite elements, each of which has a certain number of nodal degrees of freedom that define the number of elastic coordinates.

2.1.3.2. Mass matrix

In order to develop the equations of motion of a deformable body, it is necessary to develop a formulation of its mass matrix which takes into account the inertia properties of the body. In the case of a continuous body, the kinetic energy can be written as follows:

$$\mathrm{T}^i = \frac{1}{2}\int \rho^i \dot{r}^{i^T} \dot{r}^i dV^i \qquad 2.15$$

Where $\dot{r}^i$ is the velocity equation for a deformable body already introduced in subsection 2.1.3, taking into account the effect of the elastic coordinates and obviously the shape functions. $\rho^i$is the density of the continuous body, and V^iits volume. It follows that equation 2.12 can be rewritten as:

$$\dot{r}^i = \dot{R}^i - \mathrm{A}^i\tilde{\bar{u}}^i\bar{G}^i\dot{\vartheta}^i + \mathrm{A}^i S^i \dot{q}_f^i \qquad 2.16$$

Or in a matrix form as:

$$\dot{r}^i = \begin{bmatrix} I & -\mathrm{A}^i\tilde{\bar{u}}^i\bar{G}^i & \mathrm{A}^i S^i \end{bmatrix} \begin{bmatrix} \dot{R}^i \\ \dot{\vartheta}^i \\ \dot{q}_f^i \end{bmatrix} = L^i \dot{q}^i \qquad 2.17$$

I represents a 3x3 identity matrix since we are dealing with a 3D case, $\bar{G}^i$is a matrix which depends on the particular set of orientation parameters used to define the orientation of a body in space, Euler angles, Rodriguez Parameters, or Euler Parameters, and relates the angular velocity vector to the time derivatives of the orientation coordinates of the body according to the following relation:

$$\bar{\omega}^i = \bar{G}^i \dot{\vartheta}^i \tag{2.18}$$

Finally $\dot{q}^i$is the vector which contains all the generalized coordinates used to describe the motion of the body. The dimensions of this vector depends on the number of elastic coordinates used to define the behavior of the deformable body since the coordinates related to the body translation, $\dot{R}^i$, and orientation, $\dot{\vartheta}^i$are respectively three for the position and three or four for the orientation depending on the set of orientation parameters used. Substituting equation 2.17 in equation 2.15, one can define the mass matrix for a deformable body as

$$\mathrm{T}^i = \frac{1}{2} \dot{q}^{i^T} \left[\int \rho^i L^{i^T} L^i dV^i \right] \dot{q}^i \tag{2.19}$$

$$\mathrm{T}^i = \frac{1}{2} \dot{q}^{i^T} M^i \dot{q}^i \tag{2.20}$$

with M^i the symmetric mass matrix of the deformable body defined as

$$\mathrm{M}^i = \int \rho^i {L^i}^T L^i dV^i \tag{2.21}$$

$$\mathrm{M}^i = \int \rho^i \begin{bmatrix} I \\ -{\bar{G}^i}^T {\tilde{\bar{u}}^i}^T {\mathrm{A}^i}^t \\ {S^i}^T {\mathrm{A}^i}^T \end{bmatrix} \begin{bmatrix} I & -\mathrm{A}^i \tilde{\bar{u}}^i \bar{G}^i & \mathrm{A}^i S^i \end{bmatrix} dV^i \tag{2.22}$$

This mass matrix can be written in a partitioned form as:

$$\mathrm{M}^i = \begin{bmatrix} m^i_{RR} & m^i_{R\vartheta} & m^i_{Rf} \\ m^i_{\vartheta R} & m^i_{\vartheta\vartheta} & m^i_{\vartheta f} \\ m^i_{fR} & m^i_{f\vartheta} & m^i_{ff} \end{bmatrix} \tag{2.23}$$

Where the matrices along the main diagonal represent respectively the mass matrix associated with the pure translation of the body, m^i_{RR}, the mass matrix associated with the pure rotation, $m^i_{\vartheta\vartheta}$, and finally the mass matrix associated with the deformation, m^i_{ff}. The other matrices represent the inertia coupling between the rigid body translation and rigid body rotation, $m^i_{R\vartheta}$ or $m^i_{\vartheta R}$, and the coupling between the elastic and the reference motion, m^i_{Rf} and $m^i_{\vartheta f}$. In the case of the rigid body, the formulation of the mass matrix is much more straightforward since the contribution of the deformation and it's coupling with the reference motion are not present. In addition to this, for a rigid body if

the coupling between the rotational and translation coordinates can be eliminated by the choice of a centroidal body reference system for the body, i.e. a body reference with origin fixed at the body center of mass. This is not possible, in general, in the case of the deformable body since the body deformation will move its reference from that point. For convenience, the formulation of the mass matrix of the deformable body is now summarized.

2.1.3.3. Stiffness matrix

In order to complete the study of the deformable body, it is necessary to take into account of the effects that arise from the deformation of the body and particularly from the elastic forces. According to the principle of the virtual work, the virtual work of the elastic forces can be expressed in the following form [1]:

$$dW_s^i = -\int {\sigma^i}^T \delta\varepsilon^i \, dV^i \qquad 2.24$$

Where $\delta\varepsilon^i$ represents the virtual change of the elastic strain, while σ^i the stress vector. The strain can be expressed as the product of the differential operator D^i and the deformation vector $\bar{u}_f^i$:

$$\varepsilon^i = D^i \bar{u}_f^i = D^i S^i q_f^i \qquad 2.25$$

$$\sigma^i = E^i \varepsilon^i = E^i D^i S^i q_f^i \qquad 2.26$$

E^i is the symmetric matrix of the elastic coefficients. Substituting equations 2.25 and 2.26 into equation 2.24, one can define the stiffness matrix of the deformable body.

$$dW_s^i = -\int {q_f^i}^T \left(D^i S^i\right)^T E^i D^i S^i \delta q_f^i dV^i \quad 2.27$$

$$dW_s^i = -{q_f^i}^T K_{ff}^i \delta q_f^i \quad 2.28$$

$$K_{ff}^i = -\int \left(D^i S^i\right)^T E^i D^i S^i dV^i \quad 2.29$$

K_{ff}^i represents the stiffness matrix of the deformable body associated with its elastic coordinates.

2.1.3.4. Equations of motion

Many formulations can be used to solve the dynamics of a system of bodies, and one of them is the Lagrangian formulation of the equations of motion in which the constraint forces are obtained from the constraint Jacobian matrix and the vector of Lagrange multipliers, λ . As previously explained, a rigid body is characterized by 6 independent coordinates defining its position and orientation in space. If we would like to consider a multibody system, in order to connect the bodies, a certain number of its degrees of freedom will be eliminated as the result of the constraints, each of which has its own algebraic equation. The constraint forces that arise from the motion constraints are evaluated using Lagrange multipliers in the Lagrangian formulation.

.

$$M^i\ddot{q}^i + K^i q^i + C_{q^i}^T \lambda = Q_e^i + Q_v^i \qquad 2.30$$

Equation 2.30 represents the general formulation of the equations of motion for a 3D case. q^i is the vector of the generalized coordinates employed to study the deformable body, λ is the vector of the Lagrange multipliers, $C_{q^i}^T$ is the transpose of the constraint Jacobian matrix of the multibody system, Q_e^i is the vector of the external forces and finally $Q_v^i$is the vector of the centrifugal forces, a quadratic velocity vector that contains the gyroscopic and Coriolis force components. Using the generalized coordinate partitioning, the equations can be written in a more explicit form as:

$$\begin{bmatrix} m_{RR}^i & m_{R\vartheta}^i & m_{Rf}^i \\ m_{\vartheta R}^i & m_{\vartheta\vartheta}^i & m_{\vartheta f}^i \\ m_{fR}^i & m_{f\vartheta}^i & m_{ff}^i \end{bmatrix} \begin{bmatrix} \ddot{R}^i \\ \ddot{\vartheta}^i \\ \ddot{q}_f^i \end{bmatrix} + \begin{bmatrix} 0 & 0 & 0 \\ 0 & 0 & 0 \\ 0 & 0 & K_{ff}^i \end{bmatrix} \begin{bmatrix} R^i \\ \vartheta^i \\ q_f^i \end{bmatrix} + \begin{bmatrix} C_{R^i}^T \\ C_{\vartheta^i}^T \\ C_{q_f^i}^T \end{bmatrix} \lambda = \begin{bmatrix} Q_{eR}^i \\ Q_{e\vartheta}^i \\ Q_{ef}^i \end{bmatrix} + \begin{bmatrix} Q_{vR}^i \\ Q_{v\vartheta}^i \\ Q_{vf}^i \end{bmatrix}$$

2.31

2.1.4. Turbine blade model

The brief introduction to the concept of multibody systems and the development of the Floating Frame of Reference Formulation were necessary to understand the analysis of the simplified model of turbine blade studied in this thesis. The main equations of motion of a deformable body will now be applied to this practical case in which the complex shape of the turbine blade will be discretized in a set of finite elements, each of which has its own formulation in terms of stiffness and mass. The simulation of this multibody system model was performed using a general purpose code, called SAMS/2000. Note that the turbine blade motion is essentially a rotation with large displacement about a fixed axis, which means that since the motion can be represented inside a plane orthogonal to the axis of rotation, the rotation of the blade can be studied using a planar model as a first approximation. This simplification has been allowed by the fact that the case of study is a simplified model with constant thickness. Figure 2.2 shows the blade geometry and dimensions.

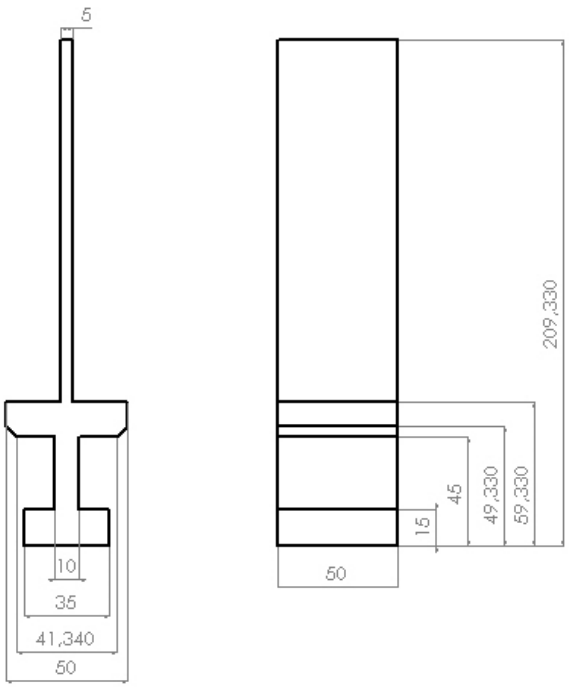

Figure 2.2 Turbine Blade Geometry

In order to obtain a more complete analysis of the case study, the blade is also examined using a solid element model based on the equations of motion introduced in the subsection 2.1.3.4. Obviously the 2D analysis is simpler since the approximation of a planar motion of a 2D model requires a smaller number of degrees of freedom and allows a faster computation. It is very important to mention that the development of the planar analysis has been made possible by the formulation of certain 2D finite elements: a 2D rectangular element and a 2D triangular element. Since these two finite elements have not been present in the program SAMS/2000 yet, the formulation has been performed purposely for this application first in Matlab environment and then implemented in Fortran code in order to update the libraries and the interface of SAMS/2000. The implementation of the two finite elements has been examined comparing the results of a test

case with Ansys. The solid model used in the second part of the simulation uses solid elements already implemented in the code, and for this reason no validation was required.

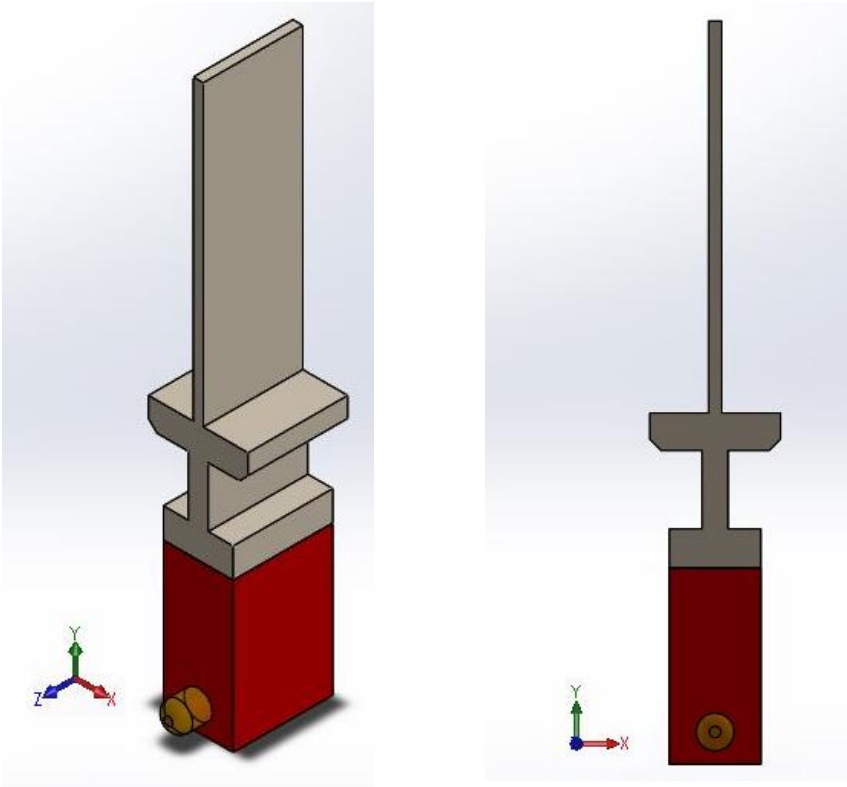

Figure 2.3 Blade model built in SAMS/2000 environment (reproduction in SolidWorks).

2.1.4.1. Planar analysis

In the special case of planar motion, the equation of motion of deformable body can be simplified by reducing the number of degrees of freedom of the model. The position of a body in a plane can be expressed specifying the position of its local reference system, two translations, and its orientation with respect to the global system. It follows that the number of generalized coordinates is lower. For rectangular and triangular elements, there are two approaches that can be used to formulate the elastic forces. These approaches are [2]:

- Plane stress problem: a problem in which a structure with a small constant thickness is subjected to an in-plane loading.
- Plane strain problem: the problem in which a long structure is loaded along its length.

Since in the turbine blade model considered in this thesis the thickness of the structure is constant and it is smaller than the length, it is possible to assume valid the 2D approximation of plane stress. In the case of plane stress, the only stress components present are all contained inside a plane, in our case the xy plane, and the stresses are related to the deformation through the constitutive equation of the plane stress problem using the following matrix of elastic coefficients:

$$\mathrm{E}^{i} = \frac{\mathrm{E}}{1-\nu^{2}}\begin{bmatrix} 1 & \nu & 0 \\ \nu & 1 & 0 \\ 0 & 0 & \frac{1-\nu}{2} \end{bmatrix} \qquad 2.32$$

The plane stress problem has been studied taking into account two different kinds of elements used to discretize the turbine blade model. The first element to be developed is a four nodes rectangular element, and the second one is a three node triangular element. For both the cases, an analytical expression of the mass and the stiffness matrices can be obtained with no need of a numerical integration.

2.1.4.1.1. Four nodes rectangular element

In the case of a 2D rectangular element, the analytical formulation of the mass and the stiffness matrices can be developed using the assumed displacement field which is expressed in terms of element shape functions. Using the theory of elasticity, the strain can be related to the displacement field as expressed in equation 2.25, where D is the differential operator and E^i is the matrix of the elastic coefficients, in this case ofplane stress, one has:

$$\mathrm{D} = \begin{bmatrix} \frac{\partial}{\partial x} & 0 \\ 0 & \frac{\partial}{\partial y} \\ \frac{\partial}{\partial y} & \frac{\partial}{\partial x} \end{bmatrix} \qquad 2.33$$

A 2D rectangular element has four nodes, each of which is characterized by 2 degrees of freedom, a translation along the x-axis, u, and a translation along the y-axis, v. It follows that the mass and the stiffness matrices will be 8x8 square matrices, while the matrix containing the shape functions will be 2x8. The shape functions are expressd in terms of the natural coordinates, which are dimensionless coordinates over the main $[-1, 1]$.

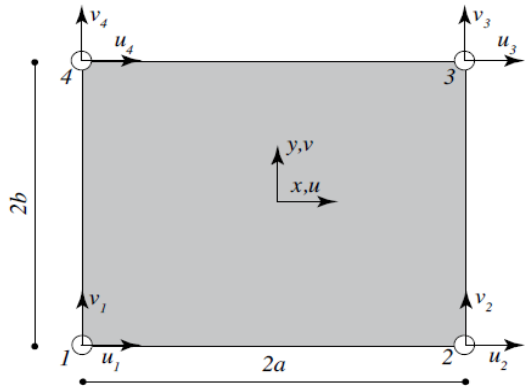

Figure 2.4 Rectangular element domain. Reprinted from Moharos István, Oldal István, Szekrényes András. *Finite element methode*. Budapest: Typotex Publishing House, 2012.

The shape functions used to define the assumed displacement field are four, one per each node and defined as follow:

$$\begin{cases} N_1(\xi,\eta) = \frac{1}{4}(1-\xi)(1-\eta) \\ N_2(\xi,\eta) = \frac{1}{4}(1+\xi)(1-\eta) \\ N_3(\xi,\eta) = \frac{1}{4}(1+\xi)(1+\eta) \\ N_4(\xi,\eta) = \frac{1}{4}(1-\xi)(1+\eta) \end{cases} \qquad 2.34$$

With

$$\begin{cases} \xi = \frac{x}{a} \\ \eta = \frac{y}{b} \end{cases} \qquad 2.35$$

And can be arranged in the matrix S in the following way:

$$\mathrm{S} = \begin{bmatrix} N_1 & 0 & N_2 & 0 & N_3 & 0 & N_4 & 0 \\ 0 & N_1 & 0 & N_2 & 0 & N_3 & 0 & N_4 \end{bmatrix} \tag{2.36}$$

Combining the differential operator with the shape functions, it is possible to get to the formulation of the stiffness matrix of the 2D rectangular element according to the definition of subsection 2.1.3.3.

$$\mathrm{B} = \mathrm{DS} = \begin{bmatrix} \frac{\partial}{\partial x} & 0 \\ 0 & \frac{\partial}{\partial y} \\ \frac{\partial}{\partial y} & \frac{\partial}{\partial x} \end{bmatrix} \begin{bmatrix} N_1 & 0 & N_2 & 0 & N_3 & 0 & N_4 & 0 \\ 0 & N_1 & 0 & N_2 & 0 & N_3 & 0 & N_4 \end{bmatrix} =$$

$$\begin{bmatrix} \frac{\partial N_1}{\partial x} & 0 & \frac{\partial N_2}{\partial x} & 0 & \frac{\partial N_3}{\partial x} & 0 & \frac{\partial N_4}{\partial x} & 0 \\ 0 & \frac{\partial N_1}{\partial y} & 0 & \frac{\partial N_2}{\partial y} & 0 & \frac{\partial N_3}{\partial y} & 0 & \frac{\partial N_4}{\partial y} \\ \frac{\partial N_1}{\partial y} & \frac{\partial N_1}{\partial x} & \frac{\partial N_2}{\partial y} & \frac{\partial N_2}{\partial x} & \frac{\partial N_3}{\partial y} & \frac{\partial N_3}{\partial x} & \frac{\partial N_4}{\partial y} & \frac{\partial N_4}{\partial x} \end{bmatrix} \tag{2.37}$$

The matrix B contains the first derivatives of the interpolating functions expressed in terms of x and y, it means that the stiffness matrix for the case of plane stress can be evaluated through equation 2.38, where t represents the constant thickness of the element.

$$\mathrm{K} = \int \int B^T E B \; t \; dx \; dy \tag{2.38}$$

In addition to the stiffness matrix, the calculation of the mass matrix is very straight-forward, since it depends on the matrix of the shape functions expressed again in terms of the spatial coordinates, x and y. Since the thickness and the density of the element are assumed constant, they can be taken outside the integral.

$$\mathrm{M} = \int \int \rho \, S^T S \, t \, dx \, dy \qquad 2.39$$

One of the main advantages of this kind of element, is the very simple definition of its property, as a matter of fact the integration of the derivatives of the shape functions and the integration of the shape functions themselves can be obtained in a close form and do not require numerical integration. A specialized code was developed in Matlab Environment in order to obtain the mass and stiffness matrices of the element in a closed form, so that only the nodal coordinates, the thickness and the density of the plate are necessary in order to evaluate its mass and stiffness. The rectangular element is also implemented in SAMS/2000 in order to mesh the blade and perform the simulation.

2.1.4.1.1.1. 2D Plate element validation

Before running the simulation, it is necessary to verify that the analytical solution obtained through the Matlab code is correct. In order to achieve this goal, a numerical validation of the rectangular element has been performed using simple case of a constrained beam with a constant force applied to its free end. The validation model has been built in Ansys Environment using an equivalent element to the four nodes rectangular element, following also the same mesh, i.e. the discretization of the model in finite elements. A 10 m bar with 1 m height and 0.01 m constant thickness is considered and discretized with ten rectangular elements. The left end of the beam is constrained, imposing zero displacements to all its nodes, while a constant force of 100000 N is applied along the –y direction. All the data related to the beam are contained in the following table.

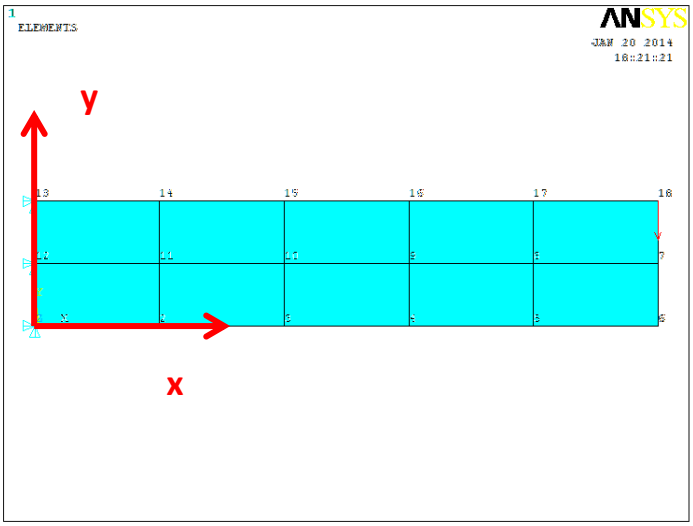

Figure 2.5 Constrained beam, validation model for 2D plate in Ansys.

TABLE I BEAM CHARACTERISTICS

BEAM CHARACTERISTICS		
Length	10	m
Height	1	m
Thickness	0,01	m
Density	8000	kg/m^3
Young Modulus	$2 \cdot 10^{11}$	Pa
Poisson's Ratio	0,25	
Force	100000	N

The deformed beam can now be plotted through Ansys using an automatic scale, i.e. a scale which is proportional to the real one. Obviously the greatest displacement is reached on the free end of the beam. The validation is concluded creating the same model in terms of physical characteristics and finite elements discretization in the SAMS/2000 code, performing a static analysis and comparing the results obtained by Ansys in terms of nodal displacements.

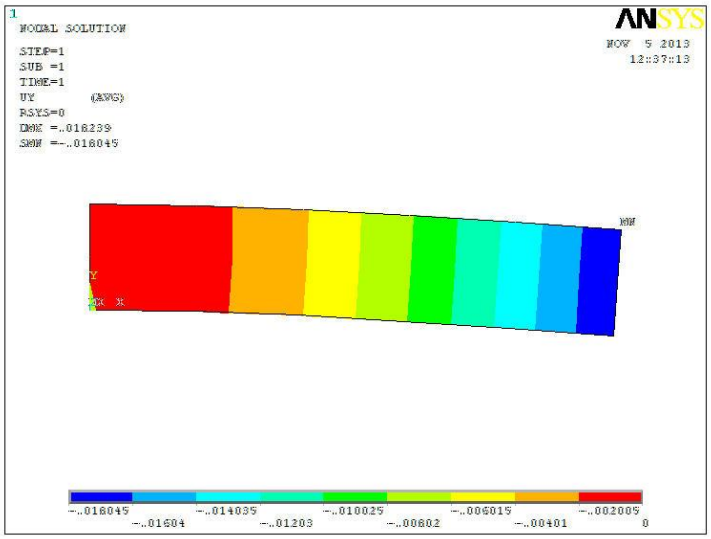

Figure 2.6 Nodal solution with Ansys.

TABLE II NODAL SOLUTION: COMPARISON BETWEEN ANSYS AND SAMS NODAL DISPLACEMENTS.

2D RECTANGULAR ELEMENT VALIDATION							
Nodal Deformation with Sams			Nodal Deformation with Ansys			Difference	
NODE	UX (m)	UY (m)	NODE	UX (m)	UY (m)	ε_x (m)	ε_y (m)
1	0,000000000	0,000000000	1	0,0000000000	0,0000000000	0,000000000	0,000000000
2	-0,000940735	-0,001098852	2	-0,0009392700	-0,0010987000	0,000001465	0,000000152
3	-0,001684642	-0,003829595	3	-0,0016834000	-0,0038299000	0,000001242	0,000000305
4	-0,002209444	-0,007846664	4	-0,0022133000	-0,0078465000	0,000003856	0,000000164
5	-0,002529120	-0,012707076	5	-0,0025285000	-0,0127110000	0,000000620	0,000003924
6	-0,002641019	-0,017994350	6	-0,0026269000	-0,0179670000	0,000014119	0,000027350
7	0,000003384	-0,017989894	7	-0,0000006211	-0,0179820000	0,000004005	0,000007894
8	0,000001246	-0,012694963	8	-0,0000036423	-0,0126960000	0,000004888	0,000001037
9	-0,000001319	-0,007819225	9	0,0000012094	-0,0078188000	0,000002528	0,000000425
10	-0,000000434	-0,003793785	10	-0,0000002606	-0,0037943000	0,000000173	0,000000515
11	0,000001052	-0,001029980	11	0,0000000331	-0,0010298000	0,000001019	0,000000180
12	0,000000000	0,000000000	12	0,0000000000	0,0000000000	0,000000000	0,000000000
13	0,000000000	0,000000000	13	0,0000000000	0,0000000000	0,000000000	0,000000000
14	0,000942720	-0,001098869	14	0,0009391800	-0,0010986000	0,000003540	0,000000269
15	0,001683794	-0,003828982	15	0,0016838000	-0,0038298000	0,000000006	0,000000818
16	0,002207066	-0,007846923	16	0,0022118000	-0,0078487000	0,000004734	0,000001777
17	0,002531658	-0,012707915	17	0,0025299000	-0,0126960000	0,000001758	0,000011915
18	0,002647690	-0,017994944	18	0,0026531000	-0,0180450000	0,000005410	0,000050056

Looking at TABLE II it is possible to see that the difference between the two sets of results is very small and it is probably due to the differences in the numerical methods used to compute the results.

2.1.4.1.2. Three nodes triangular element

The meshing of a body with some corners or complex shape can be difficult using the rectangular element. This is the reason why a new kind of 2D finite element is also considered in this analysis; a 2D three nodes triangular element is implemented in SAMS/2000 program. The formulation of this kind of element is very similar to the one used for the 2D plate, with the only difference that the triangular element has lower number of nodes, three, and obviously different interpolating functions. As in the case of rectangular element, each node has two degrees of freedom, translations along the x-axis and y-axis.

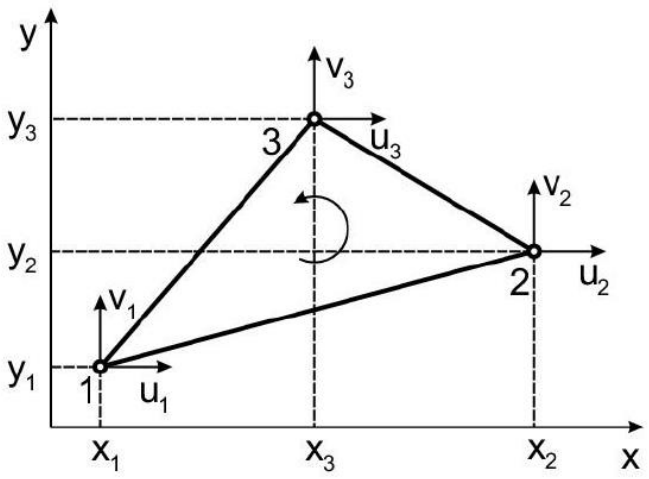

Figure 2.7 Linear Triangular element. Reprinted from Moharos István, Oldal István, Szekrényes András. *Finite element methode*. Budapest: Typotex Publishing House, 2012.

Also in this 2D case the thickness and the density of the element are taken constant. The interpolating functions used to describe the position of a generic point inside the element are considered linear and dependent. If we consider a point moving inside the triangle, its displacement will be a function of the three nodal points as shown in Figure 2.8. The three areas created by the point will be related in the following way:

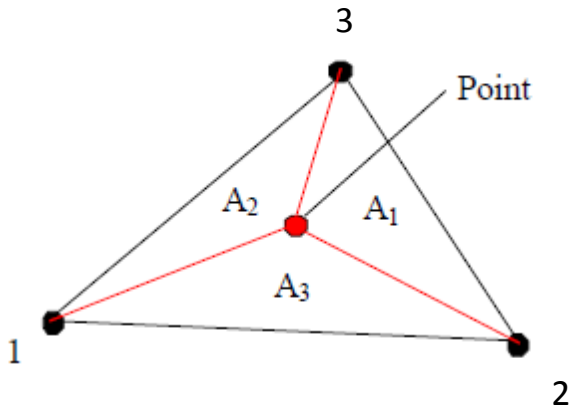

Figure 2.8 Triangular element interpolating functions.

$$\frac{A_1}{A}+\frac{A_2}{A}+\frac{A_3}{A}=1 \qquad 2.40$$

$$\begin{cases} N_1=\frac{A_1}{A} \\ N_2=\frac{A_2}{A} \\ N_3=\frac{A_3}{A} \end{cases} \qquad 2.41$$

According to this shape functions, the displacement of a generic point inside the element can be evaluated in this way:

$$\begin{cases} x = N_1 x_1 + N_2 x_2 + N_3 x_3 \\ y = N_1 y_1 + N_2 y_2 + N_3 y_3 \end{cases} \quad 2.42$$

$$\begin{cases} N_1 = \mathcal{Z} \\ N_2 = \eta \\ N_3 = 1 - \mathcal{Z} - \eta \end{cases} \quad 2.43$$

With $\mathcal{Z}$ and η, natural coordinates, i.e. dimensionless coordinates ranging between 0 and 1. Once of the shape functions are defined, it is necessary to compose the matrix of the shape functions can be developed and used to evaluate the stiffness and mass matrices. The differential operator used in this case is the same adopted for the 2D plate. Below is a summary of the equations used.

$$\mathrm{S} = \begin{bmatrix} N_1 & 0 & N_2 & 0 & N_3 & 0 \\ 0 & N_1 & 0 & N_2 & 0 & N_3 \end{bmatrix} \quad 2.44$$

$$\mathrm{B} = \mathrm{DS} = \begin{bmatrix} \frac{\partial}{\partial x} & 0 \\ 0 & \frac{\partial}{\partial y} \\ \frac{\partial}{\partial y} & \frac{\partial}{\partial x} \end{bmatrix} \begin{bmatrix} N_1 & 0 & N_2 & 0 & N_3 & 0 \\ 0 & N_1 & 0 & N_2 & 0 & N_3 \end{bmatrix} \quad 2.45$$

The equations for u and v are expressed in terms of η and $\mathcal{Z}$. Chain rule of differentiation can be used to evaluate the derivatives with respect to the natural coordinates as

$$\begin{cases}\frac{\partial u}{\partial \xi}=\frac{\partial u}{\partial x}\frac{\partial x}{\partial \xi}+\frac{\partial u}{\partial y}\frac{\partial y}{\partial \xi}\\ \frac{\partial u}{\partial \eta}=\frac{\partial u}{\partial x}\frac{\partial x}{\partial \eta}+\frac{\partial u}{\partial y}\frac{\partial y}{\partial \eta}\end{cases} \quad 2.46$$

Or written in a matrix form:

$$\begin{bmatrix}\frac{\partial u}{\partial x}\\ \frac{\partial u}{\partial y}\end{bmatrix}=\begin{bmatrix}\frac{\partial x}{\partial \xi} & \frac{\partial y}{\partial \xi}\\ \frac{\partial x}{\partial \eta} & \frac{\partial y}{\partial \eta}\end{bmatrix}^{-1}\begin{bmatrix}\frac{\partial u}{\partial \xi}\\ \frac{\partial u}{\partial \eta}\end{bmatrix} \quad 2.47$$

Substituting equation 2.43 into equation 2.42 it is possible to evaluate the partial derivatives with respect to the natural coordinates. Note that:

$$\begin{cases}x=(x_1-x_3)\xi+(x_2-x_3)\eta+x_3\\ y=(y_1-y_3)\xi+(y_2-y_3)\eta+y_3\end{cases} \quad 2.48$$

according to which:

$$\begin{cases}\frac{\partial x}{\partial \xi}=x_1-x_3\\ \frac{\partial x}{\partial \eta}=x_2-x_3\\ \frac{\partial y}{\partial \xi}=y_1-y_3\\ \frac{\partial y}{\partial \eta}=y_2-y_3\end{cases} \quad indicating\ with \begin{cases}x_{ij}=x_i-x_j\\ y_{ij}=y_i-y_j\end{cases} \quad 2.49$$

The 2x2 matrix of equation 2.47 is also known as the Jacobian matrix whose determinant is twice the area of the triangle according to equation 2.50. Substituting equation 2.49 and 2.50 into equation 2.47, one can show:

$$Area = \frac{1}{2}|\det(J)| \tag{2.50}$$

$$\begin{bmatrix} \frac{\partial u}{\partial x} \\ \frac{\partial u}{\partial y} \end{bmatrix} = \begin{bmatrix} x_{13} & y_{13} \\ x_{23} & y_{23} \end{bmatrix}^{-1} \begin{bmatrix} \frac{\partial u}{\partial \xi} \\ \frac{\partial u}{\partial \eta} \end{bmatrix} \tag{2.51}$$

$$\begin{bmatrix} \frac{\partial u}{\partial x} \\ \frac{\partial u}{\partial y} \end{bmatrix} = \frac{1}{\det(J)} \begin{bmatrix} y_{23} & -y_{13} \\ -x_{23} & x_{13} \end{bmatrix}^{-1} \begin{bmatrix} \frac{\partial u}{\partial \xi} \\ \frac{\partial u}{\partial \eta} \end{bmatrix} \tag{2.52}$$

After some mathematical derivations, and differentiating the matrix of the shape function S, the matrix B of equation 2.53 can be written as:

$$\mathrm{B} = \frac{1}{\det(J)} \begin{bmatrix} y_{23} & 0 & y_{31} & 0 & y_{12} & 0 \\ 0 & x_{32} & 0 & x_{13} & 0 & x_{21} \\ x_{32} & y_{23} & x_{13} & y_{31} & x_{21} & y_{12} \end{bmatrix} \tag{2.53}$$

Finally the stiffness matrix of the triangle will be obtained without integration since the matrices depends only on the coordinates of the triangle. As already explained, the thickness t of the element is assumed constant.

$$\mathrm{K} = \mathrm{Area} \cdot t \cdot B^T C B = \frac{\det(J)}{2} \cdot t \cdot B^T C B \qquad 2.54$$

Once the stiffness matrix of the element has been defined, it is necessary to compute its mass matrix. The formulation of the mass matrix is similar to the one of the 2D plate with the only difference due to the fact that the matrix is obtained by integrating with respect to the natural coordinates.

$$\mathrm{M} = \int_0^1 \int_0^1 \rho \, \mathrm{t} \det(\mathrm{J}) \; S^T \, \mathrm{S} \, d\eta \, d\zeta \qquad 2.55$$

2.1.4.1.2.1. Triangular element validation

Following the same procedure adopted for the 2D plate element, also the triangular element requires a numerical validation in order to check the implementation in the program SAMS/2000. The simple model of a constrained beam is built first in Ansys environment applying to its free end a vertical force along –y, and then in SAMS/2000. The same discretization is adopted in the two models in order to directly compare the nodal displacements.

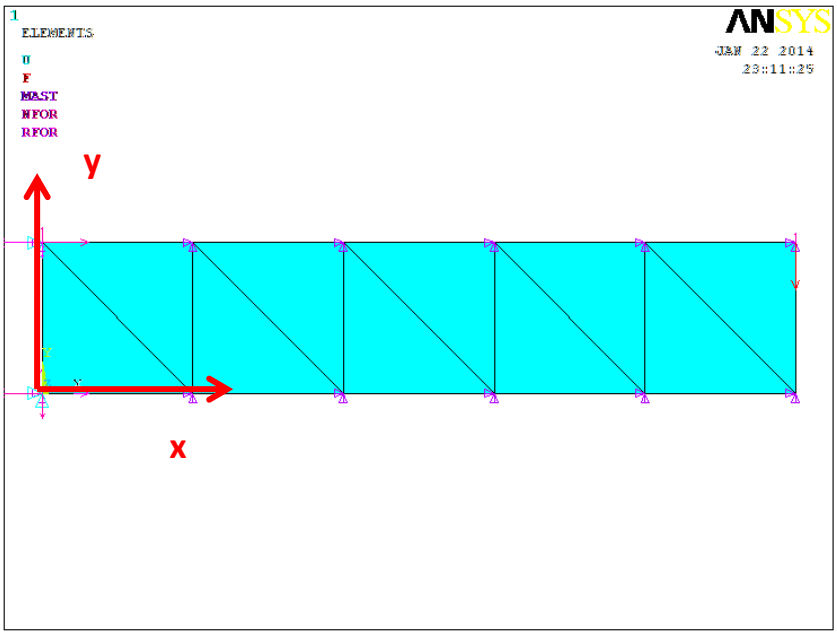

Figure 2.9 Beam discretization with triangular elements

The 5 m beam is discretized in 10 elements and constrained at its left end putting to zero all the displacements of the nodes. Finally a constant force of 10000 N is applied at

its free end. The same model is built in SAMS/2000 following the same discretization used in Ansys in order to allow a fast comparison of the nodal displacements. All the beam data are presented in TABLE III while the representation of the nodal displacement along y in Ansys environment is shown in Figure 2.10.

TABLE III BEAM CHARACTERISTICS.

BEAM CHARACTERISTICS		
Lenght	5	m
Height	1	m
Thickness	0,1	m
Density	7730	kg/m^3
Young Modulus	$2{,}2 \cdot 10^{11}$	Pa
Poisson's Ratio	0,3	
Force	10000	N

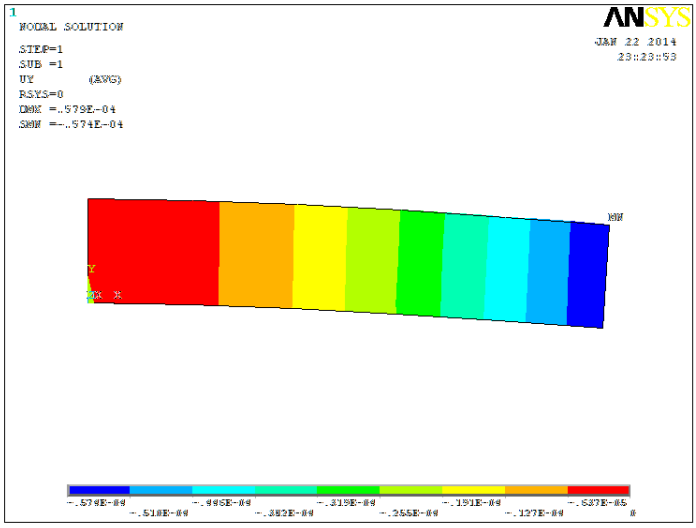

Figure 2.10 Nodal displacement of the beam along the y-axis.

Finally the validation is completed once the results obtained in SAMS/2000 are in good agreement with the results obtained from Ansys. The following table shows the results obtained from both programs.

TABLE IV COMPARISON BETWEEN ANSYS AND SAMS/2000 RESULTS

TRIANGULAR ELEMENT VALIDATION							
Nodal Deformation with Sams			Nodal Deformation with Ansys			Difference	
NODE	UX (m)	UY (m)	NODE	UX (m)	UY (m)	ε_x	ε_y
1	0,000000000	0,000000000	1	0,0000000000	0,0000000000	0,000000000	0,000000000
2	-0,000002744	-0,000003995	2	-0,0000027768	-0,0000038845	0,000000033	0,000000110
3	-0,000004816	-0,000012784	3	-0,0000048587	-0,0000128260	0,000000043	0,000000042
4	-0,000006366	-0,000025330	4	-0,0000063251	-0,0000254500	-0,000000041	0,000000120
5	-0,000007200	-0,000040710	5	-0,0000071798	-0,0000405220	-0,000000020	0,000000188
6	-0,000007351	-0,000056700	6	-0,0000074537	-0,0000567220	0,000000102	0,000000022
7	0,000007921	-0,000056805	7	0,0000081765	-0,0000573670	-0,000000255	0,000000562
8	0,000007653	-0,000040982	8	0,0000076394	-0,0000407550	0,000000014	0,000000227
9	0,000006680	-0,000025576	9	0,0000066491	-0,0000256690	0,000000031	0,000000093
10	0,000005038	-0,000012964	10	0,0000050513	-0,0000130450	-0,000000013	0,000000081
11	0,000002852	-0,000004207	11	0,0000028403	-0,0000040962	0,000000011	0,000000111
12	0,000000000	0,000000000	12	0,0000000000	0,0000000000	0,000000000	0,000000000

As we can see from TABLE IV, the results of nodal displacement of the two different solutions are in good agreement; the small differences between the two solutions can be attributed to the differences between the numerical procedures used in the two computer programs.

2.1.4.1.3. Discretization with 2D plates element

The first analysis of the turbine blade model is performed through a discretization consisting only of 2D rectangular elements, with the only exception that the two corners at the blade base, are with two triangular elements.

The main aim of the planar analysis is to simulate the rotation of the blade fixed on a rotor modeled as a rigid body and rotating at a constant angular velocity. In all the analysis performed in SAMS/2000 the angular velocity is assumed to be constant and equal to 300 rad/s simulating 10 s of rotation.

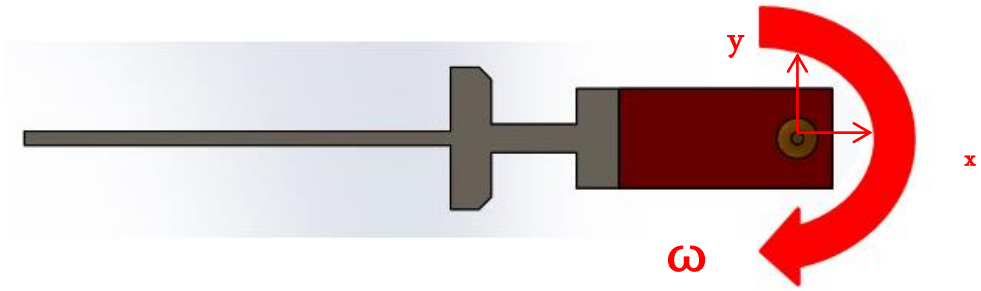

Figure 2.11 Planar model

The first step of the analysis consists of the model discretization into rectangular elements using the Ansys environment. The mesh is built manually in order to maintain a certain size of each element. The element chosen in Ansys to represent the 2D plate or the 2D triangular element is the plane182 with 4 nodes and 2 degrees of freedom per node.

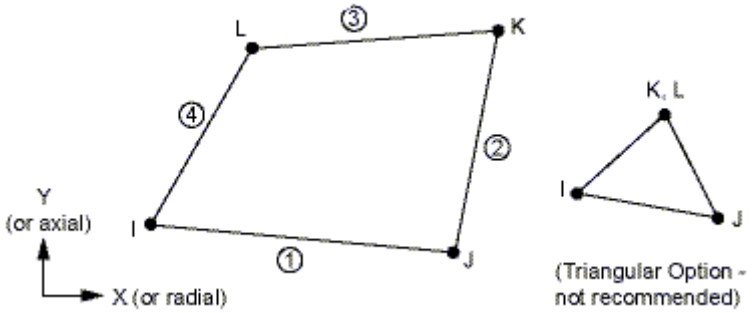

Figure 2.12 Plane182 Ansys Element. Reprinted from Ansys 14.0 Help (2011), *Plane182 element.*

The first weakness of this kind of model is that the rectangular element, does not allow the discretization of very complex models because of its geometry. An additional proof of this weakness was shown by the program itself which was not able to directly mesh the model in a mapped way. As already expected, the two corners at the blade base require the use of two triangular elements to represent their shapes. Once the mesh has been built in Ansys, the lists of node coordinates and the elements connectivity are introduced in SAMS/2000 to rebuild the flexible body model.

SAMS/2000 allows for using finite elements that have different properties, i.e. it is necessary to specify the density ρ, the Young's Modulus E, the tangential elastic Modulus G and finally the nodal masses m_n. The nodal mass consists of the mass of the single node, taking into account the portion of the mass of each element which contains that node. The nodal mass of the single element is evaluated as the element volume multiplied by its density and divided by the number of nodes. Since a node of the deformable body ca be shared by different elements, the nodal mass will be the sum of the contribution of the elements sharing this node. The thickness of the elements is considered constant and equal to the blade's thickness. The effect of gravity is taken into account using the values of the nodal masses. Figure 2.13 shows the blade discretization with 2D plates.

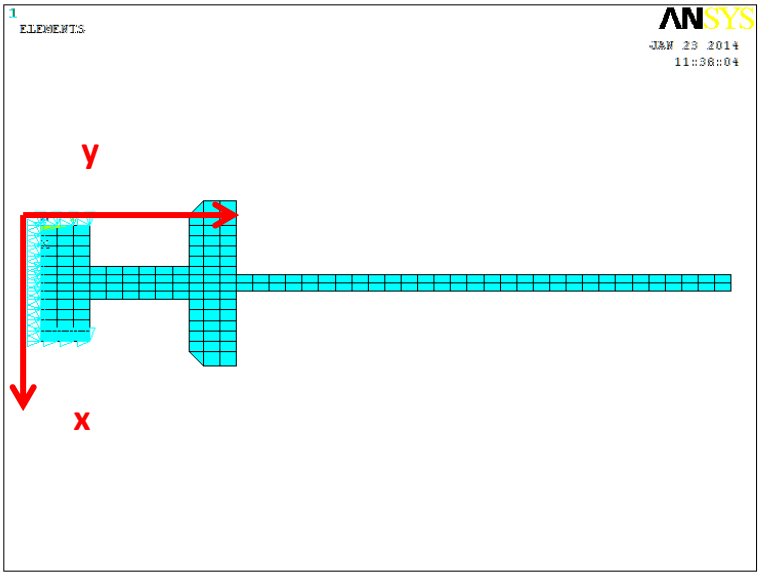

Figure 2.13 Blade discretization with 2D plates

As we can see from the figure, the model consists of 168 elements, 166 plates and 2 triangles used to approximate the corners. The blade is constrained at its base to the rigid rotor putting to 0 all the degrees of freedom of the selected nodes. Since each element has 4 nodes, the system has 233 nodes.

After the discretization of the model in Ansys, the lists of nodes and connectivity between elements are exported to SAMS/2000 to define the mesh of the deformable body. The turbine blade has been considered as one of the three bodies forming the multibody system: the ground which is fully constrained, the rotor, which is assumed to be a rigid block with a certain mass and moments of inertia, and finally the blade which is the deformable body, which is the only one to have elastic coordinates. After constraining the base of the blade to the rotor, a constant angular velocity is applied to the rotor and the numerical simulation of a 10 s rotation is performed; each simulation requires the specification of a certain error, a time step, and convergence criteria.

Once the simulation is completed, all the information related to the nodal displacement of each node along x and y direction at a certain time step obained. The main aim of the simulation is to identify how the blade deforms when it rotates at a certain angular velocity; it is clear that the displacement of the nodes on the top of the airfoil is bigger than the one of the nodes at the root of the blade. Consider 2 nodes of the blade:

- One node on the top of the airfoil, node 10.
- One node on the middle of the airfoil, node 165.

Different sets of nodes can be chosen depending on the region of interest. Figure 2.14 shows the locations of the selected nodes on the blade model.

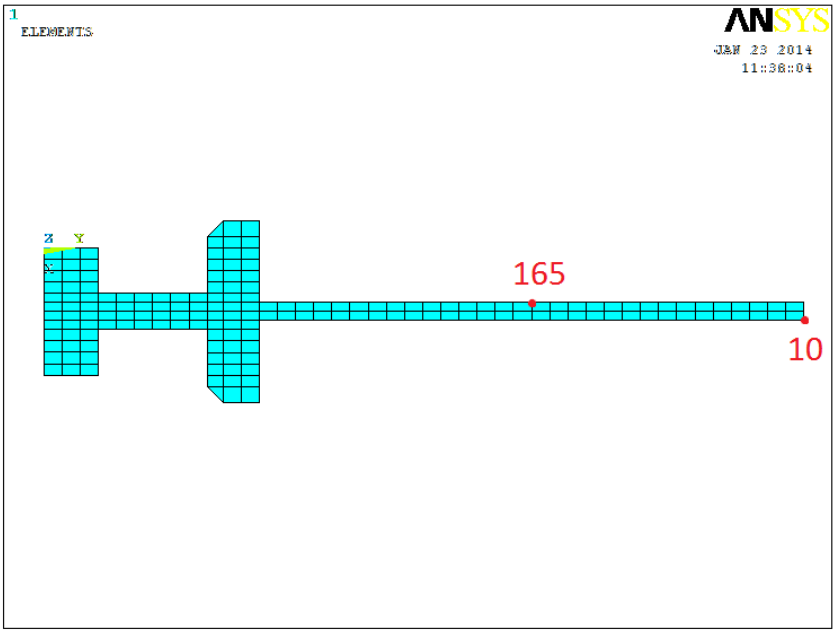

Figure 2.14 Nodes location, Ansys.

Once the nodes have been selected, a Matlab script can be developed to read the data from the nodal displacement file produced by SAMS/2000 in order to plot the displacement of the node of interest. The script will be shown in the appendix. Starting from

the first set of nodes located on the airfoil, it is possible to see how the displacement increases from the bottom to the top of the airfoil. The nodal displacement has been plotted with respect to the x-axis and y-axis respectively.

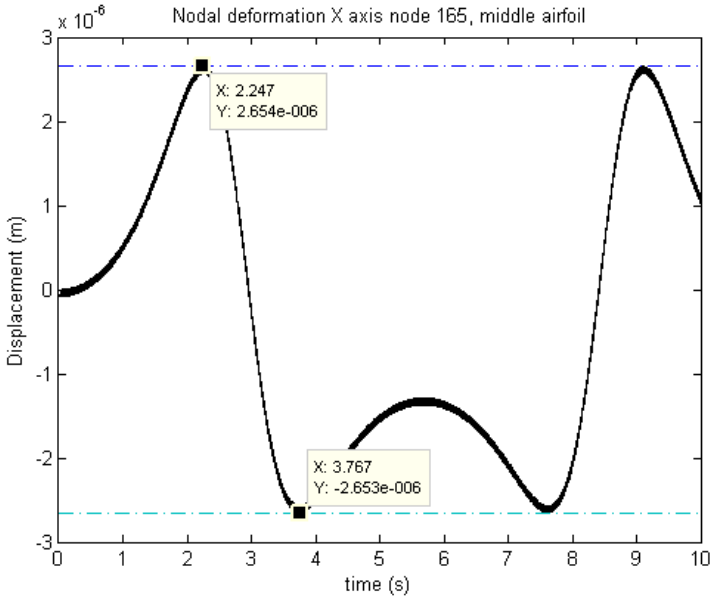

Figure 2.15 Nodal displacement node 165, middle of the airfoil, Matlab.

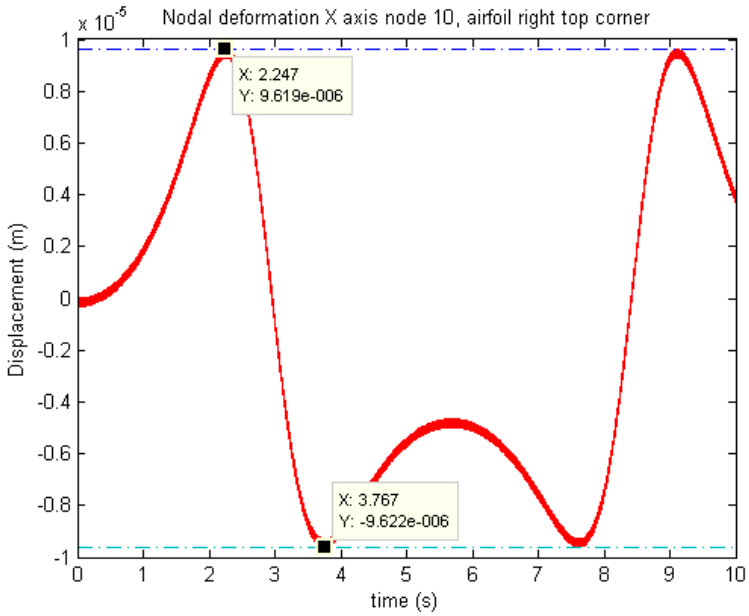

Figure 2.16 Nodal displacement node 10, top of the airfoil, Matlab.

It is now possible to plot the y-axis displacements of the same nodes; in this particular case of study, the x-axis displacement is more interesting since it represents the motion of the blade one next to the other.

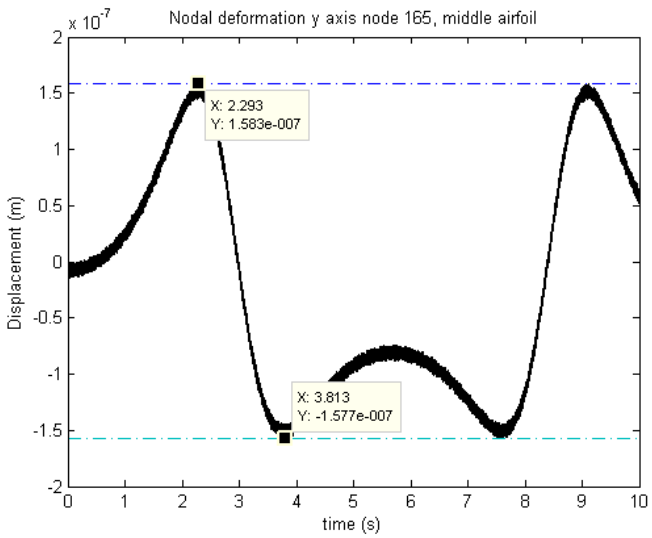

Figure 2.17 Nodal displacement node 165, top of the airfoil, Matlab.

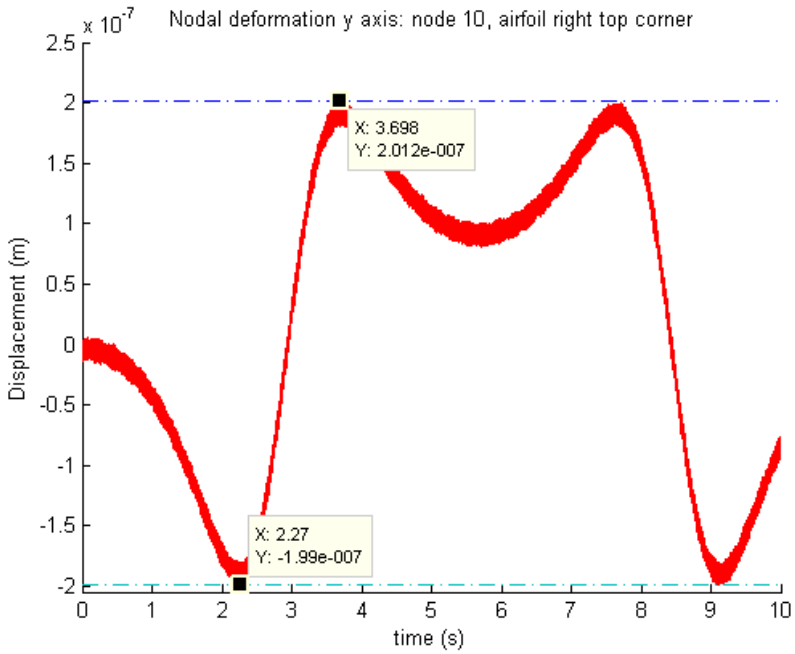

Figure 2.18 Nodal displacement node 10, top of the airfoil, Matlab.

As it is possible to see from the plots, it is evident that magnitude of the nodal displacement reduces moving from the top of the blade to the bottom, since the structure becomes stiffer. The base of the airfoil and the root are characterized by very small displacements and this is the reason why they are not considered in this analysis. The movement of the lower part of the blade is associated with only the higher frequency of the structure, and consequently the higher modes.

2.1.4.1.4. Discretization with triangular elements

While the mesh developed using rectangular elements only allows for simple discretization of the model, it can lead to some problems since the rectangular shape of the elements cannot describe easily more complex geometry.

This is the main reason for developing a triangular element which will be very useful in many cases where the shape of the model is characterized by a very large amount of geometric discontinuities. The procedure followed in this analysis is essentially the same as the one adopted for the 2D case with plate element. The first step consists in a model discretization made in Ansys environment using Plane182 element shown in Figure 2.12, exporting the list of nodes, and the element connectivity. In this case since it not possible to identify a base and a height for each triangle, the SAMS/2000 input has been compiled in order to evaluate the triangle area from its nodal positions. Again, the thickness (constant) has been specified for each element as well as Young's Modulus E, density ρ and Modulus of rigidity G. An example of Presams file used to build the deformable body model for the turbine blade is shown in Figure 2.19, Figure 2.20 and Figure 2.21.

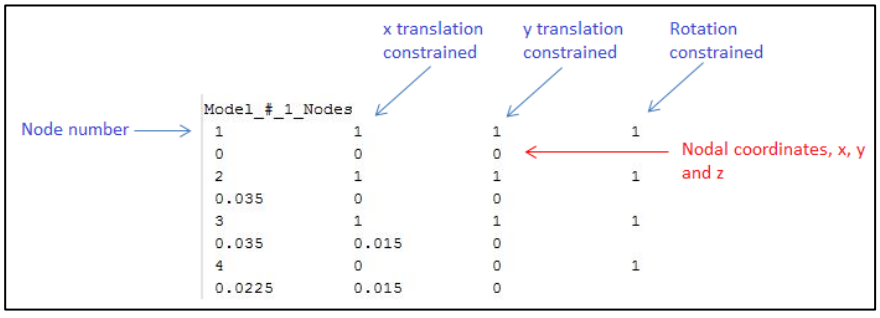

Figure 2.19 Example of Presams file: deformable body model, node list.

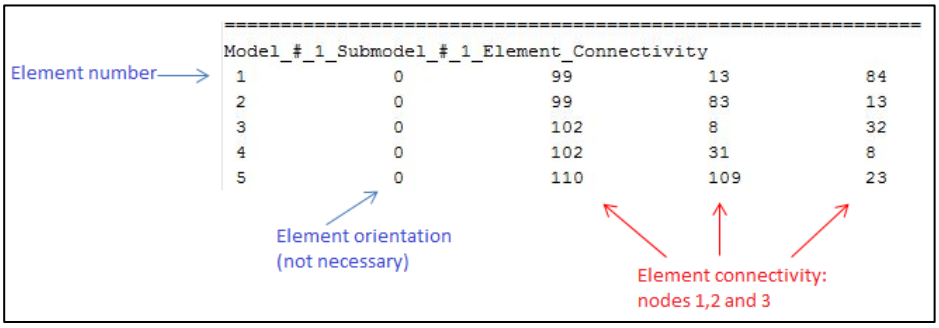

Figure 2.20 Example of Presams file: deformable body model, element connectivity.

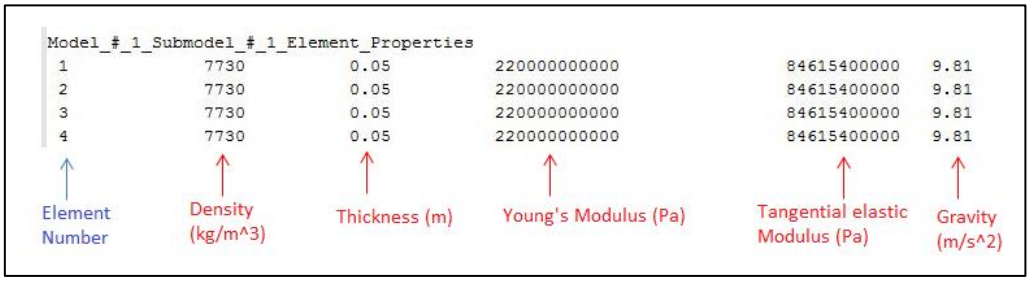

Figure 2.21 Example of Presams file: deformable body model, element properties.

The turbine blade is discretized with triangular elements as shown in Figure 2.22, it is clear how the mesh generation has less geometric restrictions as compared to the rectangular element. In addition to this, higher accuracy can be obtained reducing the size of each triangle at the expense of a higher number of elements and heavier calculations.

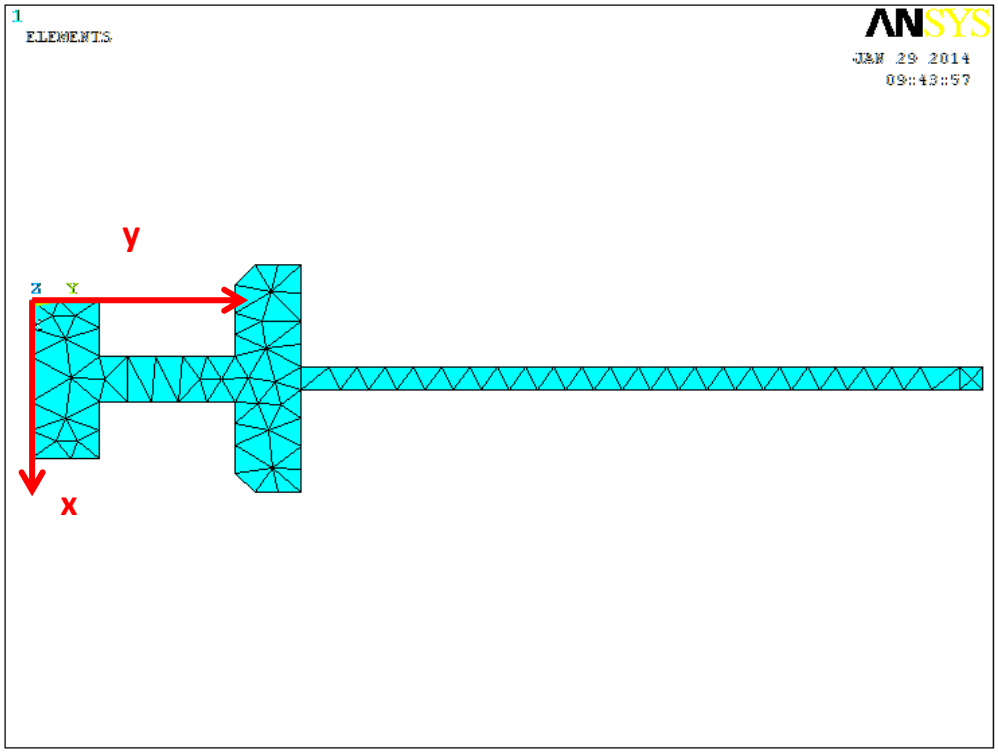

Figure 2.22 Blade discretization with 2D triangular elements.

As in the case of the 2D plate, it is possible to plot the nodal displacement of a selected set of nodes. For the sake of simplicity, the new set of nodes will be taken as similar as possible to the one of the preceding example. Despite its simplicity, the 2D triangular element results are less accurate than the results of the preceding element and the structure appears to be stiffer, this is the reason also why Ansys suggests replacing this element with a more accurate 6 nodes triangular element or equivalently reducing as much as possible the element dimension. The discretization shown in Figure 2.22 employs by 112 elements.

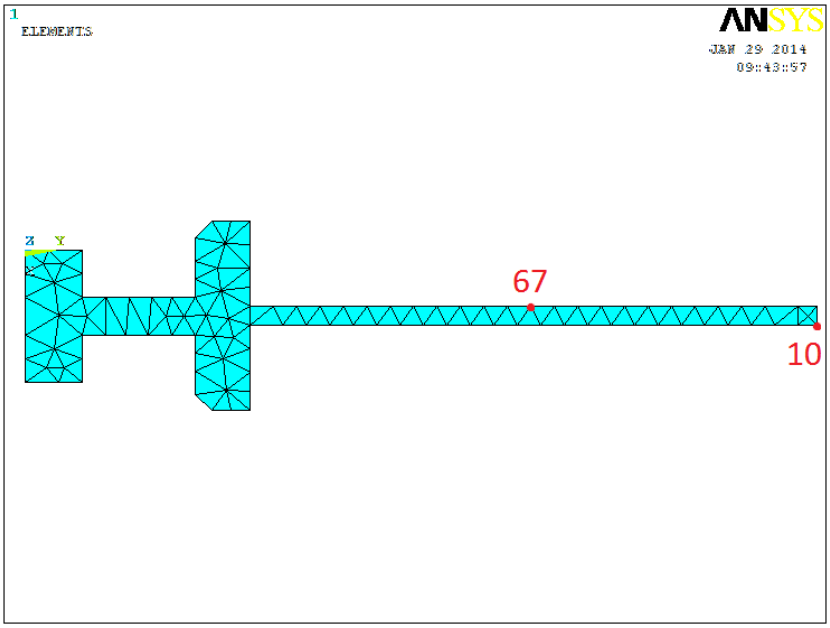

Figure 2.23 Node location, Ansys.

Since the behavior of the nodal displacement is the same as the previous case, for the sake of simplicity and in order to demonstrate the weakness of the 3 nodes triangular element discretization, the results will be shown by plotting the nodal displacement of each node compared with the equivalent case of the 2D plate discretization. In order to run the simulation the blade is constrained at its base as shown in Figure 2.13. The black curve refers to the 2D plate case, while the red one refers to the triangular element case for the x-axis displacements, blue and green will be used for the y-axis displacement. Starting from the x-axis displacement of the top of the airfoil, it is possible to get the following results:

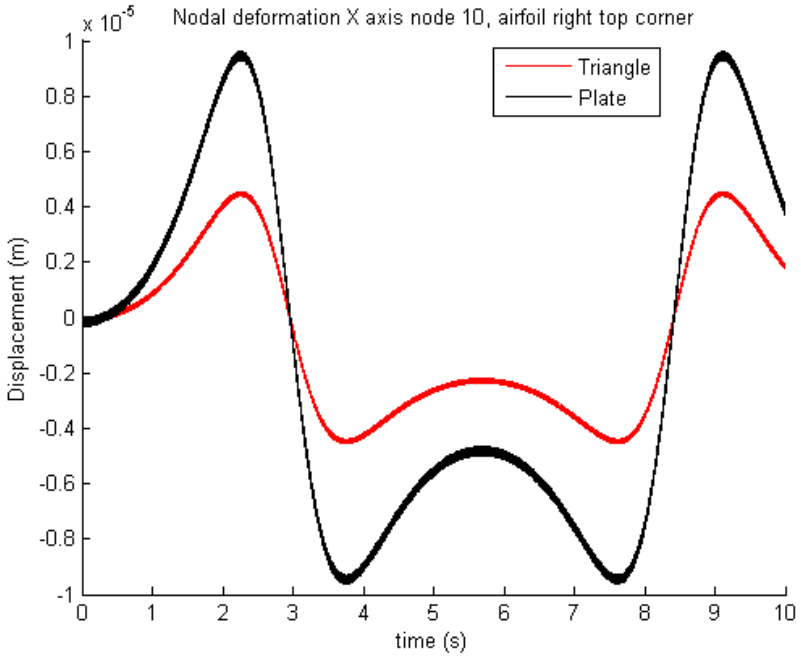

Figure 2.24 Comparison nodal displacement with 2D plate and 2D triangle discretization, top of the airfoil.

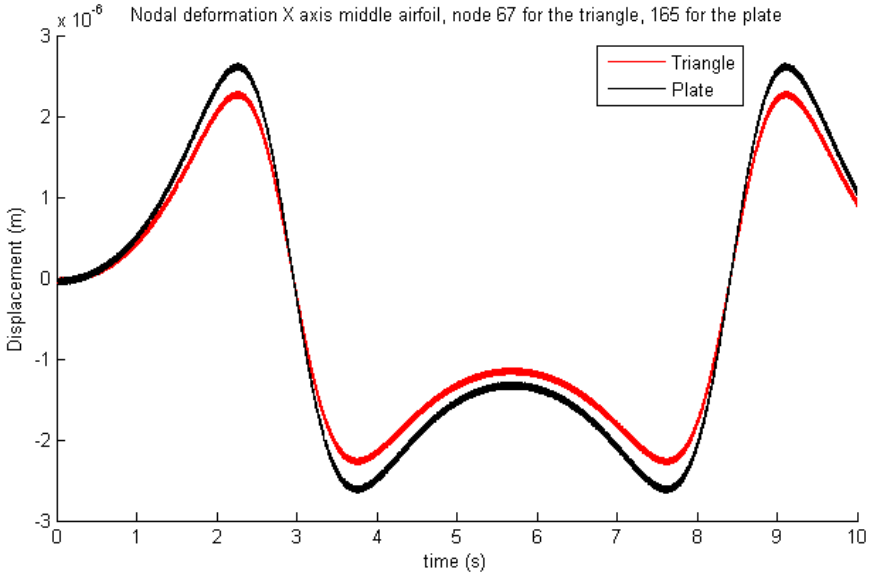

Figure 2.25 Comparison nodal displacement with 2D plate and 2D triangle discretization, middle airfoil.

The same nodal displacements can be plotted for the y-axis.

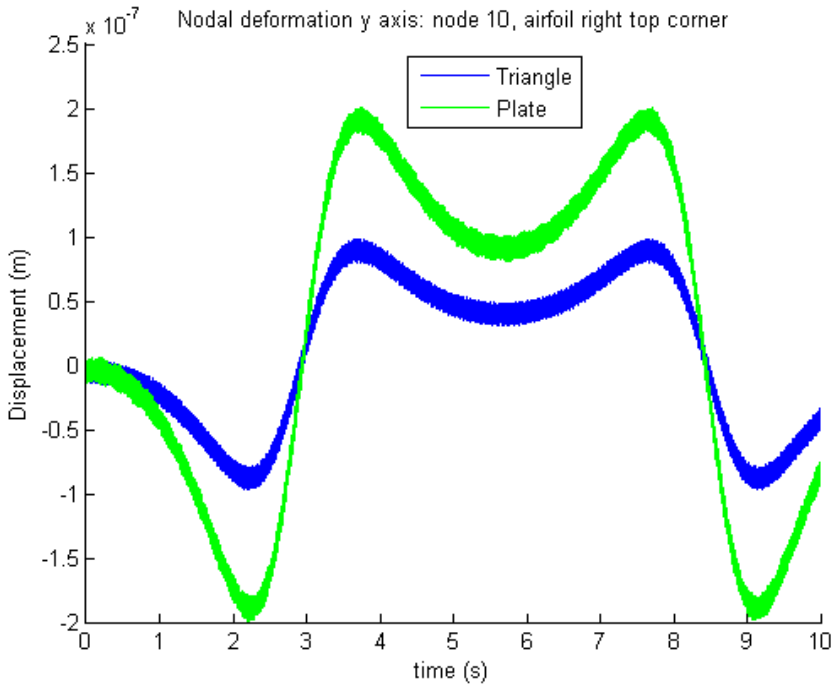

Figure 2.26 Comparison nodal displacement with 2D plate and 2D triangle discretization, top of the airfoil.

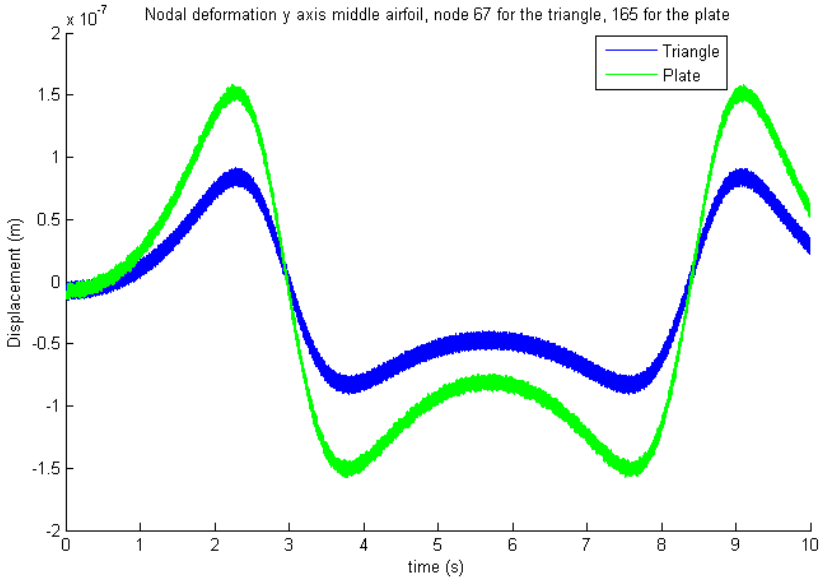

Figure 2.27 Comparison nodal displacement with 2D plate and 2D triangle discretization, middle of the airfoil.

Despite of the simplicity of programming and the high adaptability to most of the geometries, the preceding figures show that the triangular element is less accurate than the rectangular element due to its lower number of nodes. The higher stiffness of the element requires a finer mesh in order to capture the nodal displacements in a more accurate way. This is the main reason why this kind of element is usually replaced by a more complex 6 nodes triangular element. The differences in the results can also be caused by the different discretization adopted in the models.

2.1.4.2. 3D Analysis

For the sake of simplicity, the turbine blade model was assumed to have a planar rotation since the blade thickness is constant and the blade rotates in the xy plane at a specified angular velocity. But in realty, the blade represents a solid and deformable body and this is the reason why a solid element model of the turbine blade is considered in the analysis presented in this thesis. As previously mentioned, the formulation of the 3D solid element was already implemented in SAMS/2000. The element considered is a simple 8 nodes hexahedron. The definition of the solid element model is very similar to the one used for the simpler planar case with the only difference of an higher number of nodes and consequently degrees of freedom. A brief introduction to the eight nodes hexahedral element will be given in this chapter because the element was already present in the program and it requires neither a formulation nor an experimental validation.

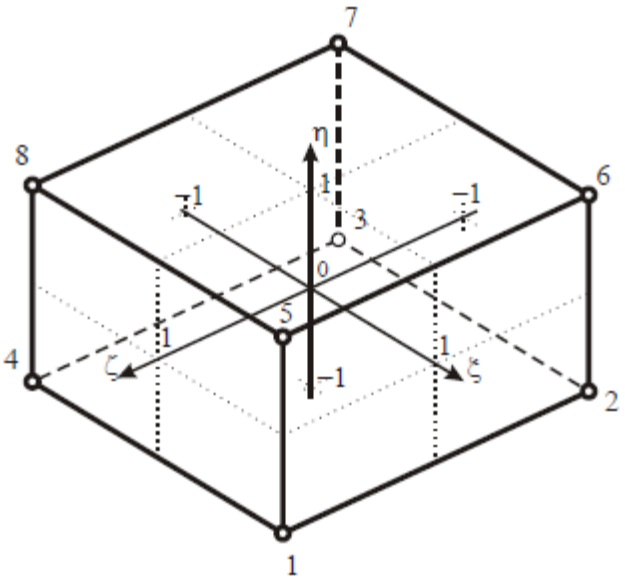

Figure 2.28 8 nodes Hexahedral element.

An analytical formulation of the solid elements in natural coordinate is possible, however SAMS 2000 employs real coordinates, that means that the shape of the element cannot be distorted. This is the reason why this 3D analysis becomes very similar to the first case of discretization of the turbine blade with 2D plates; since the element shape is rectangular it is not possible to approximate the two corners where the blade comes in contact with the damper. For this reasons, the two corners are avoided in order to allow the model discretization with these solid elements. The 8 nodes hexahedral element has three degrees of freedom per node, a translation along the x-axis, a translation along the y-axis and finally a translation along the z-axis. Eight different shape functions will be considered in order to approximate the shape of the element after its deformation and the shape function matrix will be 3x24. The procedure for formulating the stiffness and mass matrix is the same as the one used for the 2D plate element with the only difference of the higher number of nodes and one more degree of freedom per node. The basic equations are provided below:

$$\mathrm{S} = \begin{bmatrix} N_1 & 0 & 0 & N_2 & 0 & 0 & \cdots & N_n & 0 & 0 \\ 0 & N_1 & 0 & 0 & N_2 & 0 & \cdots & 0 & N_n & 0 \\ 0 & 0 & N_1 & 0 & 0 & N_2 & \cdots & 0 & 0 & N_n \end{bmatrix} \quad n = 1,2,3..,8 \qquad 2.56$$

$$\mathrm{K} = \int B^T C B \, dV \qquad 2.57$$

$$\mathrm{M} = \int S^T S \, dV \qquad 2.58$$

2.1.4.2.1. Discretization with 8 nodes hexahedral

The main procedure used to discretize the turbine model with 8 nodes hexahedral solid elements is essentially the same as the one used with 2D plates elements. The model discretization has been performed in Ansys environment with an equivalent solid element with 8 nodes and 3 degrees of freedom per node. As already anticipated before, the similarities with the 2D plate element are many since that hexahedron can be considered as a plate element with a certain thickness. However the use of a solid model is closer to the real case, the weakness of this kind of element arises during the mesh generation. Since the shape of the element cannot be changed, a mapped mesh of the model is mandatory. The element used in Ansys is the Solid45 as shown in Figure 2.29.

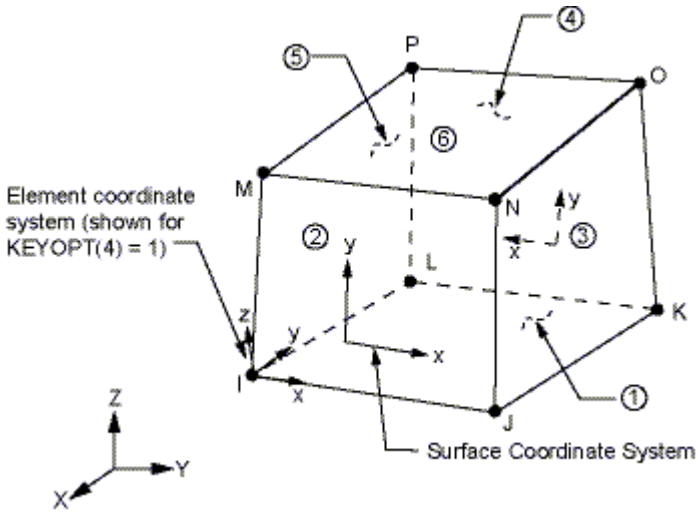

Figure 2.29 Solid45 Ansys Element. Reprinted from Ansys 14.0 Help (2011), *Solid45 element.*

As already discussed, the two corners in the real geometry must be avoided. Once the mesh is generated, the list of nodes and element connectivity is exported from Ansys to SAMS/2000 in order to generate the deformable body model. Since SAMS/2000 allows a maximum number of elements the mapped mesh is created by dividing the blade into 4 elements along the thickness, for a total of 196 elements.

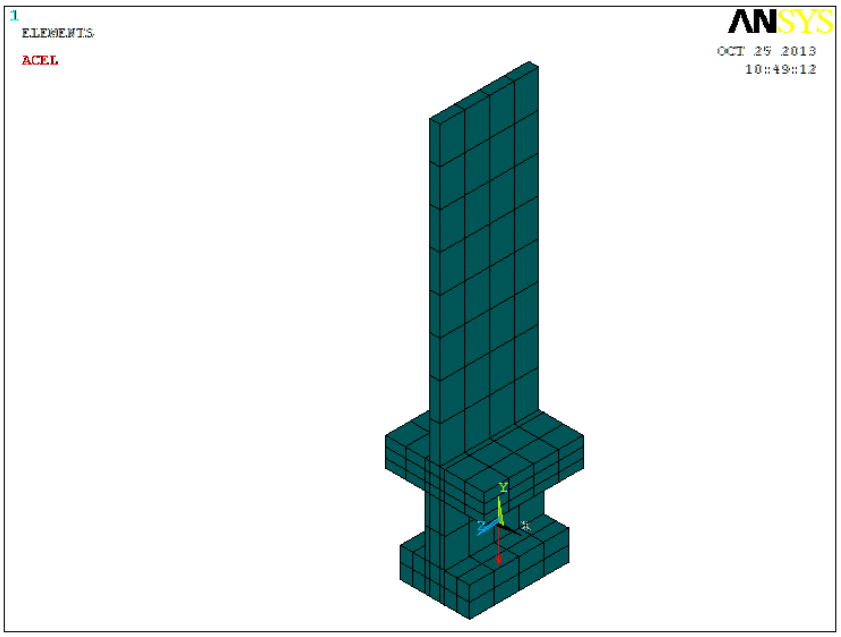

Figure 2.30 3D Solid Model: mesh generation in Ansys.

The nodal coordinates and the element connectivity have been used to recreate the 3D blade model in SAMS/2000 in order to simulate the rotation of the blade about a fixed axis at a given angular velocity of 300 rad/s for 10 s as in the planar case. The rotor is considered as a rigid body. All the information necessary to build the blade solid model are contained in the Presams file, which is very similar to the one introduced for the planar analysis.

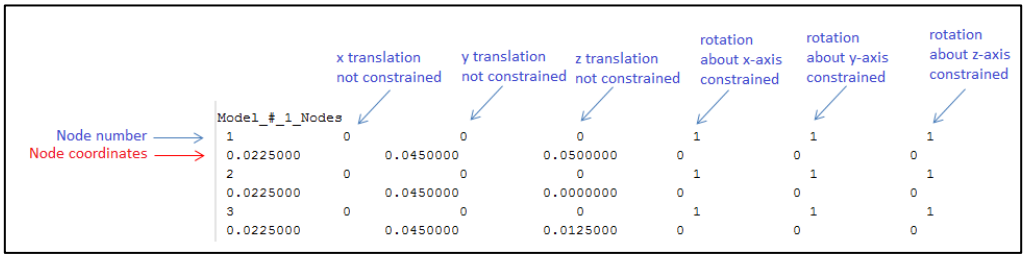

Figure 2.31 Example of Presams file: deformable 3D body model, node list.

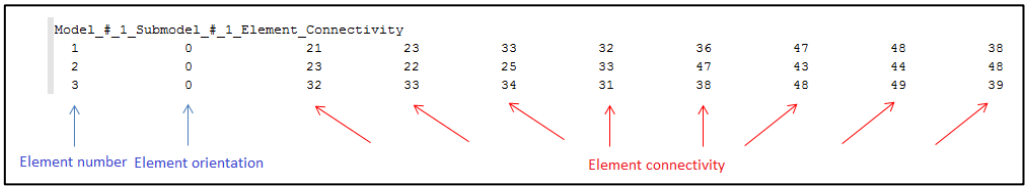

Figure 2.32 Example of Presams file: deformable 3D body model, element connectivity.

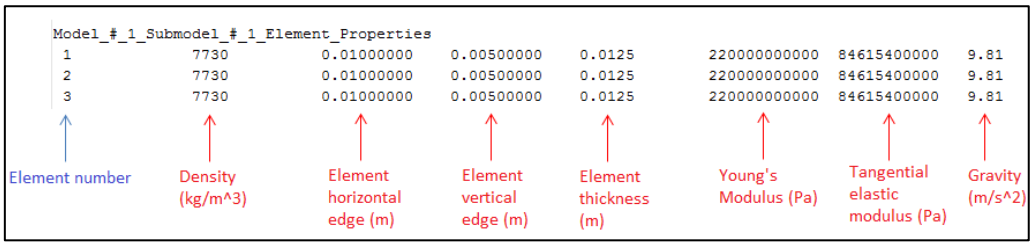

Figure 2.33 Example of Presams file: deformable 3D body model, element properties.

The same nodes used in the previous analysis will be taken into account during the simulations. It is expected that the 3D model , despite its higher complexity enables to get more accurate results since it is not represent a simplification of the model. In addition it is necessary to specify that no damping has been introduced in the model definition with the consequence of a noisy signal plotting the nodal displacement of the middle airfoil. However the solid model represents a more accurate way to investigate the dynamic be

havior of the blade, the weakness of this model consists in the higher cost in terms of computation that forced to reduce as much as possible the number of elements with the consequence of a very coarse mesh. A refinement of the analysis could be performed by the application of a finer discretization in order to catch in a more precise way the displacement of the selected nodes.

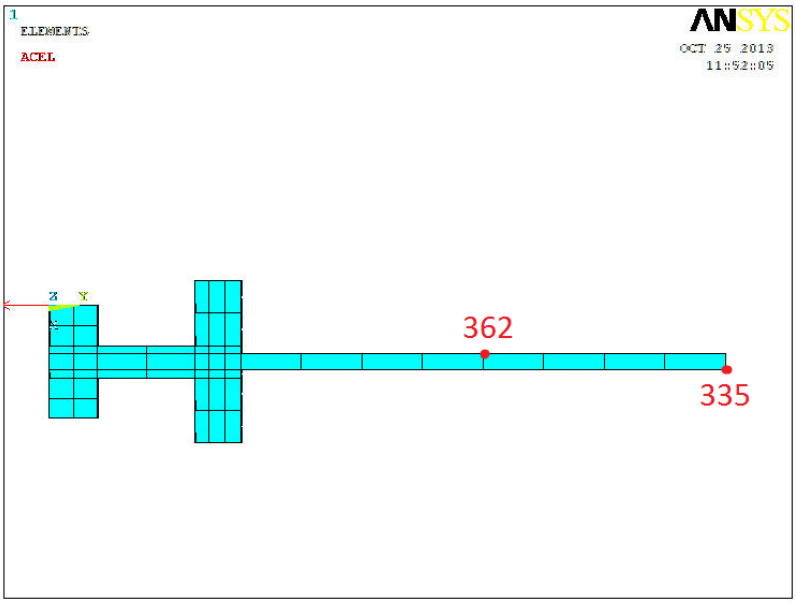

Figure 2.34 Nodes position 3D model.

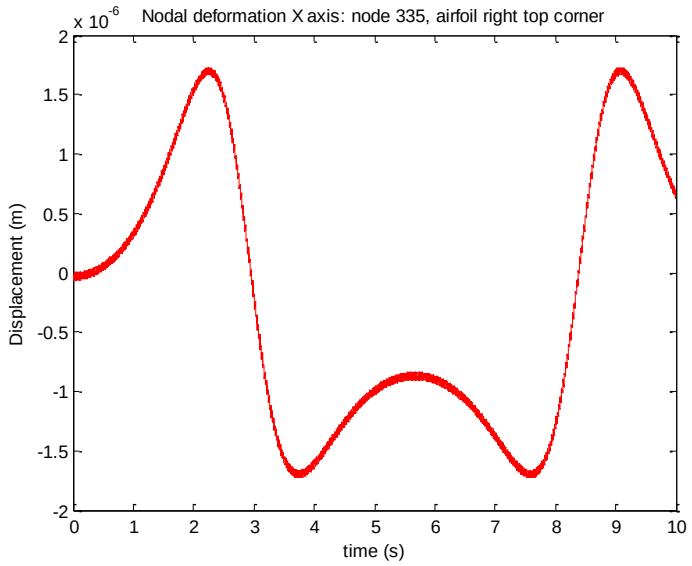

Figure 2.35 Nodal displacement x-axis node 10.

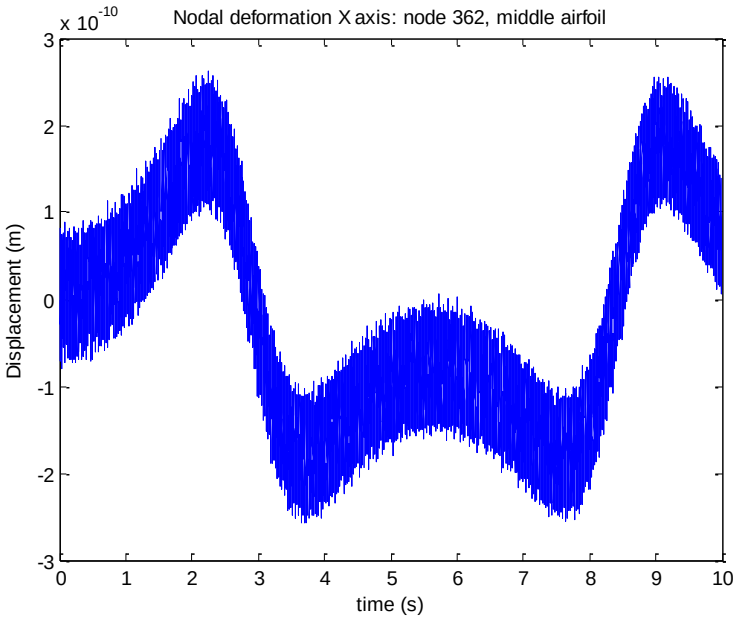

Figure 2.36 Nodal deformation x-axis, node 362.

3. DYNAMICS OF THE BLADE IN NON-LINEAR CONDITIONS

The second part of the thesis focuses the attention on the non-linear dynamics of the system of two blades, an underplatform damper and a fixture, simulating the real behavior of this set of 4 bodies during experimental measurements. The couple of blades is attached to the fixture by the presence of two wedges, used to maintain the contact between the base of the blades and the fixture. The stiffness of the whole system depends on the interference applied translating the wedges along the vertical direction. Finally the damper is interjected between the two blades, and kept in touch with them with a friction contact. The presence of the damper is necessary in order to dissipate a certain amount of energy during the blade rotation reducing the amplitude of vibration of the blades when the resonance condition occurs. The influence of the damper depends on its geometry and mass, influencing the value of the centrifugal force that arises during the blades' vibration. It follows that the fatigue failure of the blade, i.e. the failure of the component due to the application of a cyclic load, can be reduced by an optimized tuning of this solution.

The system has been analyzed in a series of steps, starting from the ideal case of the blades glued with the fixture in order to simulate the behavior of a single body without the presence of the damper.

3.1. Modal analysis of the whole system

The first step of the analysis consists in the evaluation of the dynamic behavior of the system of two blades, the fixture and the wedges without the presence of the damper in order to study the natural frequencies of the system and to understand how the presence of an underplatform damper can influence the dynamics of the system in terms of natural frequencies and modal shapes.

The dynamic analysis of the system can be expressed through its equilibrium equation, where $[\mathrm{M}]$, $[\mathrm{K}]$ and $[\mathrm{C}]$ respectively represent the mass matrix, the stiffness matrix and the damping matrix of the system, while $\{\ddot{\mathrm{U}}\}$, $\{\dot{\mathrm{U}}\}$ and $\{\mathrm{U}\}$ represent the vectors of accelerations, velocities and displacements for each degrees of freedom of the system. All these matrices have been obtained from Ansys Environment with dependence to the physical properties of the body and the number of degrees of freedom adopted in the analysis.

$$\{\mathrm{F_e}\} = [\mathrm{M}]\{\ddot{\mathrm{U}}\} + [\mathrm{K}]\{\mathrm{U}\} + [\mathrm{C}]\{\dot{\mathrm{U}}\} \qquad 3.1$$

The modal analysis of the system essentially consists in the study of the linear dynamics of the system of two blades in order to evaluate the dynamics response of the structure under the application of an excitation force. The first step in the analysis consists in the extraction of the natural frequencies as the eigenvalues and the mode shapes as the eigenvectors of the equation of motion of the not damped system.

$$0 = [\mathrm{M}]\{\ddot{\mathrm{U}}\} + [\mathrm{K}]\{\mathrm{U}\} \qquad 3.2$$

For sake of simplicity all the bodies in contact have been considered glued together in order to speed up the calculation, representing an ideal case. Once the solid model has been imported in Ansys and all the physical properties have been defined, such as material density, Young's Modulus and Poisson's ratio, the volumes have been meshed with solid95 elements, 20 node solid hexahedra with 3 degrees of freedom per node. Figure 3.1 shows the element geometry while TABLE V contains the material properties of the blade in analysis.

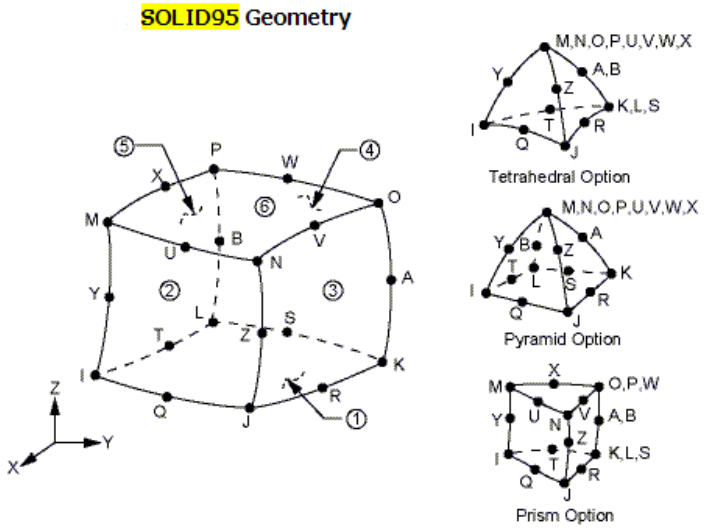

Figure 3.1 Solid95 element. Reprinted from Ansys 14.0 Help (2011), *Solid95 element.*

TABLE V MATERIAL PROPERTIES OF THE BLADE.

MATERIAL PROPERTIES OF THE BLADE		
Young Modulus	$2{,}2 \cdot 10^{11}$	Pa
Poisson's Ratio	0,33	
Density	7730	kg/m^3

Before starting the calculations, the fixture has been constrained on its base and on its lateral surfaces, applying a displacement equal to 0. After all the volumes have been meshed, it has been necessary to merge the nodes on the surfaces in contact between the volumes and to make them coincident. In this way the dynamic analysis has been performed as if the whole system can be considered as a single solid body.

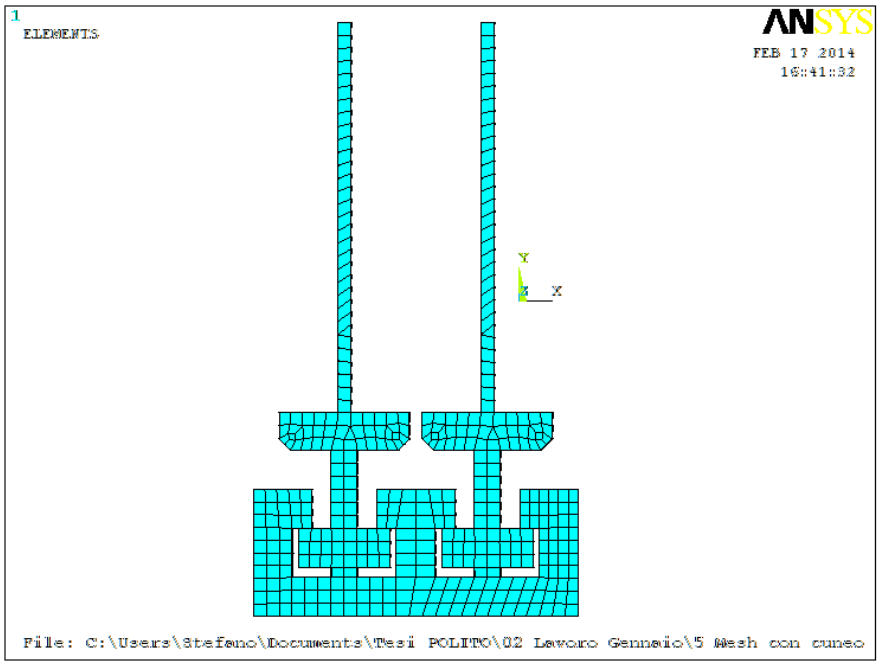

Figure 3.2 Solid model discretization in Ansys Environment.

The modal analysis carried out in this part of the thesis focuses on the first set of twenty frequencies contained in the range between 0 and $5000\,Hz$ and the modal shapes assumed by the blade during deformation. As it is possible to see from the analysis the modal shapes are all flexural or torsional and all in couples of an in-phase and out-of-phase motion. The first modal shapes usually interests the top of the airfoil and only the higher ones the body of the blade. The importance of this first kind of analysis is re

lated to the necessity to understand the dynamics of the couple of blades jointed to the fixture and consequently the natural frequencies of the system before connecting an underplatform asymmetric damper between them and appreciate its effects.

Dampers with different kinds of geometries can be interconnected between the two blades in order to optimize the dynamics of the system; in this analysis an asymmetric damper will be chosen, which means that it will be characterized by a plane contact surface on one side and of a convex contact surface on the other one, creating respectively a planar contact surface and a line contact. It is expected that the presence of an underplatform damper can increase the natural frequencies of the system and change the order of the modal shapes.

TABLE VI NATURAL FREQUENCIES OF THE GLUED SYSTEM WITHOUT DAMPER.

FREQUENCIES (Hz)	
N	**Without damper**
1	174.85
2	175.01
3	931.51
4	933.80
5	1071.1
6	1079.0
7	1123.7
8	1123.7
9	1844.5
10	1849.6
11	3236.6
12	3236.8
13	3608.8
14	3611.3
15	4058.8
16	4059.4
17	4281.0
18	4349.7

The first ten modal shapes can be represented in order to understand the shape assumed by the system once it reaches of its natural frequencies. Since the analysis has been performed in Ansys environment all the figures are taken from Ansys and the scale of the deformation is set enlarged automatically by the program and does not represent the real one.

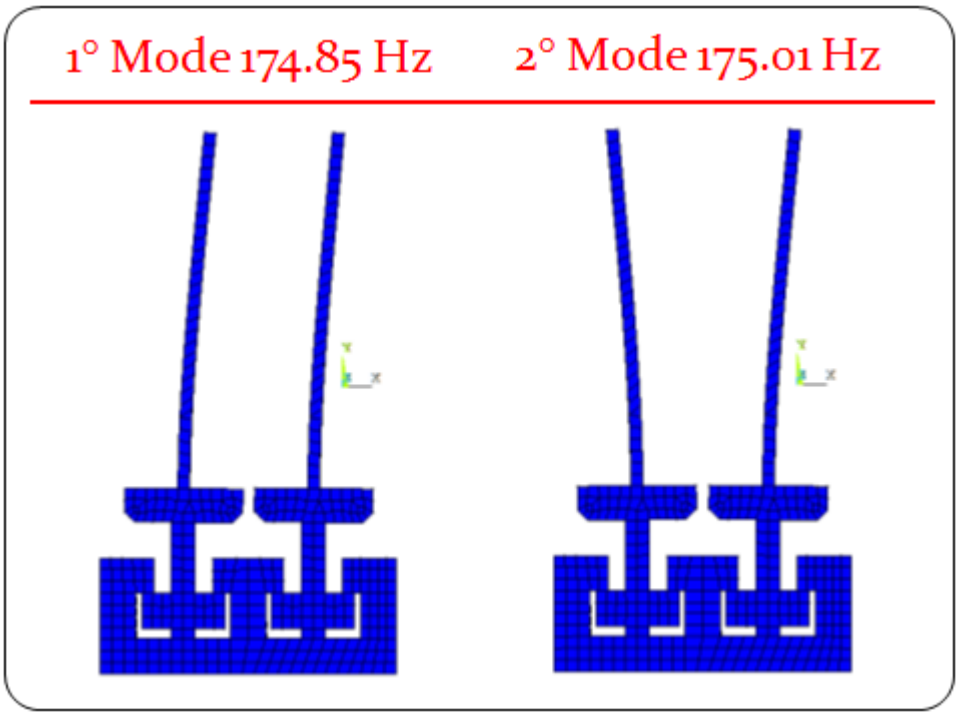

Figure 3.3 First and second modal shapes of the system from Ansys.

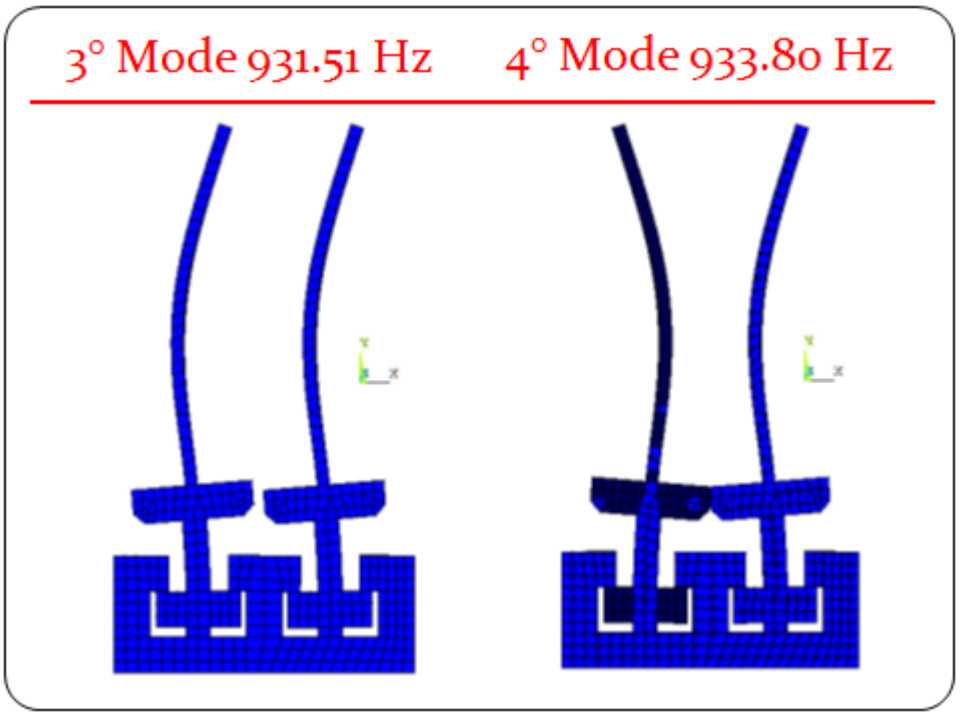

Figure 3.4 Third and Fourth modal shapes of the system from Ansys.

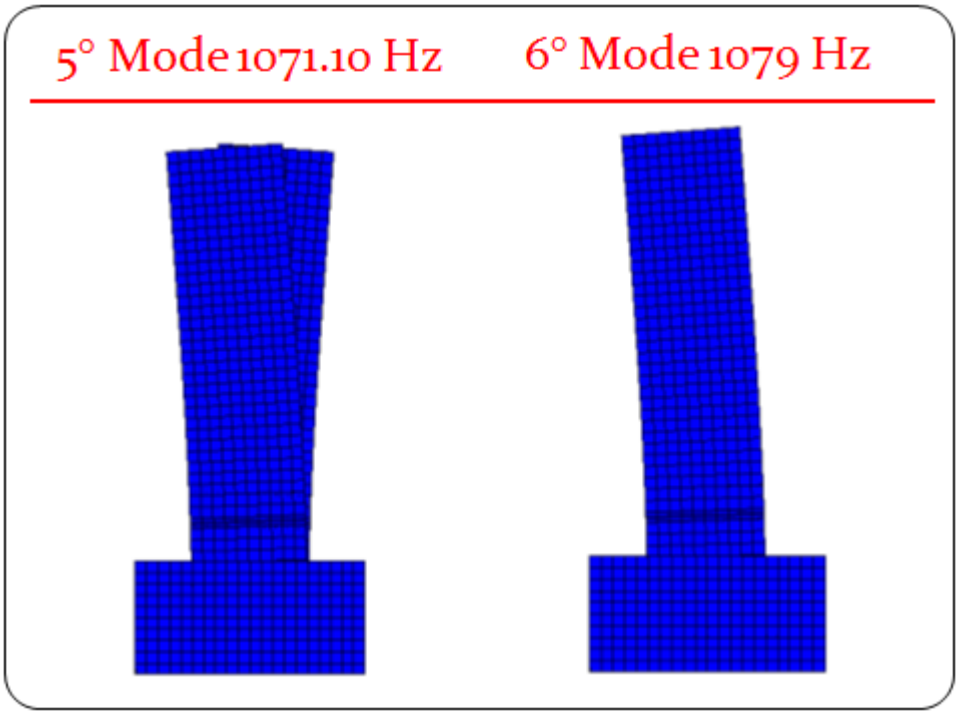

Figure 3.5 Fifth and sixth modal shapes of the system from Ansys.

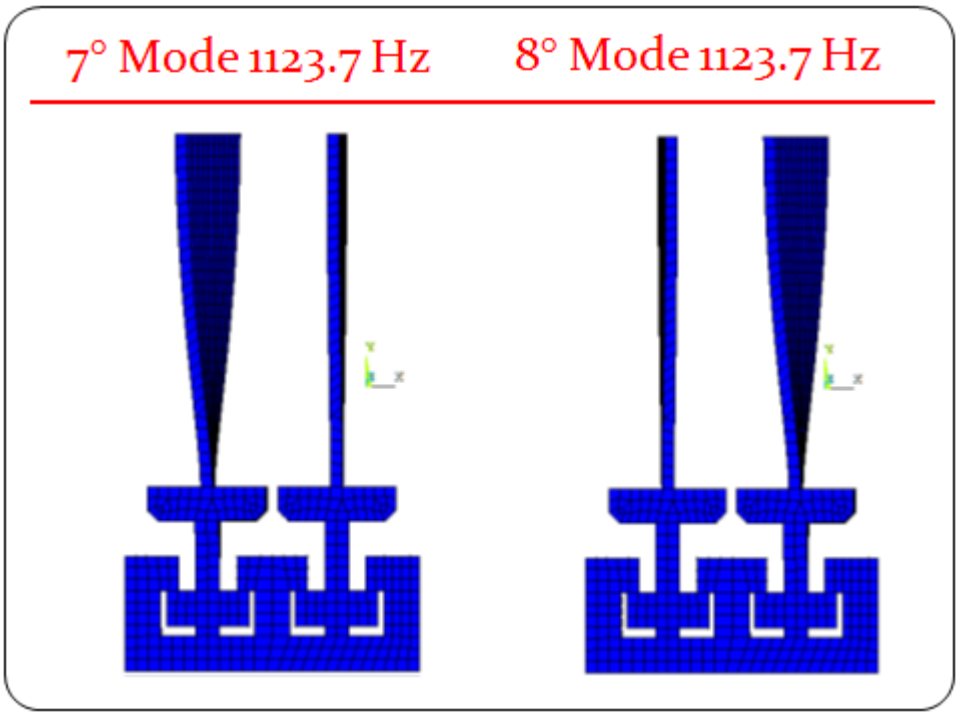

Figure 3.6 Seventh and eighth modal shapes of the system from Ansys.

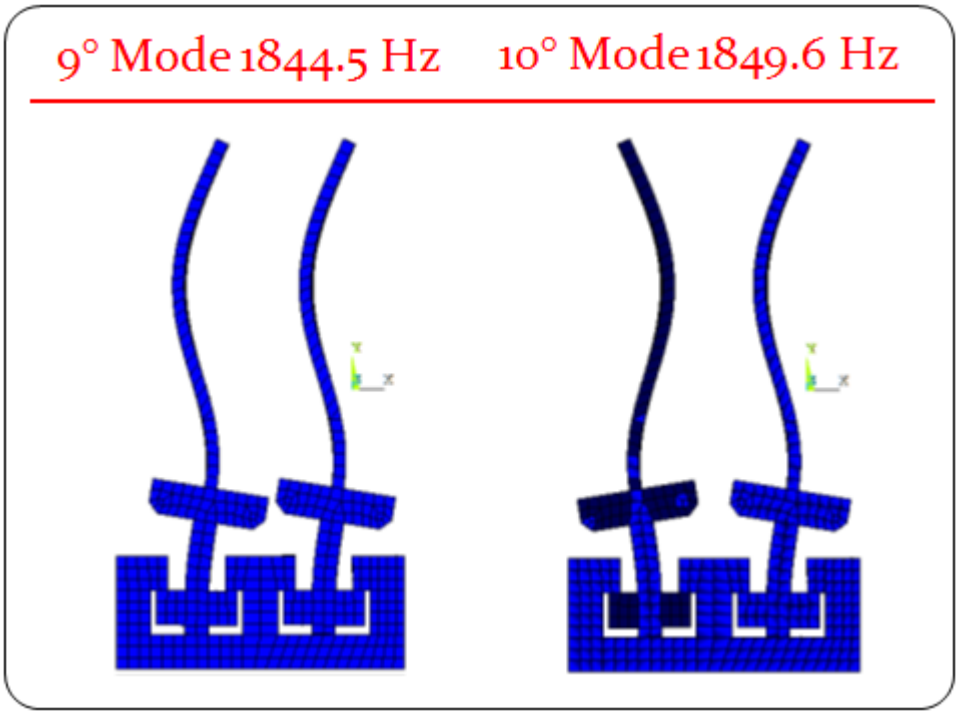

Figure 3.7 Ninth and tenth modal shapes of the system from Ansys.

3.2. Influence of the contact parameters

The first analysis on the natural frequencies of the blade has been conducted neglecting the presence of the contact between the two blades, the fixture and the wedges. In the real experimental measurement, the blades will be constrained to the fixture by the application of certain interference, i.e. the wedges will be move up of a defined displacement in order to press the blades against the arms of the fixture. The interference between the elements will be generated as well as stresses in the contact region. Due to the fact that all the bodies are in contact through plane surfaces, plane to plane contact will be created.

This contact condition can be easily simulated in Ansys environment by the creation of a “Contact Pair”, i.e. a particular surfaces in which the contact of two bodies is studied by the use of certain kinds of mesh elements [4]. Since the compenetration between the two bodies is not possible a deformation of the surfaces and consequently stresses will be generated.

The first step to ensure in order to create a contact pair in Ansys is the definition of a contact and a target surface; the choice of the two surfaces is suggested by the Ansys Help and tells that in the case of two flat surfaces, as the case of study, the target surface will be the larger of the two and the contact surface will be the smaller. The choice of the contact elements is performed automatically by the program with dependence on the type of body, planar or solid, and the type of surface. The case of study presents 4 contacts, two between the two blades and the fixture and two between wedges and blades. In the first two contacts, the fixture surface is chosen as the target one while in the contact between blades and wedges, the base of the blade is chosen as the target surface.

Since all the four contacts are very similar one to the other, the same mesh elements will be taken to study the problem. In this case the default elements set by Ansys are respectively Conta174 and Target170 because the structure has been already meshed with Solid95 elements. The contact pair creation always follows the discretization of the model. The two contact elements used in Ansys environment are shown in the following figures.

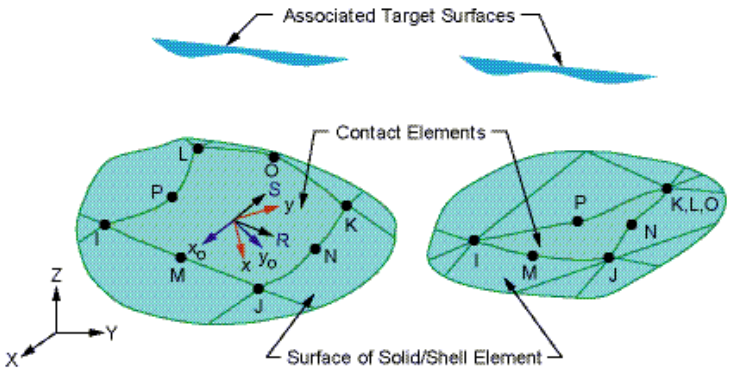

Figure 3.8 Conta174 element. Reprinted from Ansys 14.0 Help (2011), *Conta174 element.*

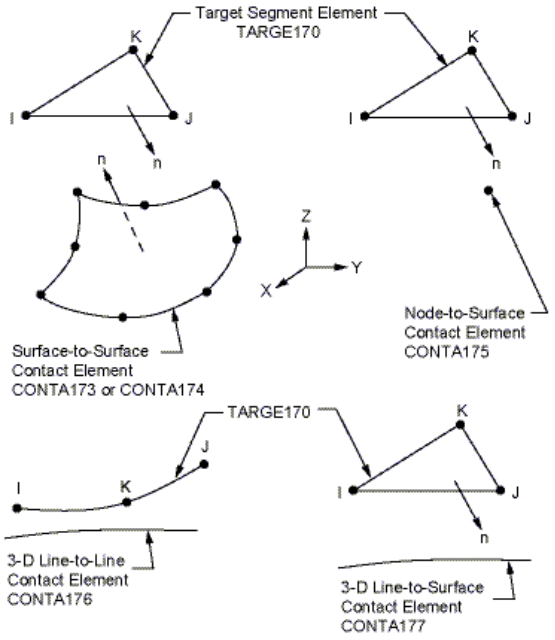

Figure 3.9 Targe170 element. Reprinted from Ansys 14.0 Help (2011), *Targe170 element.*

The definition of the contact model is usually quite complex since different kind of solution methods and contact properties can be used [5]; in this case the default Augmented Lagrange Method has been used. The model has been studied by focusing the attention on only two contact parameters: the interference applied to the system and the Normal Penalty stiffness. The interference of the system can be changed by translating the wedges along the vertical direction of a certain kind of displacement while the Normal Penalty stiffness FKN represents the stiffness of the contact along the normal direction expressed through a coefficient which ranges between 0 and 1. Different tests have been performed changing the FKN parameters for different values of interference. It is expected that a larger interference will produce a higher stress field on the contact region and consequently a little increment on the frequencies of the system.

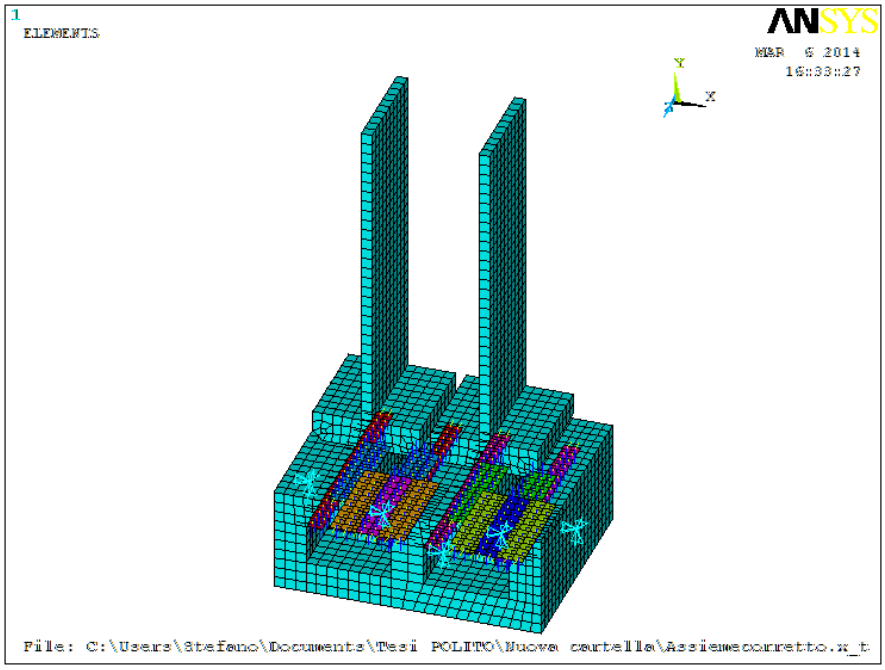

Figure 3.10 Contact Pairs creation in Ansys.

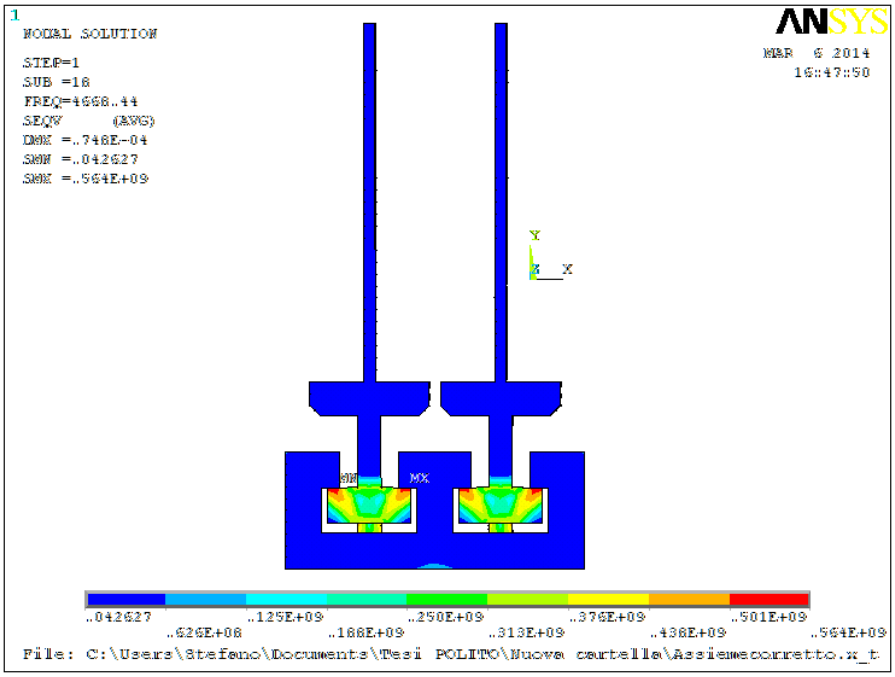

Figure 3.11 Contact due to stresses with 10^{-4} (m) interference, Ansys.

Five different values of interference have been taken as well as 5 different normal penalty stiffness coefficients FKN. The results can be plotted showing the change in the values of the natural frequencies of the system for different interferences and FKN coefficients. It is possible to see that the value of the frequency is more influenced by the interference than by the stiffness. In addition to this it is important to plot the value of each of the eight frequencies with respect to the FKN parameter chosen. In all the following graphs the values of the interferences are all expressed in m. At the right corner of each graph a little figure shows the mode shapes related to the frequency.

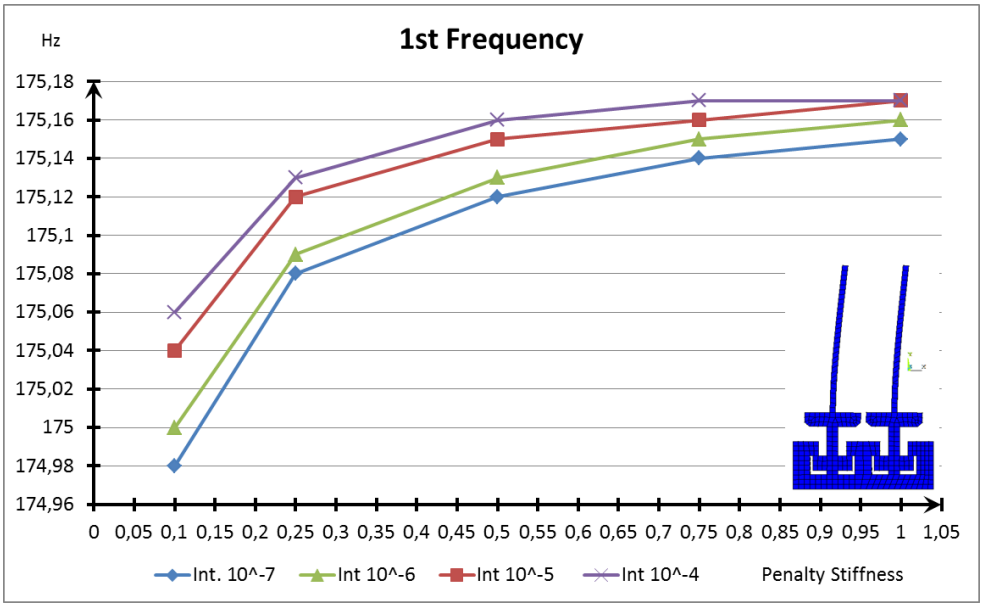

Figure 3.12 First Frequency: effects of the stiffness and interference

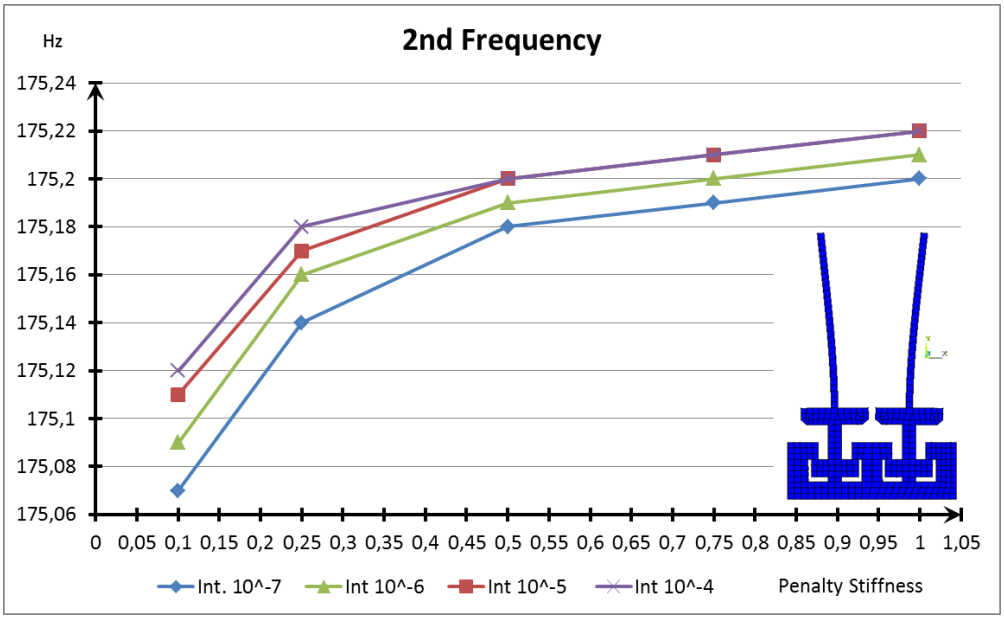

Figure 3.13 Second Frequency: effects of the stiffness and interference.

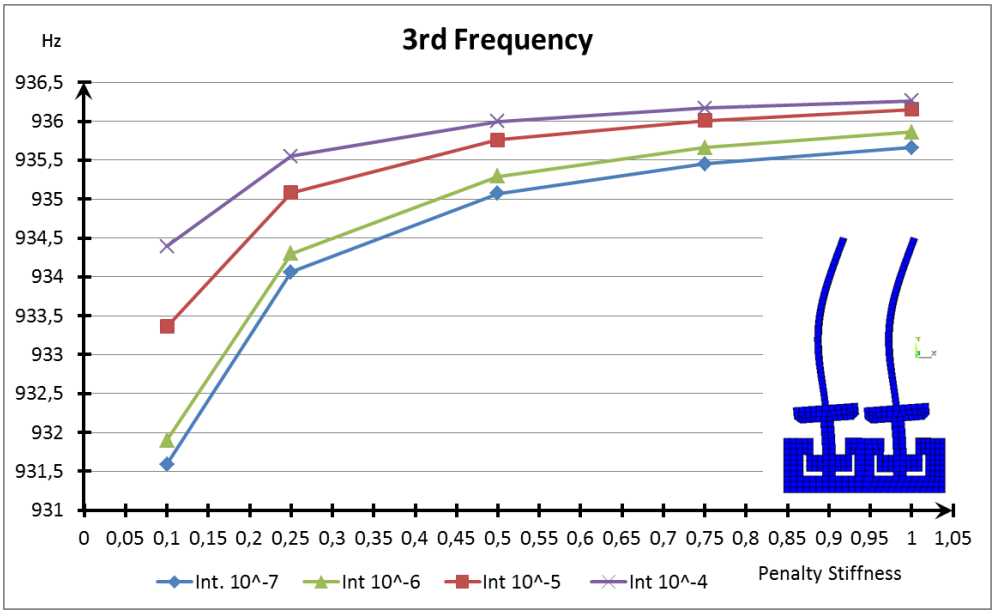

Figure 3.14 Third Frequency: effects of the stiffness and interference.

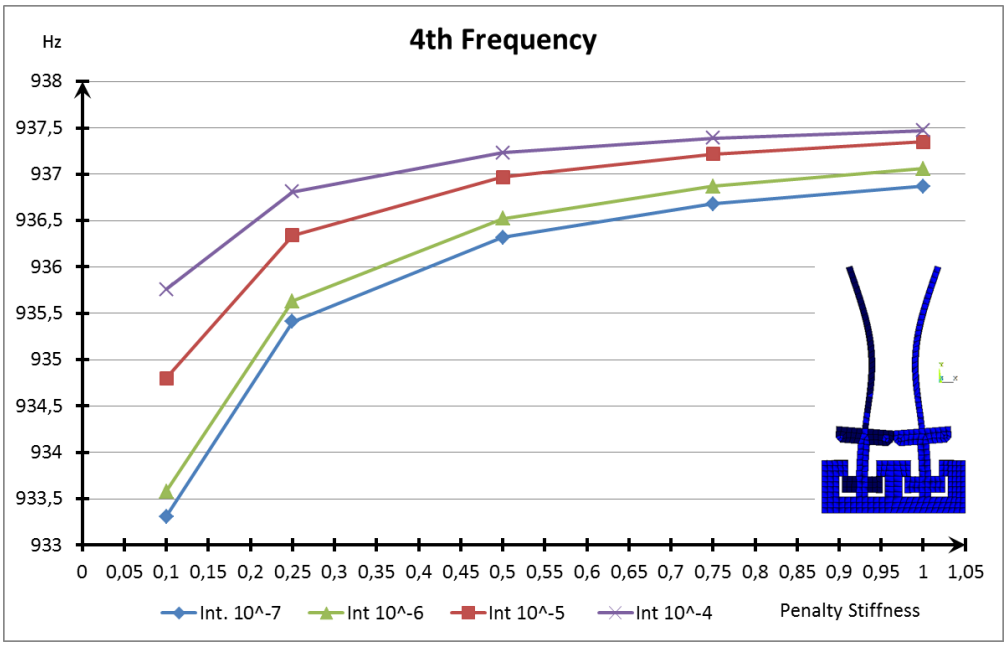

Figure 3.15 Fourth Frequency: effects of the stiffness and interference.

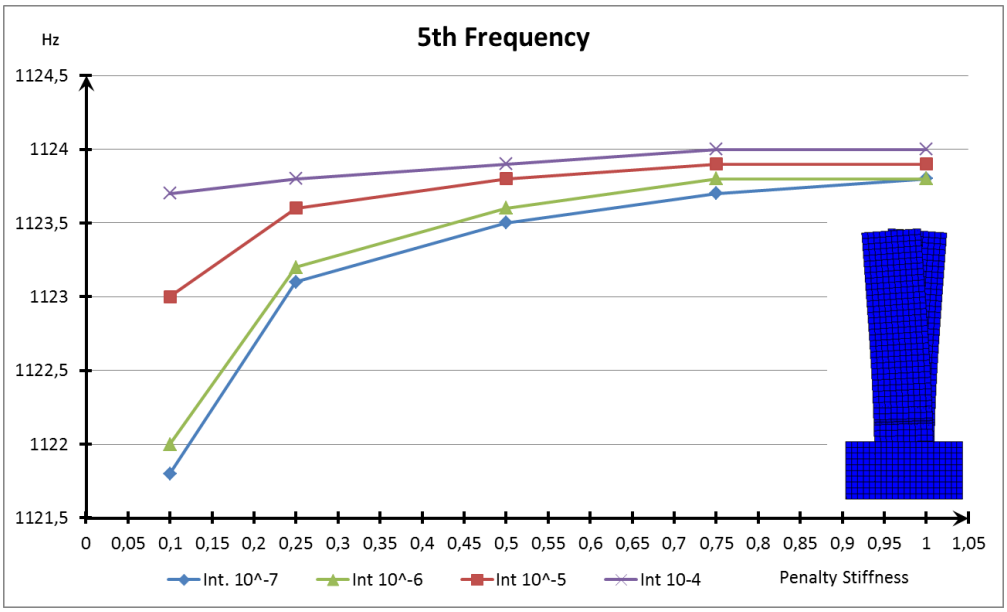

Figure 3.16 Fifth Frequency: effects of the stiffness and interference.

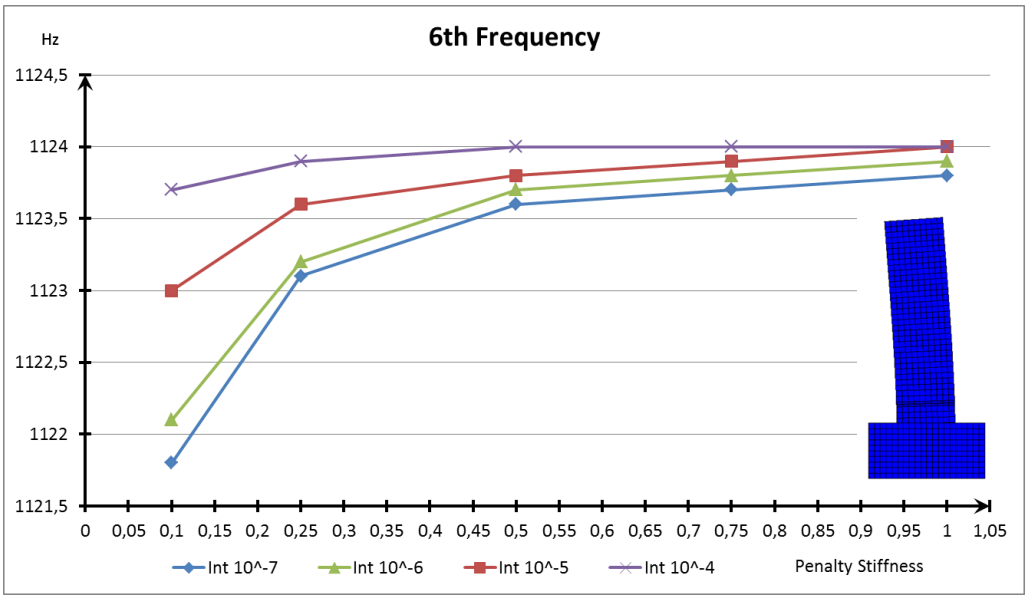

Figure 3.17 Sixth Frequency: effects of the stiffness and interference.

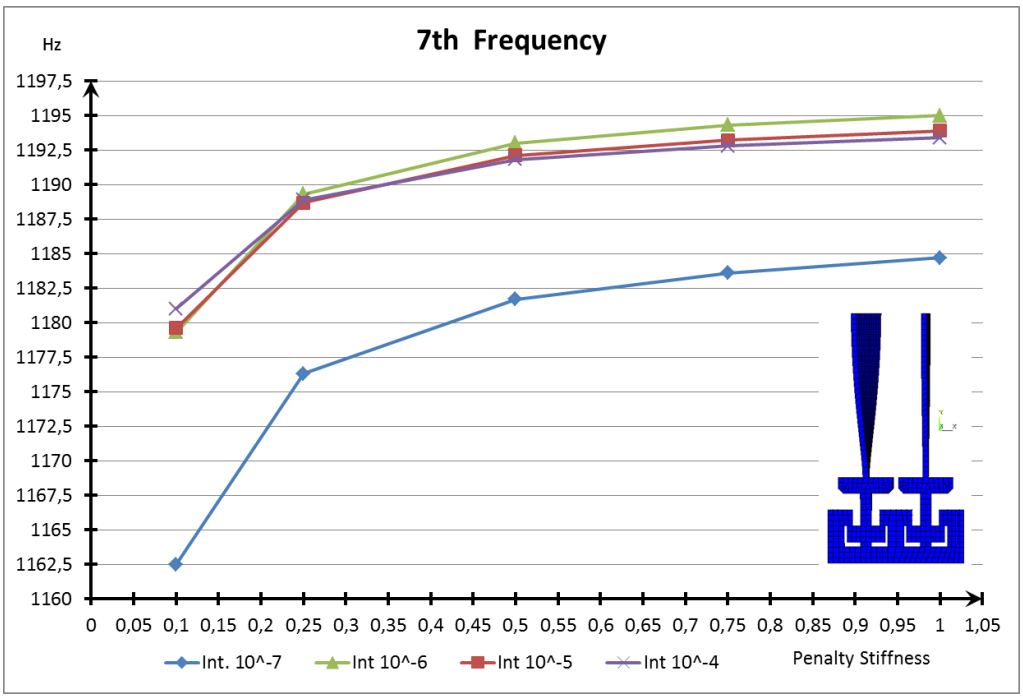

Figure 3.18 Seventh Frequency: effects of the stiffness and interference.

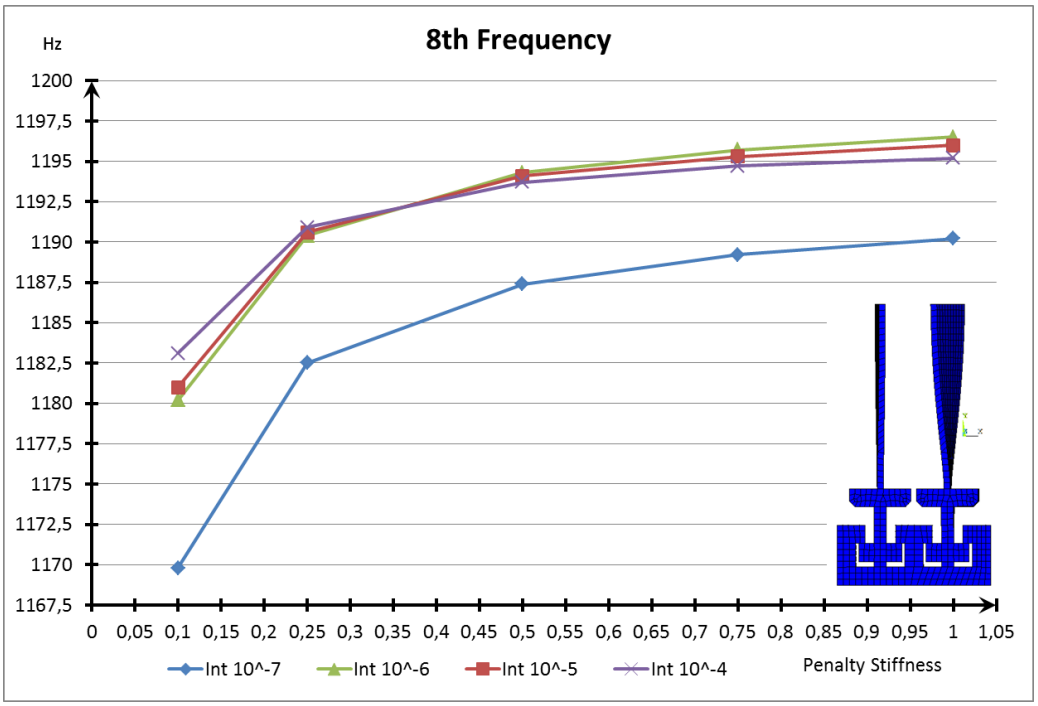

Figure 3.19 Eight Frequency: effects of the stiffness and interference.

According to the preceding figures, it is possible to notice that the effect of the interference on the natural frequencies of the system are higher at the higher frequencies while they can be considered negligible at the first ones. However an higher FKN coefficient should increase the stiffness of the system, at higher values of interference, the change in the normal penalty stiffness stops to affect the natural frequencies of the blades. Higher effects are obtained at the higher modes which interest more the lower part of the blade, and particularly its root where the contact has been established. According to the figures, the lower modes of the blades involve more the airfoil and the higher part of the base.

3.3. Forced response in frequency domain

In most of the engineering practices, it is usually interesting to predict the response of a structure or a mechanical system under the application of an external forcing; in the case of study, for example, it would be very important to understand how the system of two blades jointed to the fixture and separated by the presence of un underplatform asymmetric damper will react to the application of an excitation force.

Mathematical tools can be used in mechanical vibration analysis to model and predict vibration problems that sometimes are not obvious in engineering designs. In this part of the thesis, the forced response of the system of two blades will be studied under the application of an external force which is applied on the right side of the right blade in order to simulate the experimental measurements taking into account the frequency domain. Due to the complexity of the system, the forced response will be studied first in linear condition, evaluating how the system reacts to the application of the force without the presence of the damper and secondly in non-linear conditions. It is obvious that the presence of an underplatform damper with friction contact between the two blades will influence the dynamics behavior of the system introducing the forces due to contact. The equation of motion will be affected in the as shown in equation 3.3 with $\{F_e\}$ representing the vector of the contact forces.

$$\{F_c\} + \{F_e\} = [M]\{\ddot{U}\} + [K]\{U\} + [C]\{\dot{U}\} \qquad 3.3$$

Two steps has been followed to perform the forced response of the blades:

- Linear Response of the systems of the two blades, the fixture and the wedges without damper carried out in Ansys environment and in a purposely developed Matlab code.
- Non-linear response of the system with the presence of the asymmetric damper with a purposely developed Matlab code.

In this part of the thesis, the forced response has been evaluate through the use of a commercial software, Ansys ®, and through the use of a code developed in the Politecnico of Turin. The results obtained by the two will be compared with the one obtained through a different analysis, the numerical simulation in time domain, which, despite a much longer time to perform the calculations, enables to show the non linearities caused by the introduction of the contact forces.

3.3.1. Linear forced response

The linear forced response of the system consists in the analysis of the system response in the frequency domain under the application of an external excitation force. The same analysis has been performed in two different kinds of environments, a finite element code, Ansys, and a purposely developed Matlab code which makes use of condensed matrices and obviously simplified methods. The comparison between the results has been made possible by the use of the same physical parameters in both the methods. In this thesis both the methods will be explained focusing the attention on the main advantages and disadvantages of the two.

3.3.1.1. Linear forced response in ansys

The first step in the analysis consists in the evaluation of the forced response of the system of two blades, a fixture and two wedges using a finite element code, Ansys. The main idea of the simulation is to recreate the conditions that will be realized during experimental measurements. The analyzed system is exactly equal to the one introduced with the modal analysis. The only difference is represented by a finer discretization of the model that has been realized for the development of the Matlab code, explained in the following paragraph. Since the main goal of the analysis is to allow the comparison of the results get from the two methods, it is obvious that the same conditions must be considered in both the calculations.

The model has been discretized by solid elements analogously to the one already explained in the first part of the thesis using Ansys solid 95 elements. The only difference is the use of a mesh refinement of the two blades. Since the linear forced response of the system is used to define how the system react to the application of an external excitation force, it is necessary to define a node at which the force is applied and two nodes on the tips of the two blades in order to evaluate how the blade vibrate after the application of the external force. In this case, the two nodes have been taken at the center of the tips of the right and left airfoil respectively and the force node has been taken on the right sde of the right blade in order to respect what happens in the experimental measurement. Figure 3.20 shows the selected nodes, T1 and T2, respectively on the left and right blade and the force node F.

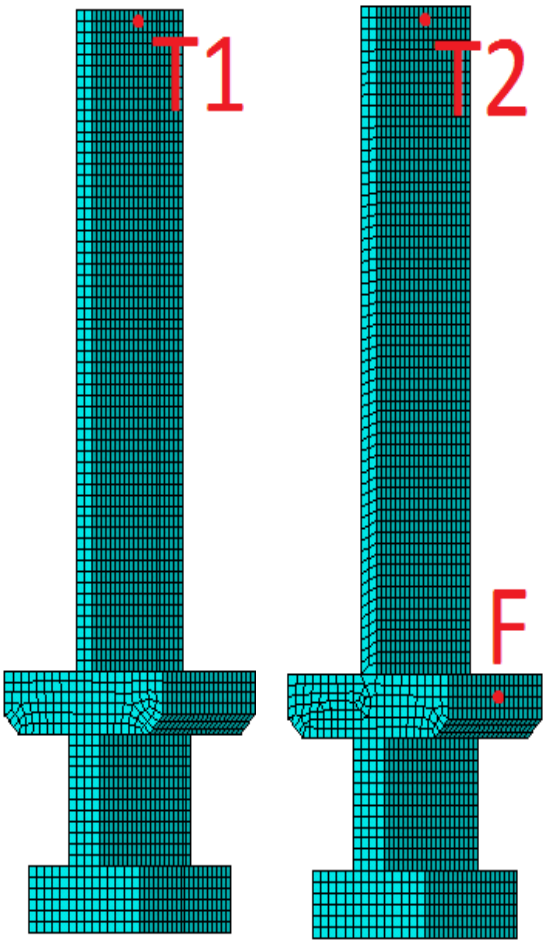

Figure 3.20 Blades discretization with solid95 elements in Ansys, linear forced response.

A coarser mesh has been used for the other parts of the system. Finally a contact has been created between the components of the system in the same way it had been already done in the subsection 0. In this case the interference between the blades and the fixture has been defined equal to 10^{-4} m, equal to the maximum value adopted in the preceding analysis. The contact properties have been set automatically by the program.

The main parameters which have been set before running the analysis where:

- Frequency range: the analysis has been performed in order to evaluate the blade response at its first frequency.
- Frequency step: a value of frequency step must be input to the code to define the accuracy of the analysis.
- External force vector.
- Modal damping: defining the analysis, it is necessary to express the value of the damping coefficient related to each mode of the structure.

All these data can be summarized in TABLE VII.

TABLE VII LINEAR FORCED RESPONSE INPUT PARAMETERS.

LINEAR FORCED RESPONSE		
Young Modulus	$2{,}2 \cdot 10^{11}$	Pa
Poisson's Ratio	0,33	
Density	7730	kg/m^3
Frequency range	170-190	Hz
Frequency step	0,01	Hz
External force vector	5	N
Modal damping	0,01	

Figure 3.21 shows the whole model discretized in Ansys environment and the node at which the force has been applied.

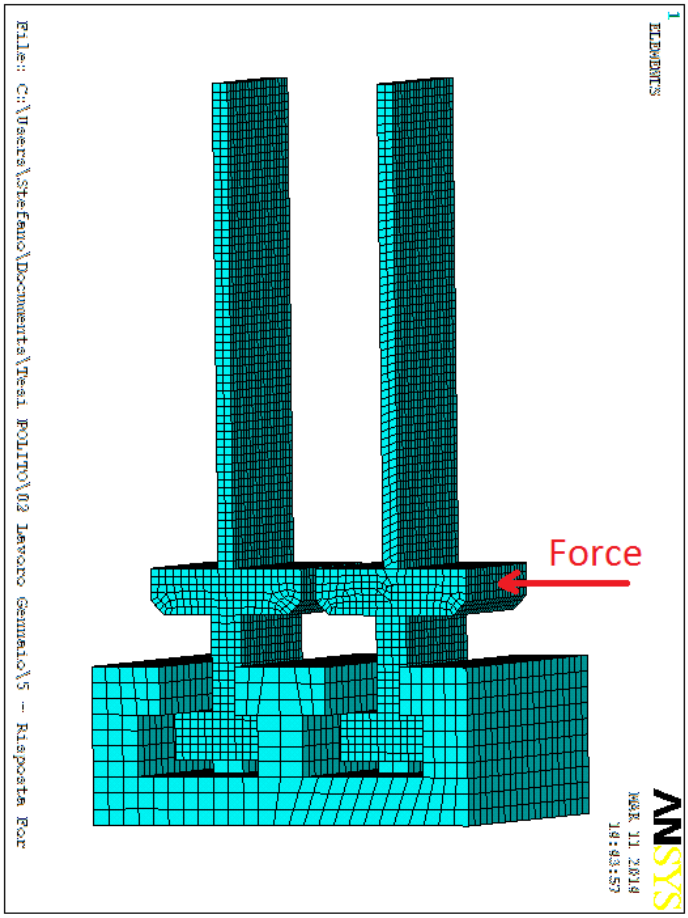

Figure 3.21 System discretization for the linear forced response, Ansys.

Once the analysis has been solved by the processor, it is possible to choose certain nodes and plot the amplitude of the response in terms of the frequency domain. The linear response has been carried out for two nodes, 6742 and 47756, respectively nodes T1 and T2 represented in Figure 3.20. Since the excitation force has been applied along the x direction at the middle of the blade thickness it is more convenient to consider the only the movement of the node along the x directions. As it is possible to see from the figure, the highest amplitude is reached at the first frequency of the system, and the amplitude of the displacement of the node on the excited blade is obviously higher with respect to the other one.

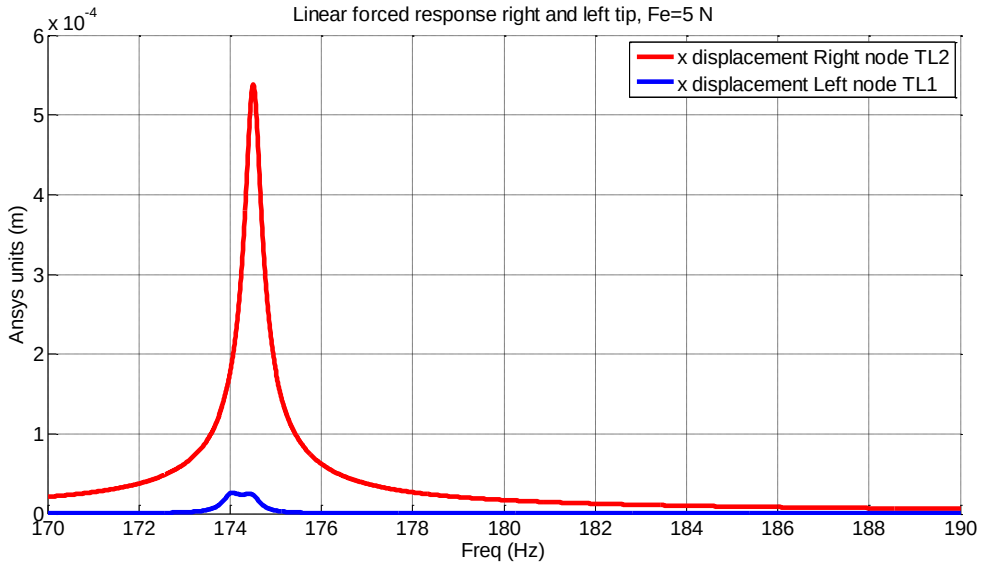

Figure 3.22 Linear forced response in Ansys, Fe =5 N.

3.3.1.2. Linear forced response in matlab

Once the linear forced response of the system has been evaluated in the finite element code, Ansys, it is very interesting to take into account the same analysis using a purposely developed code in Matlab environment which starts from the same input parameters in terms of physical model and physical properties but using a condensed model.

Sometimes the size of a finite element model used to define the dynamic behavior of a system of two turbine blades with fixture and eventually an underplatform damper between them is too large to be efficiently solved by a numerical solver, especially in the case of non-linear dynamics analysis. This is the reason why one of the two principal techniques of reduction is used to reduce the dimension of the system: the Component Mode Synthesis (CMS) using the Craig-Bampton method.

3.3.1.2.1. Component mode synthesis: the Craig Bampton method

The Craig-Bampton method is one of the most important kind of model reduction used to re-characterize large finite element models into a set of reduced mass and stiffness matrices containing the mode shapes information, capturing the low frequency response modes of the system [6]. This kind of analysis is introduced here in the linear forced response but will be used extensively in the non-linear analysis of the blades. The dimensions of the reduced system will depend on the number of nodes of interest and on the number of modes of the structures. It follows that the higher the number of modes the more accurate the analysis. These resulting matrices will be used as the reduced input parameters of the purposely developed Matlab code.

The method approach is quite straightforward: the vector of the degrees of freedom of the system is divided into a set of master degrees of freedom and slave degrees of freedom which will be approximated with a truncated series of mode shapes.

$$\begin{bmatrix} M_{B,MM} & M_{B,MS} \\ M_{B,SM} & M_{B,SS} \end{bmatrix} \begin{Bmatrix} \ddot{Q}_{B,M} \\ \ddot{Q}_{B,S} \end{Bmatrix} + \begin{bmatrix} C_{B,MM} & C_{B,MS} \\ C_{B,SM} & C_{B,SS} \end{bmatrix} \begin{Bmatrix} \dot{Q}_{B,M} \\ \dot{Q}_{B,S} \end{Bmatrix} + \begin{bmatrix} K_{B,MM} & K_{B,MS} \\ K_{B,SM} & K_{B,SS} \end{bmatrix} \begin{Bmatrix} Q_{B,M} \\ Q_{B,S} \end{Bmatrix} = \begin{Bmatrix} F_B \\ 0 \end{Bmatrix} \quad 3.4$$

Where the three matrices represent respectively the mass, the damping and the stiffness matrix of the system, $\ddot{Q}$, $\dot{Q}$ and Q the acceleration, velocity and displacement of each degrees of freedom , F_B the force vector and finally the subscripts M and S are related to the concepts of master and slaves degrees of freedom.

Since the main goal of this program is to reduce as much as possible the cost of the computations in terms of time and iterations, only very few nodes will be taken into account. As already explained before, the same condensed model will be used in the non-linear analysis of the system of blades and damper and this is the reason why also the nodes representing the contact points with the damper surfaces are kept in the reduced model. The Craig-Bampton method has been applied in Ansys environment. For sake of simplicity, 6 nodes are retained in the model reduction:

- Two tips nodes: the same introduced in Ansys to estimate the movement of the top of the blades airfoils.
- One force node: the same used in Ansys to apply the external force vector.
- Three contact nodes that will be useful for the future non-linear analysis.
- Ten modes.

Each node has three degrees of freedom that means that the resulting reduced matrices have a dimension of 28x28 considering 6 nodes and 10 modes. Figure 3.23 shows the Master dof used in the system reduction.

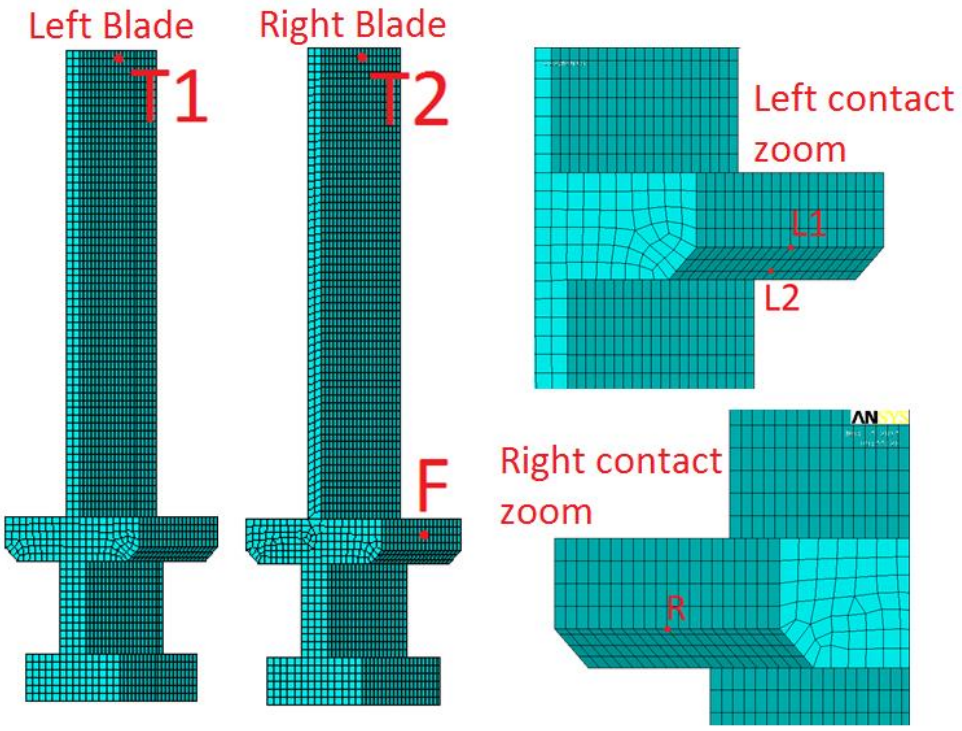

Figure 3.23 Master degrees of freedoms used in the Craig-Bamptom Method, Ansys.

The model synthesis has been performed with a purposely developed Ansys script which will pe presented in the appendix. Many steps must be executed before condensing the system:

- Model discretization: as it will be explained later in the non-linear forced response Analysis, the system discretization must be done taking into account certain features in order to allow the use of the Matlab code.
- Creation of the Contact Pairs on the contact surfaces of the model as it had been done in subsection 0 with the solution of the non-linear analysis related to the contact problem.
- Modal Analysis on the first twenty nodes.
- Matrix reduction specifying the nodes and the modes interested in the condensation.

Since the Craig-Bampton Method is directly performed by Ansys, the order of the master degrees of freedom is chosen by the program itself, which usually uses an ascending order in the nodes number. It follows that the vector of the master degrees of freedom and consequently the mass and stiffness matrices will be ordered as reported in equation 3.5.

$$\{Q_{B,M}\} = \begin{Bmatrix} \{x_R \quad y_R \quad z_R\}^T \\ \{x_{L1} \quad y_{L1} \quad z_{L1}\}^T \\ \{x_{L2} \quad y_{L2} \quad z_{L2}\}^T \\ \{x_{T2} \quad y_{T2} \quad z_{T2}\}^T \\ \{x_F \quad y_F \quad z_F\}^T \\ \{x_{T1} \quad y_{T1} \quad z_{T1}\}^T \\ \{m_1 \quad m_2 \quad m_3 \quad m_4 \quad m_5 \quad m_6 \quad m_7 \quad m_8 \quad m_9 \quad m_{10}\}^T \end{Bmatrix} \qquad 3.5$$

Where the subscripts represent respectively, R the right contact, $L1$ the first left contact, $L2$ the second left contact, $T2$ the right tip, $T1$ the left tip, F the force node and finally $m_1, m_2, \dots, m_{10}$ the ten modes of the system considered in the Craig-Bampton reduction.

3.3.1.2.2. Matlab results

Once the matrices have been obtained from Ansys, they are loaded in the Matlab code to evaluate the linear response of the system. Also in this case some input parameters must be provided to the program before running the simulation:

- Frequency range: it is chosen equal to the one adopted in Ansys in order to make the results comparable.
- Frequency step: it is equal to Ansys input, a lower step allows higher accuracy in the result.
- External force vector.
- Modal damping of the system.
- Nodes of which it is necessary to evaluate the response: since the linear response has been evaluated using the previous discretization the number of the nodes is not changed.

TABLE VIII INPUT PARAMETERS, MATLAB CODE FOR LINEAR FORCED RESPONSE.

LINEAR FORCED RESPONSE		
Young Modulus	$2{,}2 \cdot 10^{11}$	Pa
Poisson's Ratio	0,33	
Density	7730	kg/m^3
Frequency range	170-190	Hz
Frequency step	0,01	Hz
External force vector	5	N
Modal damping	0,01	

The result of the application of an external force vector of 5 N can be shown in the following graph. The same consideration made for the Ansys results can be used in this case. Since the response of the system is linear, the output result will be linearly proportional to the applied force.

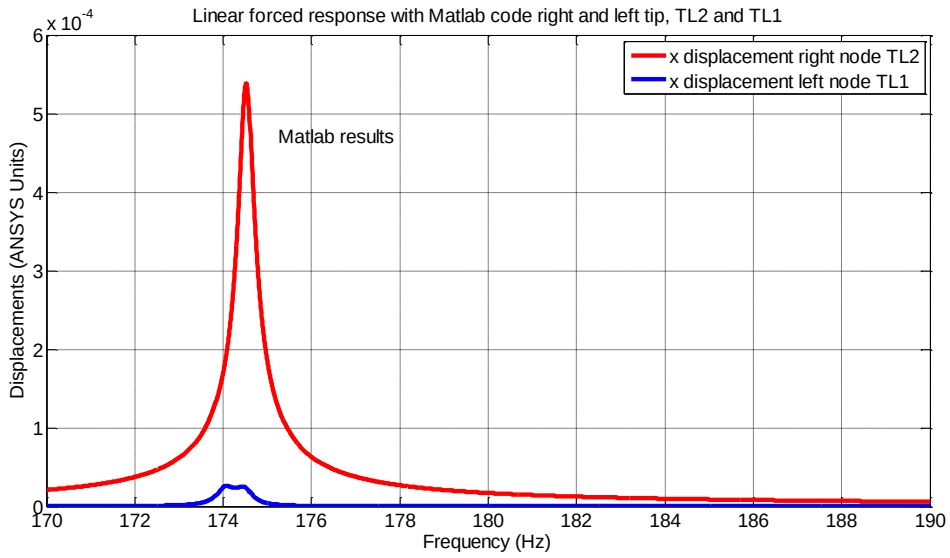

Figure 3.24 Linear forced response with Matlab code.

It is possible to plot the same response for Fe varying from $300\ N$ to $5\ N$.

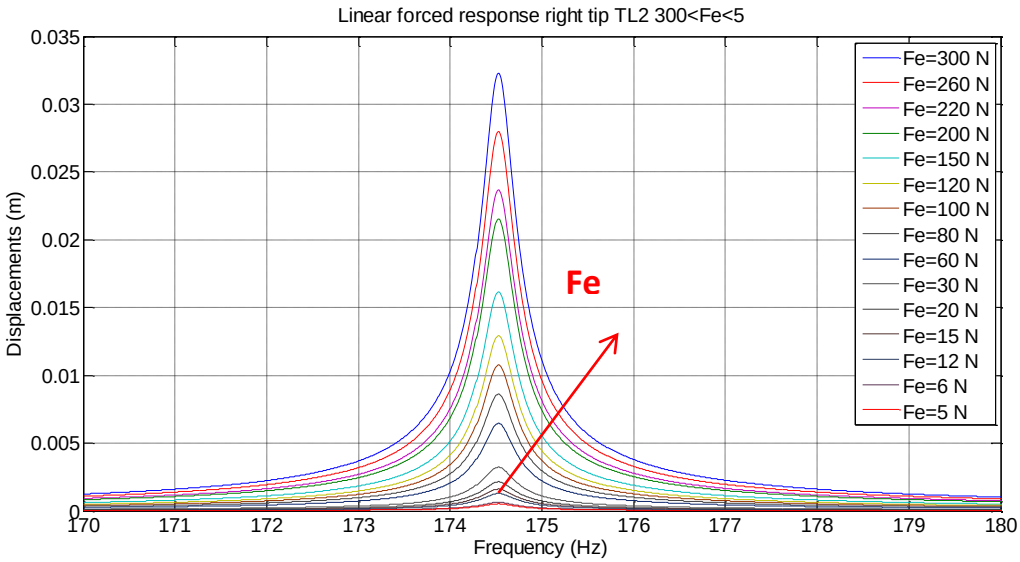

Figure 3.25 Linear forced response for Fe ranging from 5 to 300 N, Matlab.

3.3.1.3. Linear forced response comparison

The linear forced response of the system of two turbine blades, a fixture and two wedges has been evaluated through two different kind of procedure:

- Forced response with a finite element code, Ansys, which solves the analysis using all the degrees of freedom of the system, which in this case are in a very high number.
- Forced response with a purposely developed code in Matlab environment which makes use of the reduced mass and stiffness matrices of the system starting from the same initial discretization of the model. The condensed matrices have been obtained through the Craig-Bampton method operated in Ansys which allows reducing the number of degrees of freedom of the system to 28 taking into account 10 modes of the model.

It follows that the results obtained with Matlab can be validated comparing with the Ansys ones, since the same physical parameters are used in both the analysis. For sake of simplicity, only the displacements along x direction of the right tip will be compared, also because it is the most meaningful since the external force is applied to the right blade. Figure 3.26 shows that the two responses are very similar.

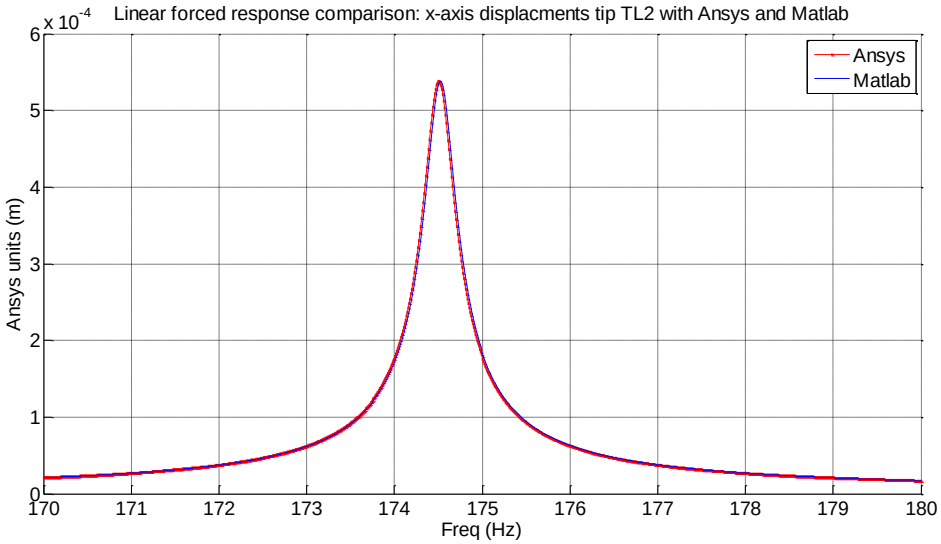

Figure 3.26 Ansys and Matlab results comparioson, right tip TL2 x-axis displacement.

However the model reduction carried out with the Craig Bampton method only involves the first ten modes of the model, it would be interesting to show how the Matlab code can be used to evaluate the other natural frequencies of the system in a range between 0 and $5000\ Hz$ comparing the results with the natural frequencies obtained in the modal analysis performed in Ansys in paragraph 3.1. Before comparing the results it is necessary to bear in mind two important considerations:

- The accuracy of the results is affected by the use of a reduced model of the system, i.e. the lower the number of dof and modes considered in the matrix reduction, the lower the accuracy of the results.

- Some of the modes are torsional and since the matrix reduction considers only few nodes in the middle of the blade thickness, i.e. coinciding with the axis of torsion, they cannot be kept by the program because the related displacement is negligible.

The complete linear response of the system is presented in Figure 3.27 and Figure 3.28 . For higher clarity, the x-axis and z-axis displacements are plotted in two different graphs due to the different magnitude of the displacement.

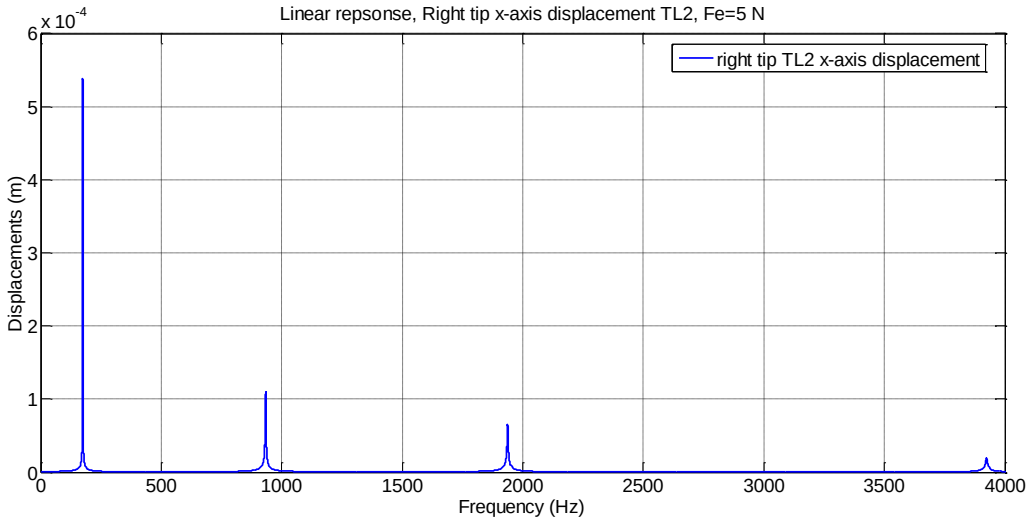

Figure 3.27 Linear response along x-axis, Matlab.

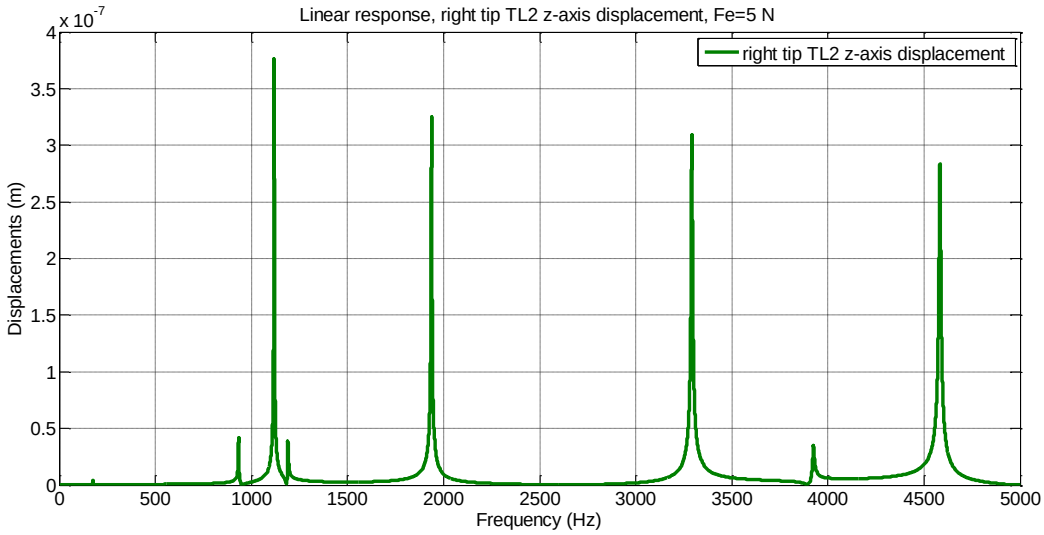

Figure 3.28 Linear response along z-axis, Matlab.

All the peaks of the preceding figures can be stored in a table to compare them with the results obtained in the modal analysis performed in Ansys. For completeness the relative error is evaluate for each frequency.

TABLE IX FREQUENCY COMPARISON: LINEAR RESPONSE IN MATLAB VS MODAL ANALYSIS IN ANSYS.

FREQUENCIES (Hz)			
SET	**Ansys**	**Matlab**	**Error (%)**
1	174,85	174,5	0,200171576
2	175,01	-	-
3	931,51	933,4	0,202896373
4	933,8	933,5	0,032126794
5	1071,1	1118	4,378676127
	1079	-	-
7	1123,7	1190	5,900151286
8	1123,7	-	-
9	1844,5	1937	5,014909189
10	1849,6	-	-
11	3236,6	3292	1,711672743
12	3236,8	-	-
13	3608,8	3924	8,734205276

As already anticipated, since all the nodes used in the matrix reduction are in the middle of the blade thickness, the displacement caused by torsional modes becomes zero due to the fact that the node lies on the axis of rotation. A more accurate analysis can be performed by including one node on the corner of the blade in order to keep all the possible nodes during vibration and including more modes in the matrix reduction performed with the Craig-Bampton Method.

3.3.2. Non-linear forced response

However the linear response of the blade during the application of an external load is very helpful in order to understand how the system reacts to an excitation, howeve it would be of great interest to focus the attention on what happens in non-linear conditions, i.e. when the dynamics of the couple of blades is influenced by the presence of an asymmetric underplatform damper. Turbine blades are usually subjected to high speed of rotation with the consequence of frequently reaching the resonance condition which may lead the blades to large amplitude vibration increasing the risk of fatigue failure of the structure. This is the main reason why a friction damper is usually used in the system in order to increase the damping of the system and control the blade response level.

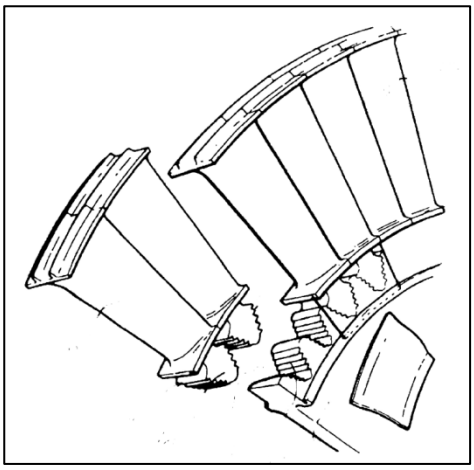

Figure 3.29 Rotor disc for gas turbine engine. Reprinted Phipps, Anthony B. (Derby, GB), *Rotor disc for gas turbine engine,* 2005.

Most of the mechanical systems are passively controlled in terms of vibrations by friction damping, and in the case of turbine blades, friction dampers are commonly in

cluded in the blade disk design. Among all the possible solutions, the underplatform damper is one of the most used: it can be considered as a metal device placed under the blades and pressed against them by the centrifugal force generated by the disk rotation. The amount of energy dissipated by the damper depends on the centrifugal force, the damper material and its geometry.

3.3.2.1. State of the art

Nowadays many different articles and researches have been made in the field of the non-linear dynamic behavior of a system of turbine blades coupled with underplatform dampers with friction contact in order to reduce the risk of fatigue failure of the structure due to the high amplitude of vibration reached by the blades in resonance conditions. When the blade detuning is not possible the only form of control of the system is represented by the introduction of a damper to reduce the response level of the blades, reducing the amplitude of the blade vibration dissipating energy through friction contact. Many different kind of solution can be adopted in the definition of the contact status between the damper and the blades platforms. In [7] a complete overview of all the possible contact elements used to couple the damper to the blade are shown, [8] gives a brief introduction to the contact model, while in [9] the stick-slip separation analysis is evaluated. All the following articles show different solution approaching the problem of vibration of turbine blades during the disk rotation.

3.3.2.1.1. Variability in the dynamics of semi-cylindrical friction dampers

The pioneering work of Zucca, Botto and Gola [10] shows the range of variability in the dynamics of semi-cylindrical underplatfrom damper coupled with turbine blades. The motion of the damper is characterized by three degrees of freedom, two in-plane translations and an in-plane rotation. The contact model on the curved surface is modeled with only one contact point while on the flat surface two contact points are present.

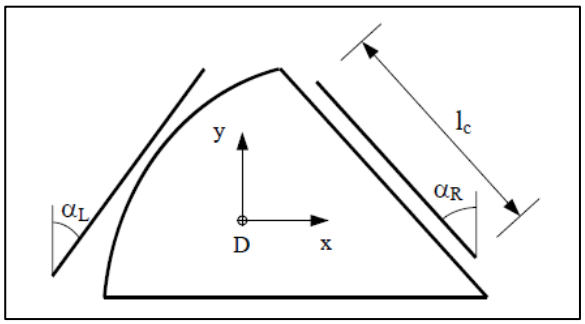

Figure 3.30 Damper model. Reprinted from [10].

A test case is performed in order to show the capabilities of the damper to influence the response level of the blades. The first step consists in the calculation of the static forces on the contact points starting from the centrifugal force acting on the damper. The model is defined as 2D contact where k_n and k_t respectively represent the contact stiffness along the normal and the tangential direction.

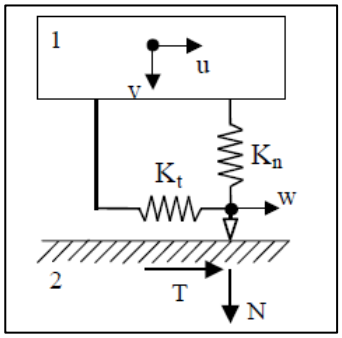

Figure 3.31 Contact model. Reprinted from [10].

The dynamic behavior of the system is simulated by the means of a set of normal modes without the damper, and the system response is evaluated around the resonance of the first bending mode.

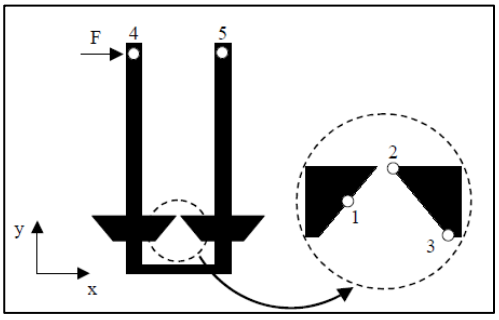

Figure 3.32 Case of study. Reprinted from [10].

The simulation has been performed in order to analyze the effects of the damper mass, the normal preload, excitation force, friction coefficient and finally damper rotation. It was shown that the damper mass affects the response of the system for the IP and OOP vibration of the system. Increasing the damper mass, the resonance ampli

tude of vibration decreases up to a minimum value, called the optimum value, and then it increases again till a condition in which the damper becomes fully stuck against the blade platforms preventing any slip.

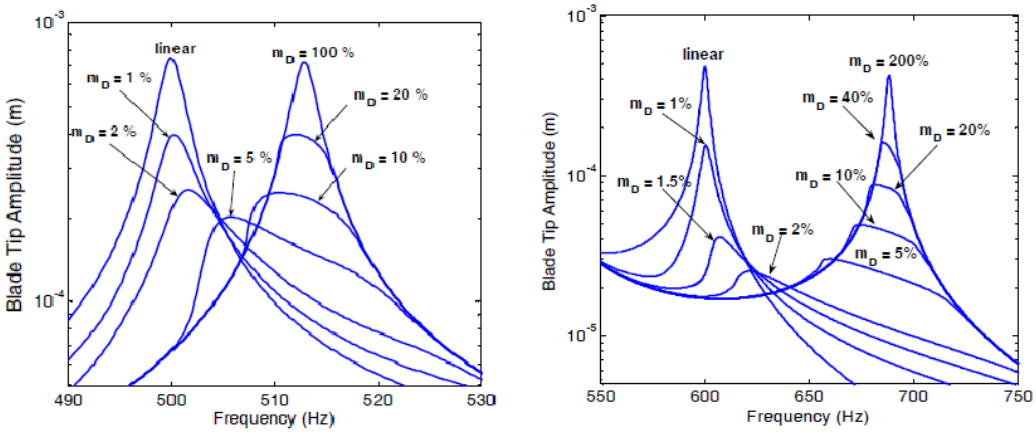

Figure 3.33 Effect of the damper mass on the IP peaks (left) and OOP peaks (right). Reprinted from [10].

The change of the normal preload acting on the damper, i.e. the variation of the centrifugal force during rotation of the system causes a relevant effect. Two limit cases had been taken into account: the first in which the tangential preloads were taken null (red curve) and a second one in which the preloads were taken equal to the limit value imposed by the Coulomb friction law (blue). According to this hypothesis it was shown that assuming a negligible tangential preloads, the maximum vibration amplitude can be 80% larger than the one evaluated through Coulomb law.

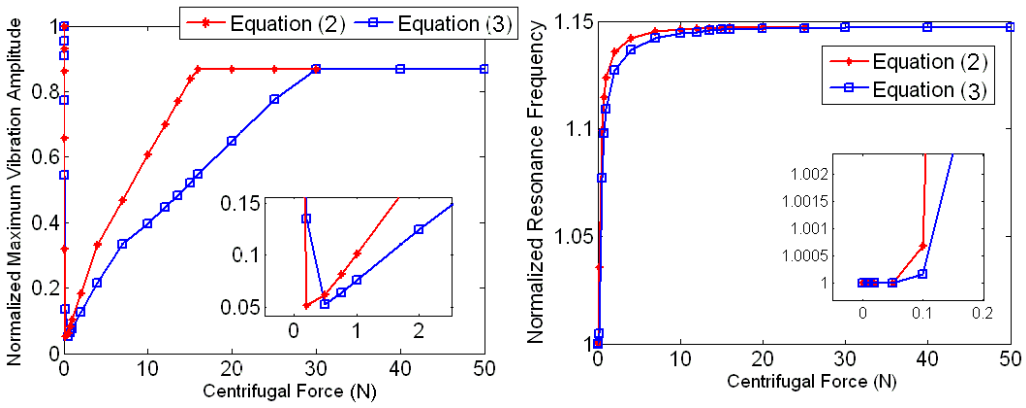

Figure 3.34 Effect of the preloads. Reprinted from [10].

Finally the effect of the friction coefficients and the external force were considered. With regards to the friction coefficients, it affects the response of the system in a similar way to the damper mass, reaching the condition of free response when it reaches a null value. Increasing the value of μ, the system response decreases up to a minimum value and finally it starts to increase again when the contact approaches the fully stuck conditions.

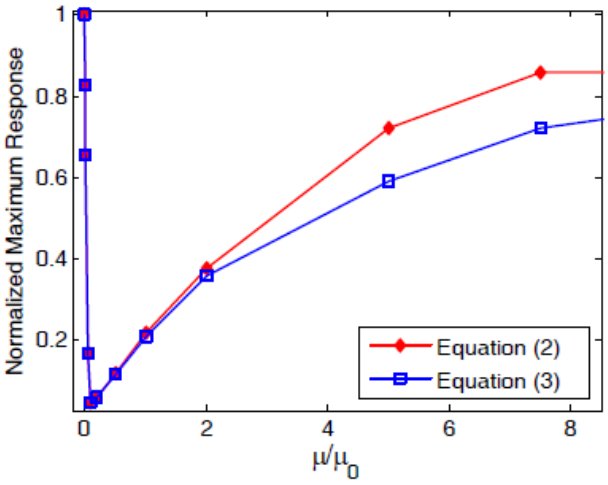

Figure 3.35 Effects of the friction coefficient. Reprinted from [10].

Finally one the most important roles in the characterization of the non-linear dynamics of the system is played by the external force. The results had been evaluated taking into account the two conditions of normal preloads. For small value of external force, the relative displacements between the blades platforms and the damper are not large enough to make slip occur. As the external force increases, the contact approaches the slip condition until it tends to the linear system without the damper.

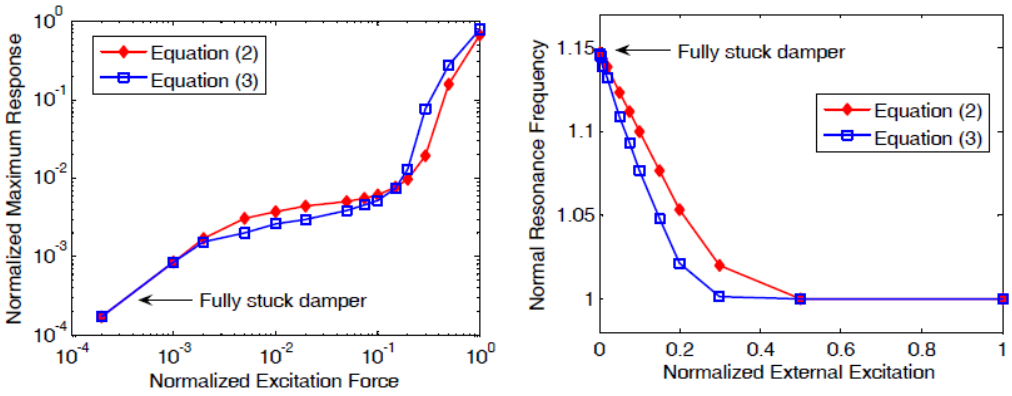

Figure 3.36 Effects of the excitation force. Reprinted from [10].

In this paper the effects of a semi-cylindrical underplatform damper coupled with a system of turbine blades have been described. Different values of the normal preloads acting on the damper lead to a great variability in the dynamic behavior of the blade which has been investigated against some of the main system parameters such as friction coefficients, damper mass and external force. A perfect set of these values could lead to an optimized tuning of the blades in dynamic condition reducing the risk of fatigue failure due to the presence of the resonance conditions.

3.3.2.1.2. A refined approach for modeling friction dampers for turbine blades

In their work, Zucca, Firrone and Gola [11] propose a coupled approach: the static and dynamic displacements of blades and damper are coupled together during the forced response calculation, defining the contact between the two through a refined version of the state of-the-art contact model. The accuracy of the model is maintained avoiding an increase of the size of the problem by modeling the blade and damper dynamics using a superposition of a truncated series of normal modes.

This methodology has been applied to a test case of dummy blade disk with 48 identical sectors, calculating the forced response on the first mode of the system.

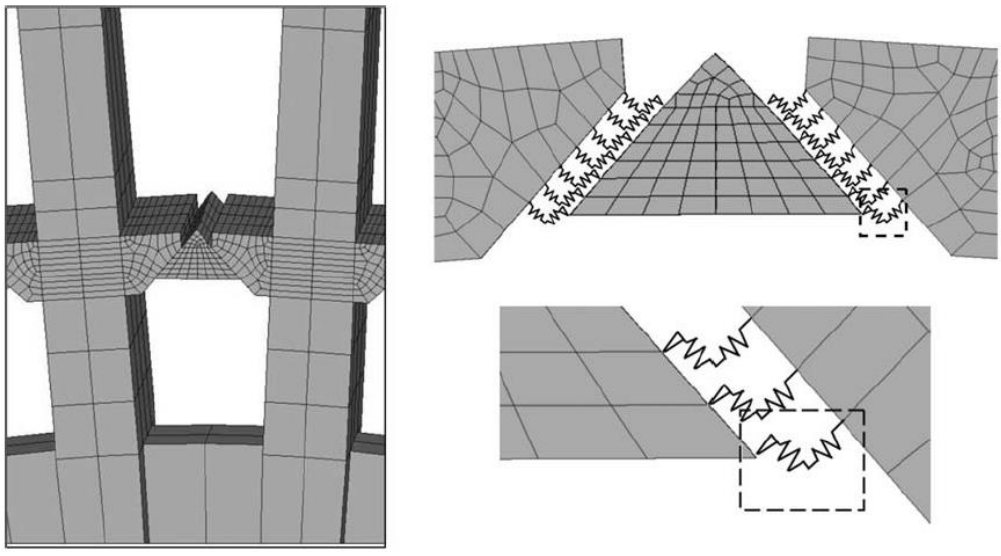

Figure 3.37 Blade model. Reprinted from [11].

The contact model has been refined involving its static component of the normal and tangential forces. Taking into account the static relative displacements between the surfaces in contact, $v^{(0)}$, the bodies are in contact with $v^{(0)} > 0$ otherwise they separate. Consequently the static normal force during contact can be evaluated as follow:

$$\mathrm{N(t)} = \max(\mathrm{k}_n v(t), 0) \tag{3.6}$$

In the case of the tangential static force, if the vibration amplitude is not large enough to enter the lift-off state or the slip state, it cannot be computed uniquely. The value of $T(t)$ will be included in the range $T_{min}^{(0)} < T^{(0)} < T_{max}^{(0)}$ corresponding to the two Coulomb limits $-\mu N$ and $+\mu N$. This is the reason why a refinement is proposed introducing a predictor corrector approach. The tangential force is defined in the full-stick case as:

$$\mathrm{T(t)} = \mathrm{k}_t u^{(0)} + \mathrm{k}_t \cdot R\left(u^{(1)} e^{i\omega t}\right) \; if \; T_{min}^{(0)} \leq \mathrm{k}_t u^{(0)} \leq T_{max}^{(0)} \tag{3.7}$$

Otherwise if during the period $\mathrm{k}_t u^{(0)}$ overtakes one of the Coulomb limits, the value of the equation is corrected in the following way.

$$\mathrm{IF} \quad \mathrm{k}_t u^{(0)} > T_{max}^{(0)} \rightarrow \mathrm{T(t)} = T_{max}^{(0)} + \mathrm{k}_t \cdot R\left(u^{(1)} e^{i\omega t}\right) \tag{3.8}$$

$$\mathrm{IF} \quad \mathrm{k}_t u^{(0)} < T_{min}^{(0)} \rightarrow \mathrm{T(t)} = T_{min}^{(0)} + \mathrm{k}_t \cdot R\left(u^{(1)} e^{i\omega t}\right) \tag{3.9}$$

This methodology is included in a numerical solver to calculate the forced response of the system for different values of the damper mass. The frequency of the response peak is shifted to values higher than the resonance frequency in the free response increasing the mass of the damper. Finally the response of the system has been evaluated for different values of external forces: starting from a low excitation where the damper is in fully stuck with the blades platform, as the external force increases the response of the curve tends to the linear one without damper.

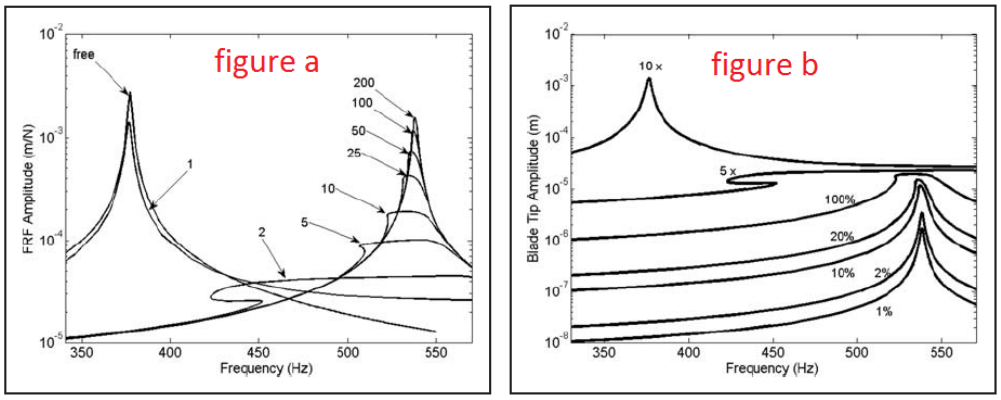

Figure 3.38 Figure a: effect of the damper mass on the frequency response, the number is the multiplier of the damper mass; Figure b: effect of the excitation force. Reprinted from [11].

The consistency of the method is checked from the map of the contact status at resonance for different values of damper mass, the white color represents the full-stick condition, the grey the alternating stick-slip and finally the black represents the alternating stick-slip-lift-off.

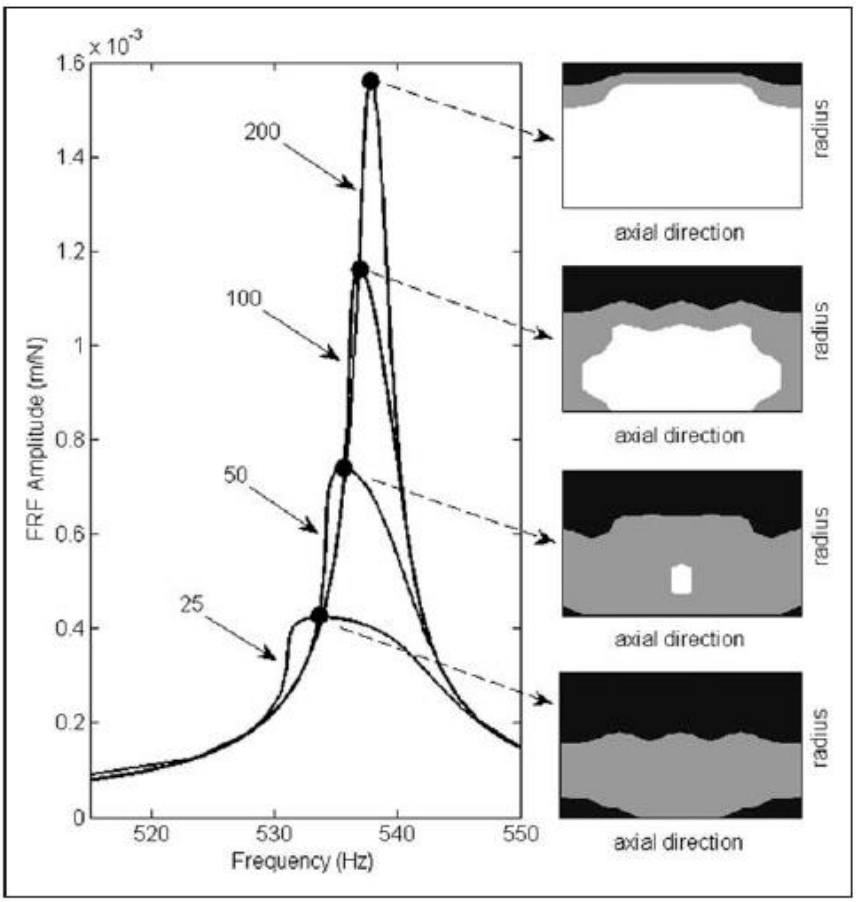

Figure 3.39 Map of the contact status. Reprinted from [11].

The results are consistent with the physical problem since the contact is in stick condition for the largest value of the damper mass and then as the mass decreases the portion of the area where slip occurs becomes larger. In conclusion, it is shown that the proposed method represents a more accurate tool for the simulation of the forced response of the bladed disks with underplatform dampers.

3.3.2.1.3. Identification of the damping coefficient

Doosan Skoda Power is continuously developing new solution for its steam turbines, modeling a new kind of shrouds with friction contact [12]. In this paper the blade damping ratio has been identified under rotation taking into account three test cases: free blades, blades with dampers and finally a new kind of blade with a new shroud. The measurement is conducted by the excitation of the set of blades rotating on the blade disk and excited by the presence of some electromagnets placed above and below the blades. In the first test the damping ratio dependence on the blade vibration was shown for 4 natural frequencies. Some of the damping values have been evaluated through regression line showing that the damping ratio slightly increases with the amplitude of the blade vibration. The damping values previously obtained are compared with the one of beam made of the same material.

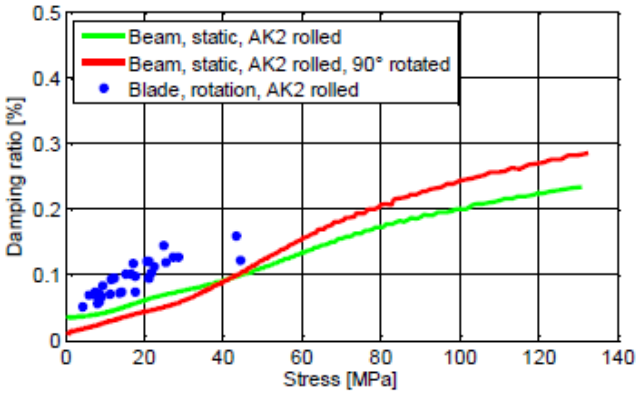

Figure 3.40 Damping ratio comparison between turbine blades and beam cut out of the same blade material. Reprinted from [12].

In the next measurements, the damping ratio is obtained for blades coupled with friction dampers; the non-linear behavior obtained is a function of the damper size in terms of centrifugal force and contact area, vibration level and nodal diameter. It is evident that the presence of a friction damper increases the damping ratio of the system. For higher accuracy, the influence of the nodal diameter on the damping ratio is shown, when phase shift of two adjacent blades increases for higher nodal diameters it causes a growth of the relative displacements and friction.

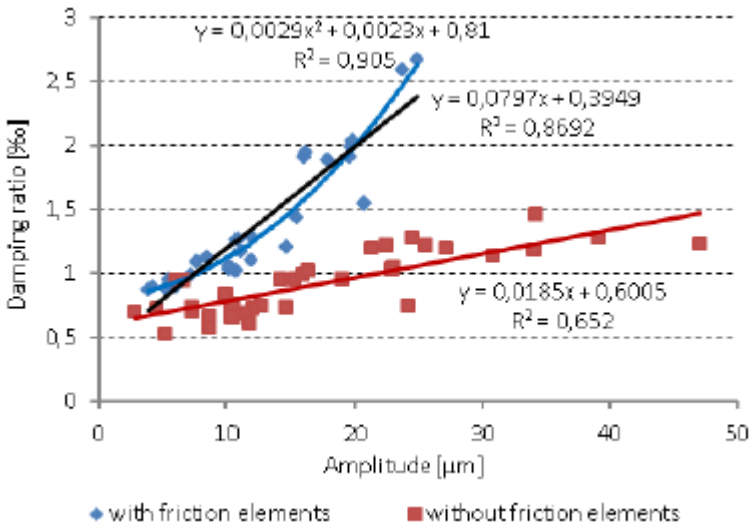

Figure 3.41 Comparison between free blades and blades modeled with friction elements. Reprinted from [12].

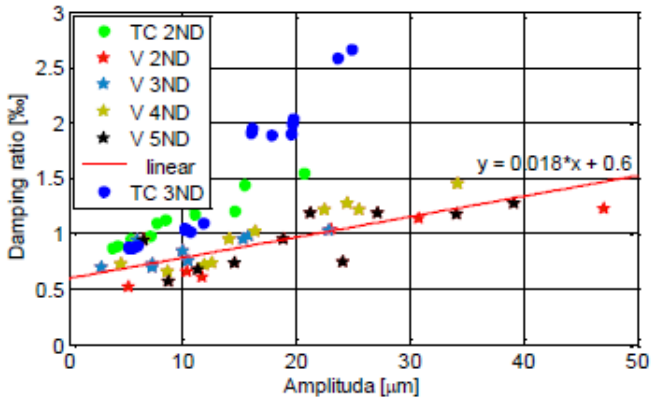

Figure 3.42 Damping ratio dependence on blade vibration amplitude and nodal diameters, TC=blades with friction damper, v=free blades. Reprinted from [12].

Finally in the third test case, a new V-shroud profile has been tested obtaining similar results to the previous one. In conclusion it was shown that the damping ratio depends on both the amplitude of the blade vibration and on the nodal diameter.

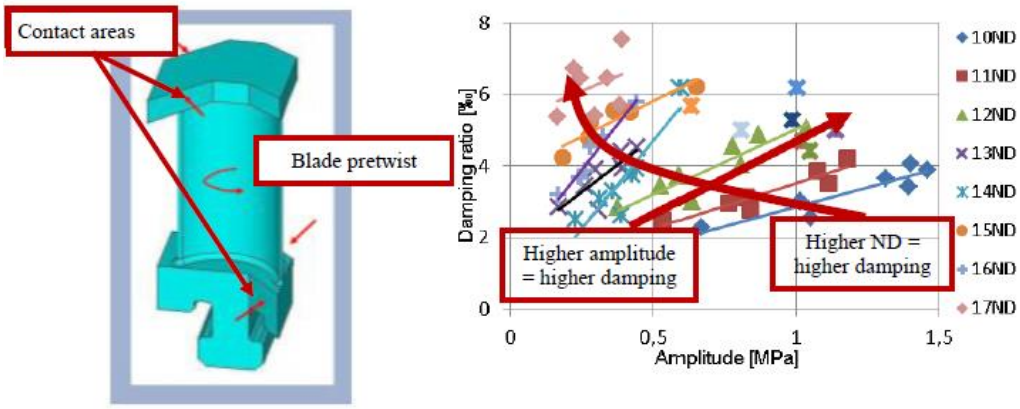

Figure 3.43 V-shroud profile and experimental results. Reprinted from [12].

3.3.2.1.4. Coupling between turbine blades and friction dampers

This paper [13] presents an investigation relative to the influence of alternate mistuning with a bladed disk assembly coupled through frictional contacts, applying simplification like cyclic symmetry and Harmonic Balance Method and by the use of a purposely developed code called DATAR [13]. This code has been used to perform vibration measurement of a Siemens gas turbine. A couple of two blades was modeled through a finite element code, to generate the model used to evaluate the forced response of the system considering the damper element coupling.

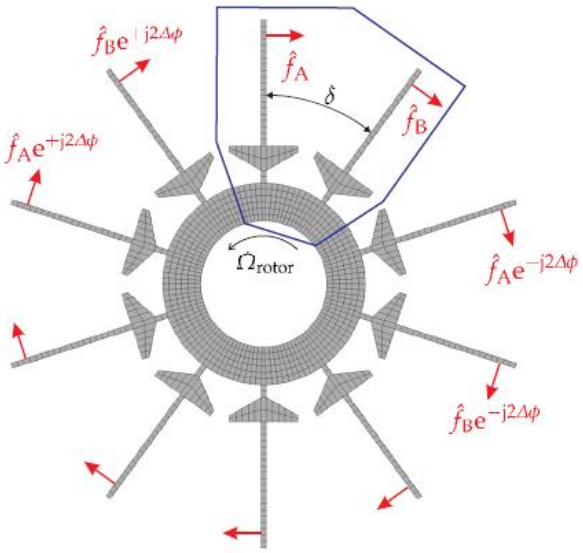

Figure 3.44 System of Blades with excitation force vector with A-B mistuning. Reprinted from [13].

The non-linear contribution of the contact force depends on the relative displacement between the contact interfaces; the contact zone has been modeled through the use of 3D point contact model. The FRF were performed with a simple blade disk, taking into account the first bending mode of the blade. In the first test, the centrifugal force acting on the underplatform damper is used as the variation parameter. After that the mistuning between the blades is obtained by the introduction of a point mass (5g) on the first blade of the disk. The consequence of the application of the mistuning between the blades is represented by an increase of the amplitude of the blade A and a decrease of the blade B.

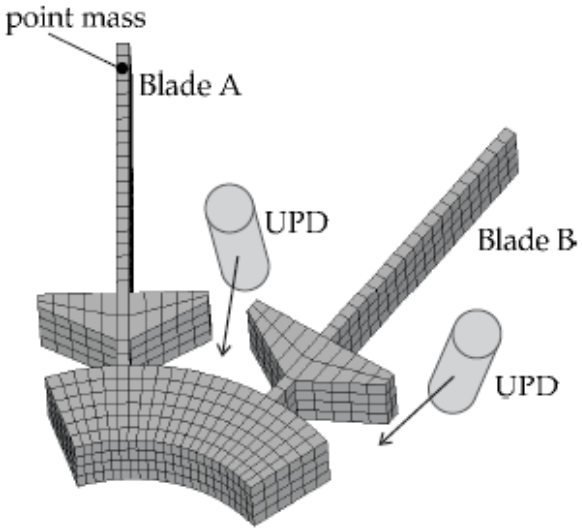

Figure 3.45 Application of the mistuning on blade A. Reprinted from [13].

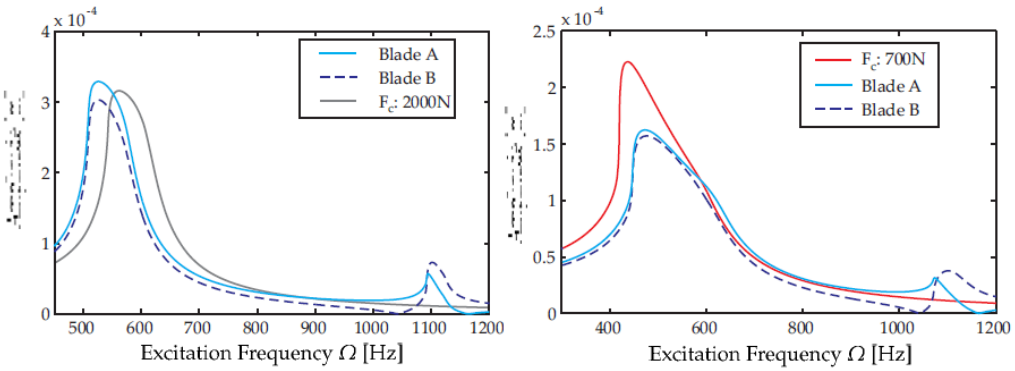

Figure 3.46 FRF of blades A and B, effect of the centrifugal force and the application of the mistuning. Reprinted from [13].

In the second part of the paper, a system of two real blades has been studied taking into account the effects of an underplatform damper with friction contact on the blades non-linear response.

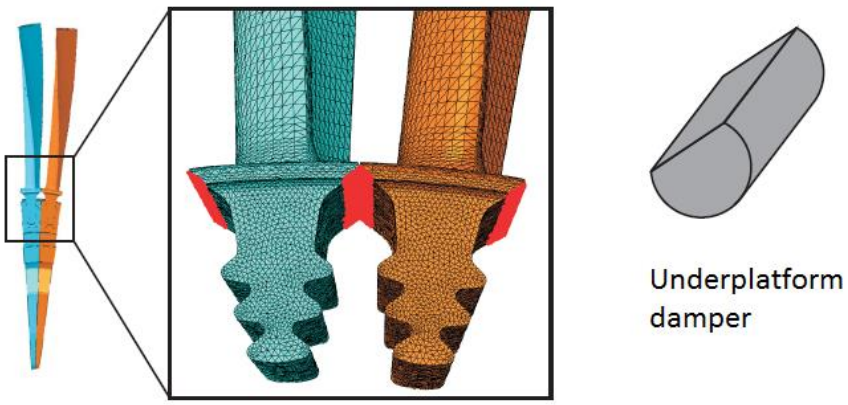

Figure 3.47 System of two blades plus underplatform damper analyzed by DATAR code. Reprinted from [13].

The forced response calculation has been performed through DATAR code taking into account different EO = N/4, i.e. engine order with N number of blades, for the first two modes in order to compare the frequencies with the measured data. Performance curves are plotted for the first mode, showing the influence of the external excitation on the frequencies of the blades. The measurement has been performed for two values of EO:

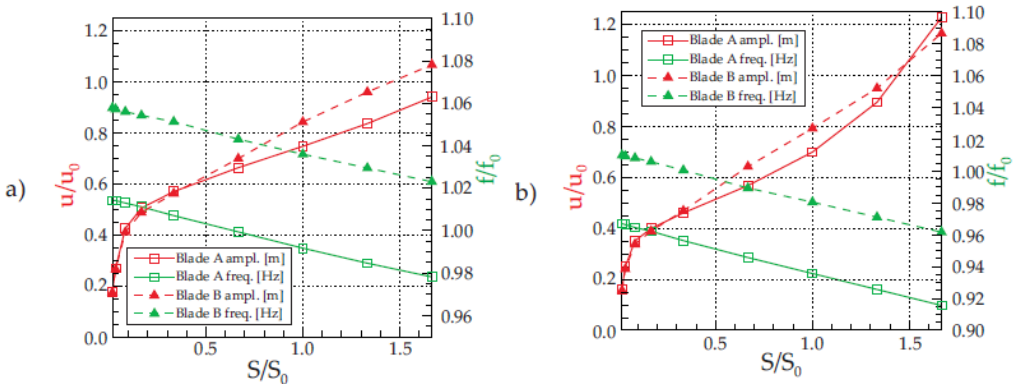

Figure 3.48 Performance for mode 1 for different value of EO. Reprinted from [13].

The forced response for modes 1 and 2 are shown for the relevant stimulus S_0 where the coupling between blades A and B is very marked for mode two by the presence of the double peak. The resulting Campbell diagram shows the comparison between the predicted and the measured blades frequencies. Frequencies are normalized with respect to the predicted static test frequency of mode 1, while rotational speed and power are normalized respectively to the nominal speed and the base load power. It is shown that the prediction matches well the test results for mode 1 and 2, and the difference increases for higher EO.

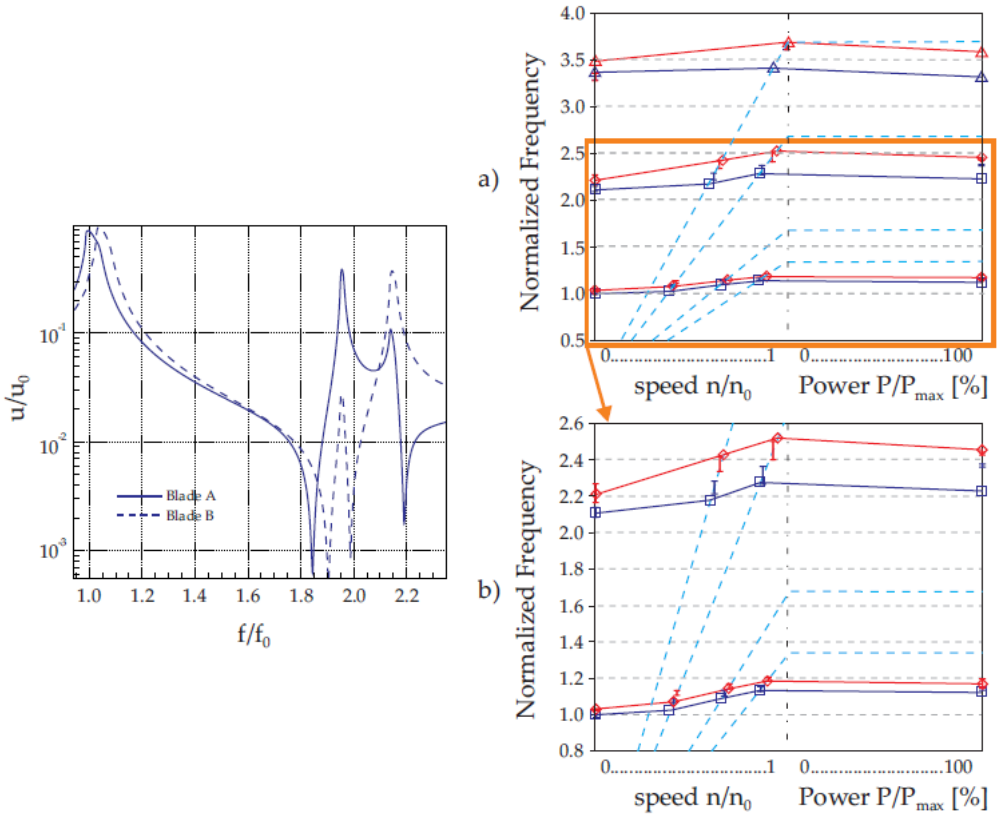

Figure 3.49 Frequency response of the system of two blades and Campbell diagrams. Figure a comparison between mode 1-3, Figure b comparison between mode 1 and 2. The red curve represents the blade A, the blue curve blade B. Reprinted from [13].

The paper shows that the forced response calculation using the mistuned double blade model matches the measured values in a good manner especially for mode 1. The effects of the excitation stimulus are shown by the performance curves for both the blade types whereas the amplitude of blade A becomes lower than blade B for higher external stimulus.

3.3.2.2. Underplatform damper

Nowadays different kinds of configurations for underplatform damper have been studied in order to develop models to be included in numerical solver to characterize the damper behavior during the blade vibration.

During vibration, energy is dissipated by friction at the contacts which can be either a line or a surface, and the normal load acting on the contact becomes a function of the centrifugal force and consequently of the damper mass. The slipping condition with consequent energy dissipation may be prevented by a too large mass of the damper or in the opposite case, a too small mass can cause the damper lift off from the blades. The damper model used in this analysis is essentially an asymmetric underplatform damper characterized by a flat surface and a cylindrical one. It follows that the damper will be in contact with the blades with a line contact on the right side and a flat contact on the left one. As already specified in the description of the model all the blades are designed with particular corners to maintain the damper in the correct position.

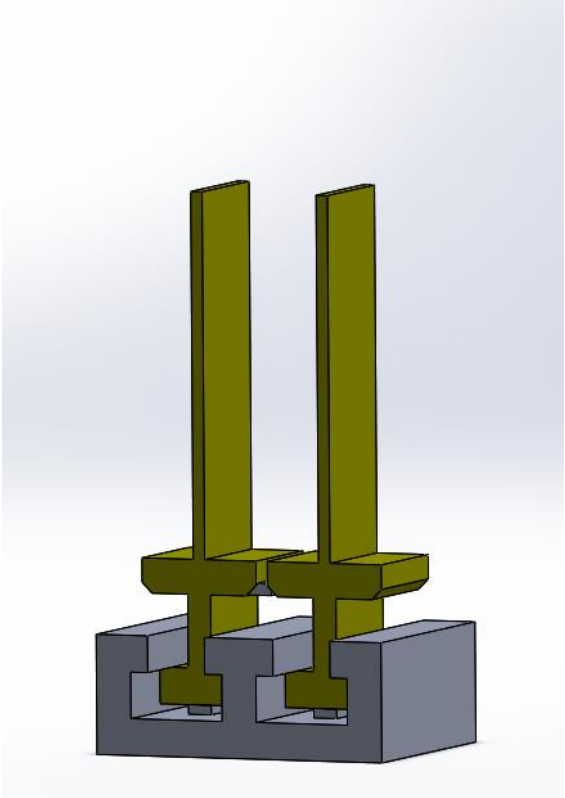

Figure 3.50 System of two blades and an underplatform damper, Solidworks.

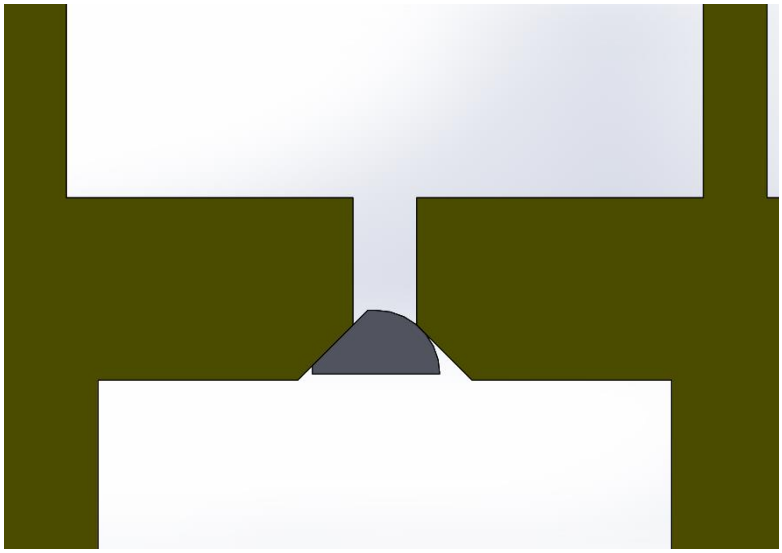

Figure 3.51 Zoom, underplatform damper in contact with the blades.

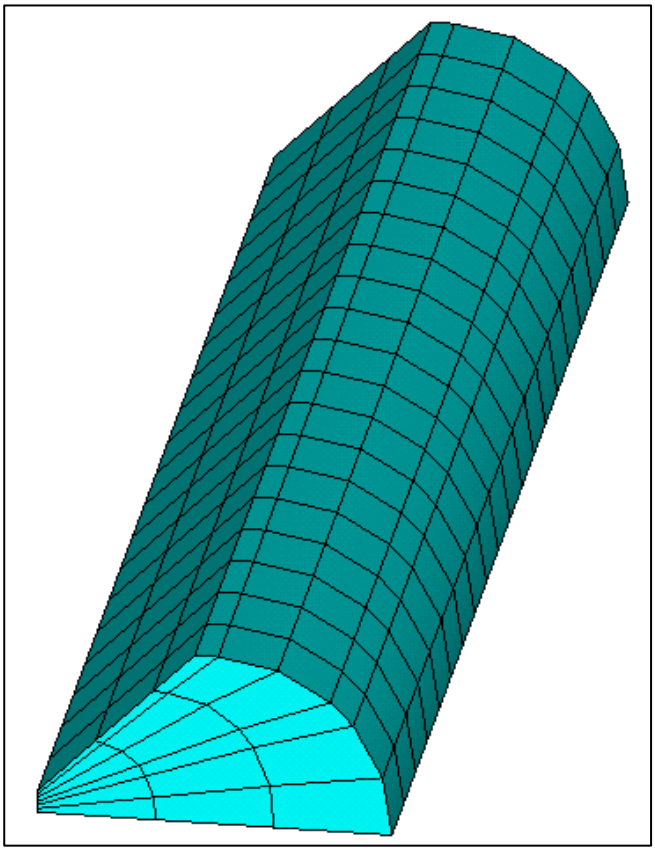

Figure 3.52 Underplatform damper, finite element model in Ansys.

3.3.2.3. Finite element model

The initial step to be performed to study the non-linear forced response of the system of two blades is the development of a finite element model of the structure very similar to the one already introduced in chapter 3.3.1. The only difference is related to the presence of the damper which will not be connected to the structure with traditional contact elements since the contact will be directly introduced in a purposely developed Matlab code. The FEM model has been created in Ansys environment as shown in Figure 3.53.

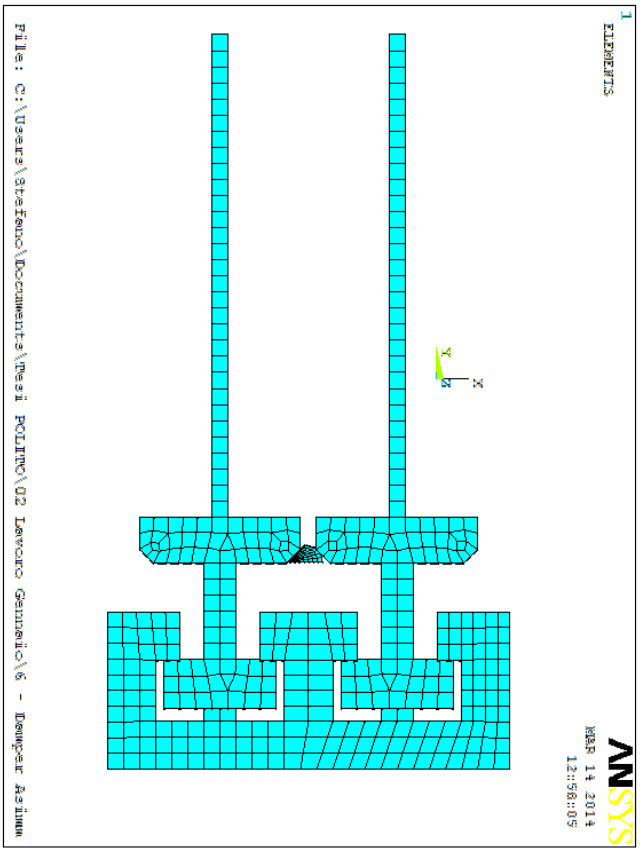

Figure 3.53 FEM of the structure for non linear analysis, Ansys.

As always in this thesis the finite element model is built in Ansys environment and the exported to another program to perform the calculation. In this case, the non-linear analysis is performed with a purposely developed Matlab code which works simultaneously with the one used to compute the linear response of the system introduced in paragraph 1.1.1.1.

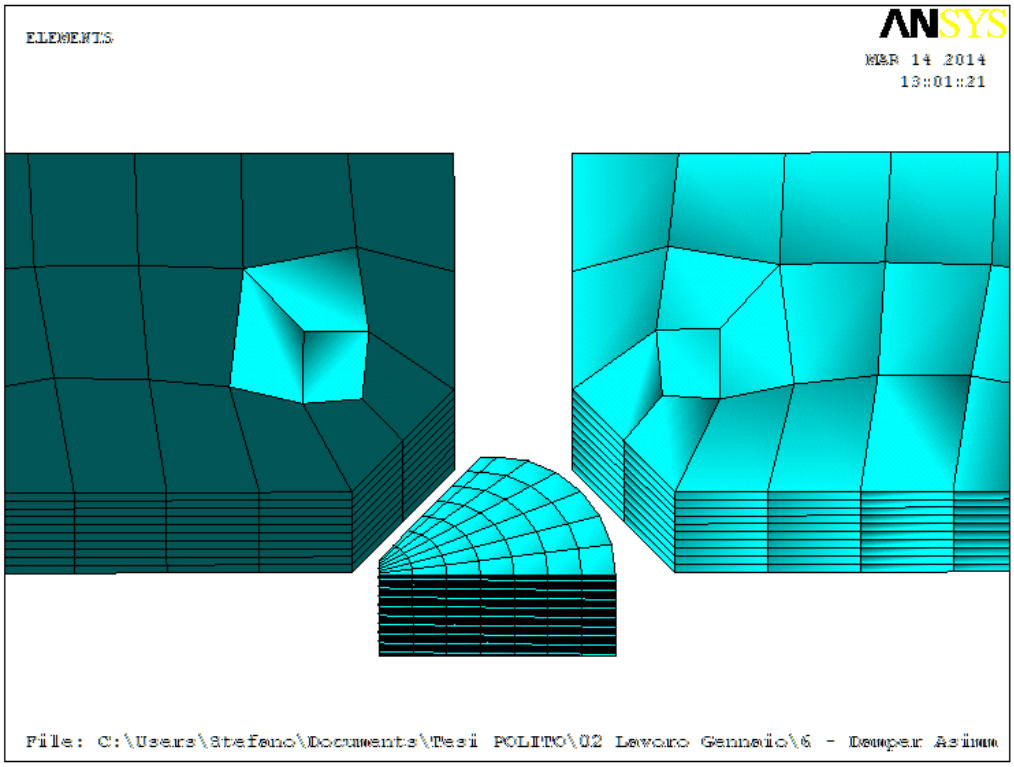

Figure 3.54 Underplatform damper, FEM model in Ansys.

Figure 3.54 shows the model of underplatform damper used to develop the calculation. Instead of using a symmetric solution with two flat surfaces in contact with the

blades, it had been decided to take an asymmetric underplatform damper with a flat surface in contact with the left blade and a cylindrical one in contact with the right blade. It follows that the contact on the right side will be a line.

3.3.2.4. Balance equations and harmonic balance method

Let's now consider the system of the blades in contact with the underplatform damper, the balance equation for the blades can be written in the following way:

$$\mathrm{M}\,\ddot{\mathrm{Q}}(\mathrm{t}) + \mathrm{C}\,\dot{Q}(\mathrm{t}) + \mathrm{K}\,\mathrm{Q}(\mathrm{t}) = \mathrm{F}_e(t) + \mathrm{F}_D(t) \qquad 3.10$$

Where M, C and K represent the mass, the damping and the stiffness matrix of the blades, Q is the vector of the system degrees of freedom, $\mathrm{F}_e(t)$ is the harmonic excitation force and F_D is the non linear force which arises from the contact between the blades and the damper, caused by the relative displacements between the two bodies. In order to reduce the amount of calculations, the HBM, harmonic balance method, can be used to compute the response of the system. Based on the assumption of the presence of an external excitation, the periodical displacements and the contact forces can be approximated with a first order Fourier series, reducing the second order differential equation of motion in non-linear algebraic equations.

$$\mathrm{Q}(\mathrm{t}) = \mathrm{Q}^{(0)} + R\left(\mathrm{Q}^{(1)} e^{i\omega t}\right) \qquad 3.11$$

$$\mathrm{F}_D(\mathrm{t}) = {\mathrm{F}_D}^{(0)} + R\left({\mathrm{F}_D}^{(1)} e^{i\omega t}\right) \qquad 3.12$$

It follows that:

$$\mathrm{KQ}^{(0)} = +\mathrm{F}_D{}^{(0)} \tag{3.13}$$

$$\mathrm{D}(\omega) = K + i\omega C - \omega^2 M \tag{3.14}$$

$$\mathrm{D}(\omega)\mathrm{Q}^{(1)} = F_e + \mathrm{F}_D{}^{(1)} \tag{3.15}$$

$\mathrm{D}(\omega)$ represents the dynamic stiffness matrix, while equation 3.9 represents the static balance of the blade and equation 3.11 the first term of the dynamic balance. The same considerations can be done in the case of the damper paying attention on the fact that in order to have a consistent model, all the contact nodes lying on the contact surfaces on the blades' platforms must be coincident with the ones lying on the damper contact surfaces. This constrain makes mandatory the presence of specific discretization in which the same finite elements are used to discretize the structure in order to impose the coincidence of the nodes. The damper equations of motion can be written in a similar way to the blades one with M_D, C_D and K_D mass, damping and stiffness matrices of the damper, Q_D vector of the damper degrees of freedom, $\mathrm{F}_D(t)$ the contact forces exerted by the blade against the damper and finally F_C the centrifugal force which presses the damper against the blades.

$$\mathrm{M}_D\,\ddot{\mathrm{Q}}_D(\mathrm{t}) + \mathrm{C}_D\,\dot{Q}_D(\mathrm{t}) + \mathrm{K}_D\mathrm{Q}_D(\mathrm{t}) = \mathrm{F}_C - \mathrm{F}_D(t) \tag{3.16}$$

By the application of the HBM method the second order differential equation is reduced to a system of non-linear algebraic equations.

$$\mathrm{Q}_D(\mathrm{t}) = \mathrm{Q}_D{}^{(0)} + R\left(\mathrm{Q}_D{}^{(1)} e^{i\omega t}\right) \quad 3.17$$

$$\mathrm{F}_D(\mathrm{t}) = \mathrm{F}_D{}^{(0)} + R\left(\mathrm{F}_D{}^{(1)} e^{i\omega t}\right) \quad 3.18$$

$$\mathrm{K}_D \mathrm{Q}^{(0)}{}_D = F_C - \mathrm{F}_D{}^{(0)} \quad 3.19$$

$$\mathrm{D}_D(\omega) = K_D + i\omega C_D - \omega^2 M_D \quad 3.20$$

$$\mathrm{D}_D(\omega)\mathrm{Q}_D{}^{(1)} = -\mathrm{F}_D{}^{(1)} \quad 3.21$$

with D_D dynamic stiffness matrix of the damper. In order to solve the non-linear balance equations, a contact model must be computed. Equations 3.11 and 3.17 can be re-written in terms of the receptance matrices of the blades and the damper, $\mathrm{r}_B$and r_C.

$$\mathrm{Q} = \mathrm{r}_B F_e + \mathrm{r}_B F_D \quad 3.22$$

$$\mathrm{Q}_D = -\mathrm{r}_D F_D \quad 3.23$$

Dividing the degrees of freedom of the system in contact C, and non-contact NC dof, the following system of equations can be written:

$$\mathrm{Q}_{B,C} = \mathrm{r}_B{}^{(C,F)} F_e + \mathrm{r}_B{}^{(C,C)} F_D \quad 3.24$$

$$\mathrm{Q}_{B,NC} = \mathrm{r}_B{}^{(NC,F)} F_e + \mathrm{r}_B{}^{(NC,C)} F_D \quad 3.25$$

$$\mathrm{Q}_{D,C} = -\mathrm{r}_D{}^{(C,C)} F_D \quad 3.26$$

$$Q_{D,NC} = -\,r_D{}^{(NC,C)}\,F_D \qquad 3.27$$

With $r_B{}^{(C,F)}$ receptance of the blade contact points due to the external force, $r_B{}^{(C,C)}$ receptance of the blade contact points due to the contact forces, $r_D{}^{(C,C)}$ receptance of the damper contact nodes due to contact forces, $r_B{}^{(NC,F)}$ and $r_B{}^{(NC,C)}$ receptances of the blades non-contact points due to the external forces and contact forces and finally $r_D{}^{(NC,C)}$ the receptance of the damper non contact points due to the contact forces.

3.3.2.5. Contact model

In literature, four different kinds of contact models [7] are present to evaluate the forced response of a mechanical system with friction contact:

- 1D contact with constant normal load and tangential relative displacement.
- 1D contact with variable normal load with tangential relative displacement.
- 2D contact with constant normal load and tangential relative displacement.
- 2D contact with variable normal load with tangential relative displacement.

In the evaluation of the non-linear dynamics of the turbine blade model it is necessary to take into account the partial separation of the damper from the blades platforms and the possible variation of the normal load. This is the reason why the first and the third contact model have been excluded from the choice. In addition to this, however the fourth model seems to be the more complete, its huge computational cost keeps it out from the possible solution. It follows that a 1D contact model with variable normal load and tangential relative displacement will be used for the calculation. In order to take into account the motion of the damper, two 1D model will be combined together to create a 2D model suitable for the application. In this way the two perpendicular slip directions are uncoupled to each other. Finally this kind of contact model will be used to connect each node of the damper with the corresponding blade node.

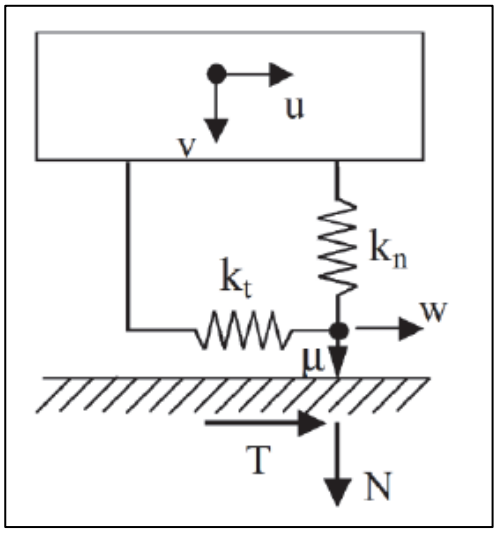

Figure 3.55 2D contact model for non linear dynamic analysis. Reprinted from Stefano Zucca, Christian M. Firrone, Muzio Gola. *Modeling underplatform dampers for turbine blades: a refined approach in the frequency domain*. Journal of Vibration and Control, 2012: 1-16.

According to this model shown in Figure 3.55, the tangential and contact stiffness are modeled as springs of stiffness k_t and k_n with a friction coefficient μ between the surfaces. $u\ (t)$ and $v(t)$ represent respectively the relative motion in the tangential and normal direction, w the amount of slip and finally T and N the tangential and the normal contact forces. During a cycle three states are possible as shown in TABLE VI.

TABLE X CONTACT CONDITIONS.

CONTACT CONDITIONS		
1	**Stick**	T < μN
2	**Slip**	T > = μN
3	**Lift-off**	T,N = 0

In stick conditions, the contact point is fixed since the tangential force is lower than the Coulomb limit force, in slip the tangential force reaches and eventually overcomes the limit while in lif-off condition, there is separation of the parts. The normal contact load can be defined as:

$$\mathrm{N(t)} = \max[\mathrm{N}_0 + k_n \tilde{v}(t),\ 0] \tag{3.28}$$

Where N_0 is the static normal load due to the presence of the centrifugal force acting on the damper and pressing it against the blades without vibration, and $\tilde{v}(t)$ the harmonic relative displacement. The contact state determines the tangential contact force:

$$\mathrm{T(t)} = \begin{cases} k_t\big(u(t) - w(t)\big) & Stick \\ sgn\big(\dot{w}(t)\big)\mu\, N(t) & Slip \\ 0 & Lift - off \end{cases} \tag{3.29}$$

A preliminary static solution is usually performed in order to evaluate the static normal load preload acting on the contact. According to the HBM method the absolute displacement of the contact points is related to the harmonic term, and can be replaced in the definition of the contact forces. Considering a linear superposition of the 0st and 1st harmonic terms the relative displacements can be written as follow:

$$\mathrm{u(t)} = \mathrm{u}^{(0)} + R\big(\mathrm{u}^{(1)} e^{i\omega t}\big) \tag{3.30}$$

$$\mathrm{v}(\mathrm{t}) = \mathrm{v}^{(0)} + R\left(\mathrm{v}^{(1)} e^{i\omega t}\right) \qquad 3.31$$

with the terms with the superscript "0" indicating the static relative normal and tangential displacements between the bodies in contact. If $\mathrm{v}^{(0)} \geq 0$ the contact is reached otherwise the two bodies are separated.

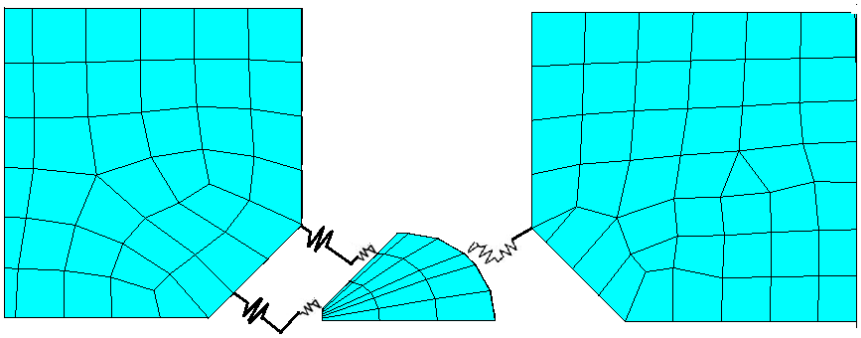

Figure 3.56 Contact between adjacent nodes.

However the problem deals with solid bodies the relative displacement along the direction parallel to the damper axis is neglected.

3.3.2.6. Model reduction and numerical solution

The non-linear behavior of the system can be obtained through the solution of the system of non-linear algebraic equations after the introduction of a 2D contact model. Since the size of the problem is very big according to the size of the finite element model, a reduction technique must be applied in order to minimize the calculation time. The same Craigh-Bampton method introduced in paragraph 3.3.1.2.1 has been used to drastically reduce the number of degrees of freedom.

The only difference with the preceding case is represented by the fact that in addition to the first reduction operated to the blades and the fixture, a second matrix reduction has been performed on the damper itself, taking into account its nodes in contact with the blade platforms. As already specified in the contact model, the contact nodes between the blades and the damper must be coincident. The blade and fixture matrix reduction involves 6 nodes of the structure and the first ten modes: one force node on the right blade, two nodes on the left platform, one on the right, and finally two nodes on the blades tips, one on the right and one on the left blade.

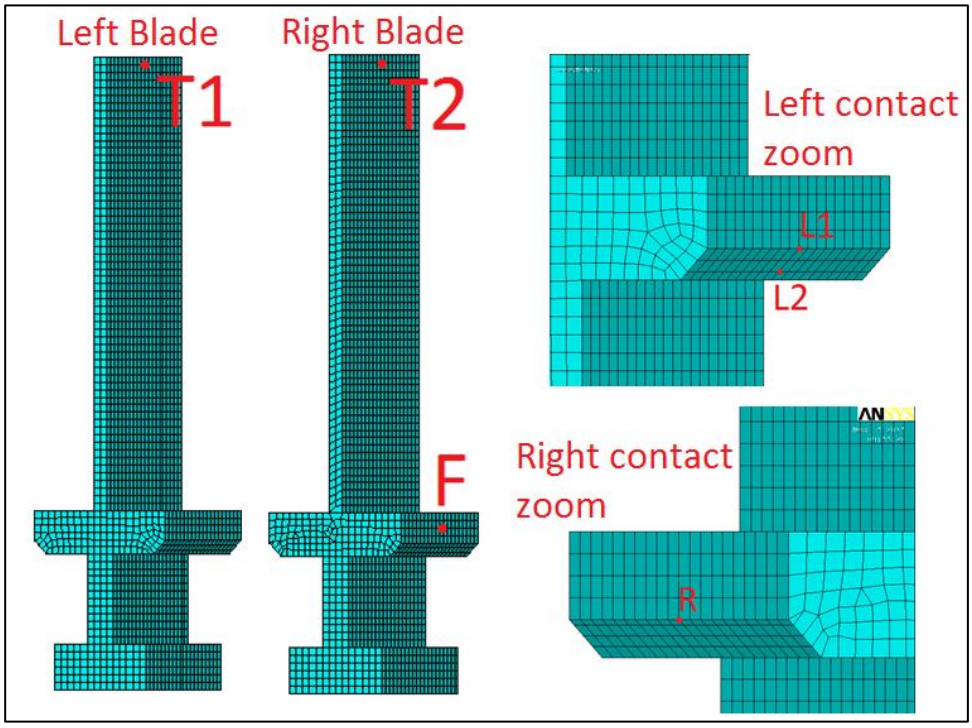

Figure 3.57 Matrix reduction in non linear analysis.

The same operation can be performed with the damper; in this case it is only interesting to take into account the contact nodes corresponding to the point $L1$, $L2$ and R. It is evident from the problem reduction that the problem of contact has been highly simplified introducing only two contact points on the left platform and one on the right one. This simplification is allowed by the fact that the relative displacement along the direction parallel to the damper axis has been considered negligible.

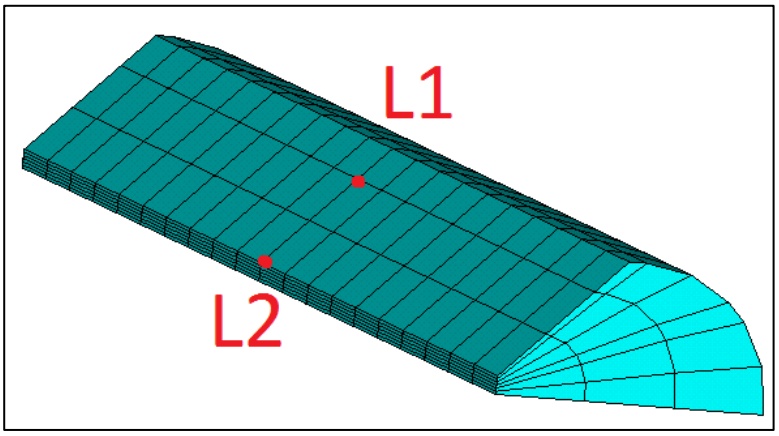

Figure 3.58 Damper discretization, left contac.

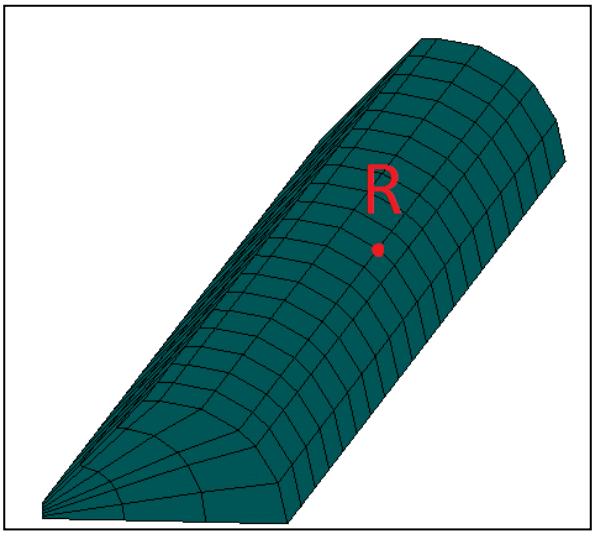

Figure 3.59 Damper discretization, right contact.

Once the reduction procedure has been concluded, all the set of equations must be solved numerically. The non-linearity has been introduced by the presence of the contact forces between the contact elements.

The numerical code computes the normalize modeshapes V and the natural frequencies of the model ω at the beginning of the solution loop in order to avoid the inver

sion of the dynamic stiffness matrices to get the receptance matrices and the coefficients of the receptance matrices are computed at each loop in the following way:

$$\mathrm{r} = \mathrm{V}(\Omega_n^2 - \omega^2 + 2i\mathfrak{Z}\Omega_n\omega)^{-1}\,\mathrm{V}^T \qquad 3.32$$

with Ω_n diagonal matrix of the natural frequencies and $\mathfrak{Z}$ modal damping. At this point an iterative solver is employed to solve the system. The equations of motion can be partitioned in real and imaginary parts as follow:

$$\begin{Bmatrix} R(Q_C) \\ I(Q_C) \end{Bmatrix} = \begin{bmatrix} R(r^{(C,F)}) & -I(r^{(C,F)}) \\ I(r^{(C,F)}) & R(r^{(C,F)}) \end{bmatrix} \begin{Bmatrix} R(F_e) \\ I(F_e) \end{Bmatrix} + \begin{bmatrix} R(r^{(C,C)}) & -I(r^{(C,C)}) \\ I(r^{(C,C)}) & R(r^{(C,C)}) \end{bmatrix} \begin{Bmatrix} R(F_D) \\ I(F_D) \end{Bmatrix}$$

3.33

Which can be condensed in the form to be solved in a frequency range $[\omega_i, \omega_f]$.

$$X = X_B + R_X\, F_{\,X}(X) \qquad 3.34$$

The resulting equation can be solved numerically by the use of the Newton Rapson Method rewriting the equation in the form $f(X) = 0$. The solution starts with an initial frequency guess and the calculation proceeds until the specified converge is reached. Then the frequency is increased of a certain step and the computation starts again. For the generic iteration i the equation becomes:

$$X_{i+1} = X_i - J(X_i)^{-1} f(X_i) \qquad 3.35$$

The time required by the numerical solver depends on the length of the frequency domain in which it is necessary to compute the forced response of the system. Obviously, an higher accuracy can be reached by reducing the frequency step in the application of the Newton Raphson Method increasing the number of computations and the time to reach the result.

3.3.2.7. Non-linear response of the system

The numerical simulation the non-linear response of the system of two blades connected through an underplatform damper is evaluated by the application of an external force used to excite the right blade, reproducing what would have been done in a real experimental measurement. As already anticipated in the brief introduction about the effect of the underplatform damper, the damper effects depend on both the damper material an damper geometry since the damper is pressed against the blades by the centrifugal force which arises during the disk rotation. The amount of force which affects the contact between the damper and the blades platforms determines the contact status and the amount of energy dissipated by friction. It is necessary to keep in mind that the main goal of the damper is to dissipate energy through friction in order to avoid the blades to reach the dangerous resonance conditions during the rotation of the disk.

The system response has been evaluated through a purposely developed Matlab code in which it is supposed to excite the right blade by the application of an external force which ranges from 5 to 300 N. For sake of simplicity, the centrifugal force acting on the damper is maintained constant and equal to 300 N. Since the numerical calculation requires a long time and it is more interesting to focus especially on the first and the second mode shapes, the frequency range in which the simulation has been performed is chosen between 170 and 190 Hz.

From paragraph 3.1 was shown that the mode shapes of the blades are always coupled in “in-phase”, IP, and “out-of-phase”, OOP, motions, i.e. in the IP condition the difference between the two phases of the blades oscillation is zero while in the OOP condition the difference between the two phases is equal to π radiants. In this simulation it will

be shown how the motion IP and OOP will be differently affected by the non linear behavior of the system and by the variation of the excitation force. It is also expected that for a very high value of the external force Fe the damper reaches the stick condition and the response of the blades becomes equal to the one reached in the linear response as if the damper is not presence between the blades. On the other and the value of the centrifugal force must be sufficient to prevent the separation of the damper.

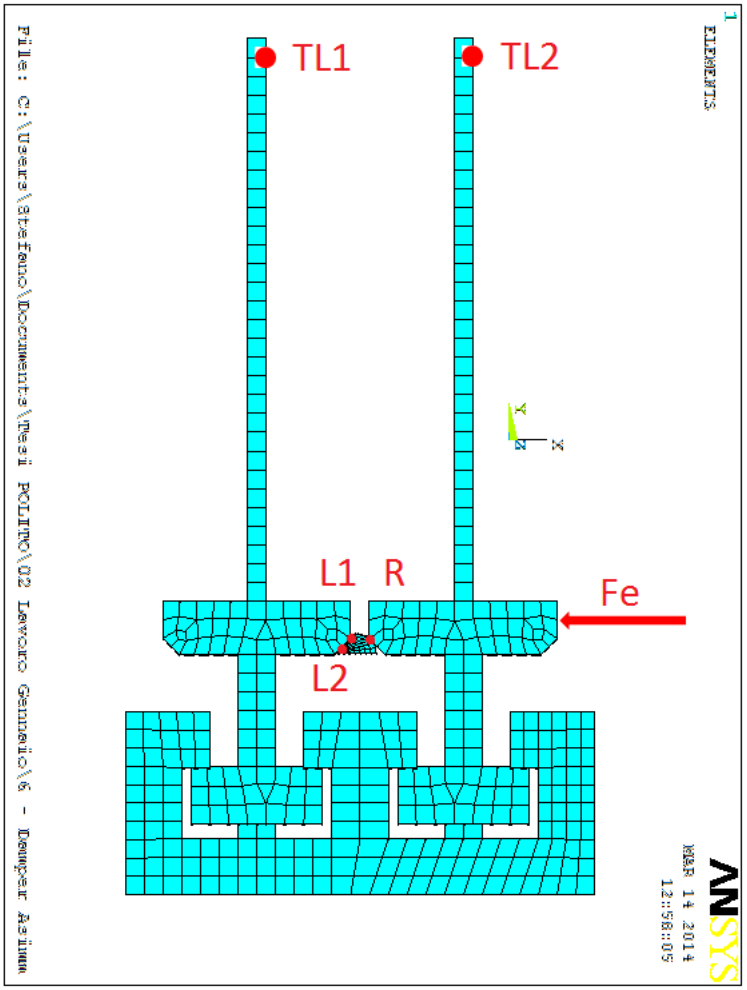

Figure 3.60 Non-linear analysis, application of the external force vector.

As already done in the linear response of the blade, it would be interesting to focus the attention on the blades tips, and particularly on the x-axis displacement of the right tip TL2, since the right blade is the one subjected to the excitation force and the most important motion is the one in the xy plane . The decision to plot only one node is enforced by the attempt to make the graphical representation as clear as possible.

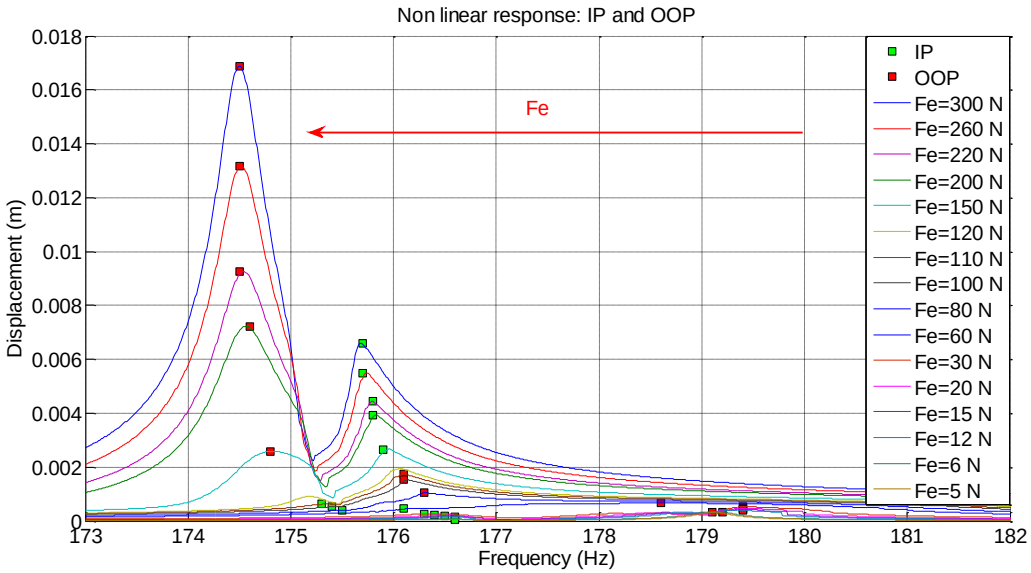

Figure 3.61 Non-linear response of the right tip TL2, IP and OOP.

Figure 3.61 shows the effect of an increasing external force vector applied to the right blade: for higher value of Fe, the system response is very similar to the one obtained in the linear response since the stick condition is reached. As soon as Fe decreases the amplitude of the peak decreases and the frequency of resonance increases moving the peak on the right. It is also possible to focus on the different behavior of the IP and OOP peaks: the OOPs seem to be more influenced by the external force and the contact condition that the IPs.

For higher clarity it would be of great interest to plot the same graph normalizing the frequency response with respect to the external force vector focusing the attention to the peaks behavior.

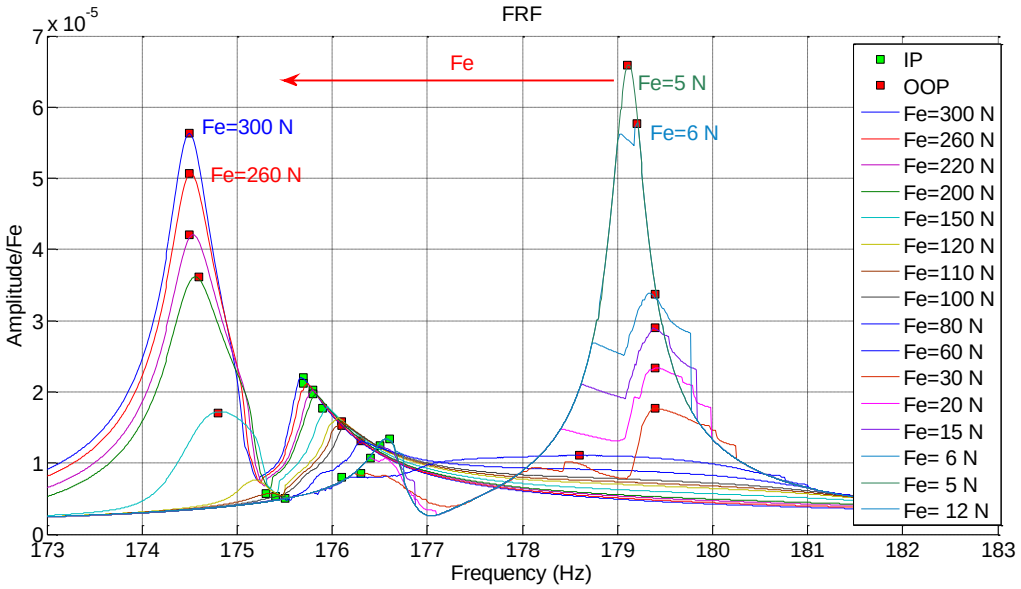

Figure 3.62 FRF right tip TL2, IP and OOP peaks.

Introducing the free response of the blade, it will appear very similar to the non-linear response of the blade for $Fe = 300\ N$ where the damper reaches the stick condition.

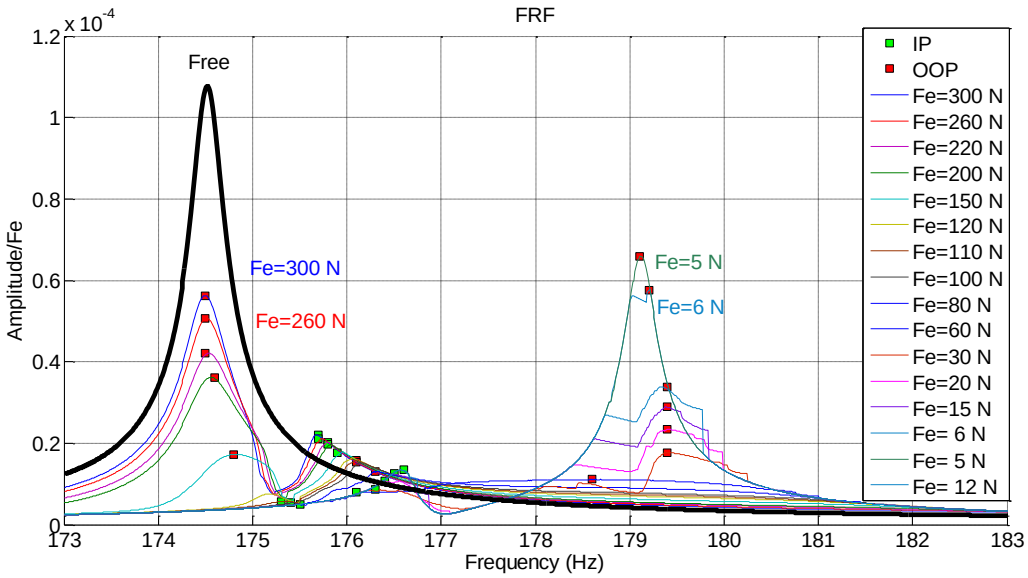

Figure 3.63 FRF with free response, right tip TL2.

Figure 3.63 shows the comparison between the system behavior with and without the damper. It is possible to see that as the external excitation force increases the contact reaches the slip condition and the system response becomes non-linear. For higher values of Fe, the system behavior tends to the linear one. TABLE XI contains all the information relatively the IP and OOP peaks of the system which can be plotted tracing the performance of the damper.

TABLE XI IP AND OOP PEAKS IN THE NON LINEAR FORCED RESPONSE, RIGHT TIP TL2.

IP AND OOP IN NON LINEAR FORCED RESPONSE							
Fe (N)	**Fc/Fe**	**IP (Hz)**	**Amplitude (m)**	**Amp/F (m/N)**	**OOP (Hz)**	**Amplitude (m)**	**Amp/F (m/N)**
300	1	175,7	0,00660500	0,00002202	174,5	0,01689000	0,00005630
260	1,1538	175,7	0,00550200	0,00002116	174,5	0,01318000	0,00005069
220	1,3636	175,8	0,00445800	0,00002026	174,5	0,00925900	0,00004209
200	1,5	175,8	0,00393900	0,00001970	174,6	0,00723100	0,00003616
150	2	175,9	0,00266400	0,00001776	174,8	0,00256300	0,00001709
110	2,7273	175,3	0,00062820	0,00000571	176,1	0,00174000	0,00001582
100	3	175,4	0,00053800	0,00000538	176,1	0,00152600	0,00001526
80	3,75	175,5	0,00039970	0,00000500	176,3	0,00104700	0,00001309
60	5	176,1	0,00048060	0,00000801	178,6	0,00066500	0,00001108
30	10	176,3	0,00025710	0,00000857	179,4	0,00053140	0,00001771
20	15	176,4	0,00021410	0,00001071	179,4	0,00046800	0,00002340
15	20	176,5	0,00018770	0,00001251	179,4	0,00043420	0,00002895
12	25	176,6	0,00016100	0,00001342	179,4	0,00040520	0,00003377
6	50	176,6	0,00008047	0,00001341	179,2	0,00034580	0,00005763
5	60	176,6	0,00006707	0,00001341	179,1	0,00032970	0,00006594

In order to show how the IP and OOP peaks are differently influenced by the presence of the damper, it could be of great interest tracing the performances of the peaks in terms of resonance frequency and resonance amplitude with respect to the value of the external force used to excite the system. The same scale has been used in the graph to focus on the differences between the two cases.

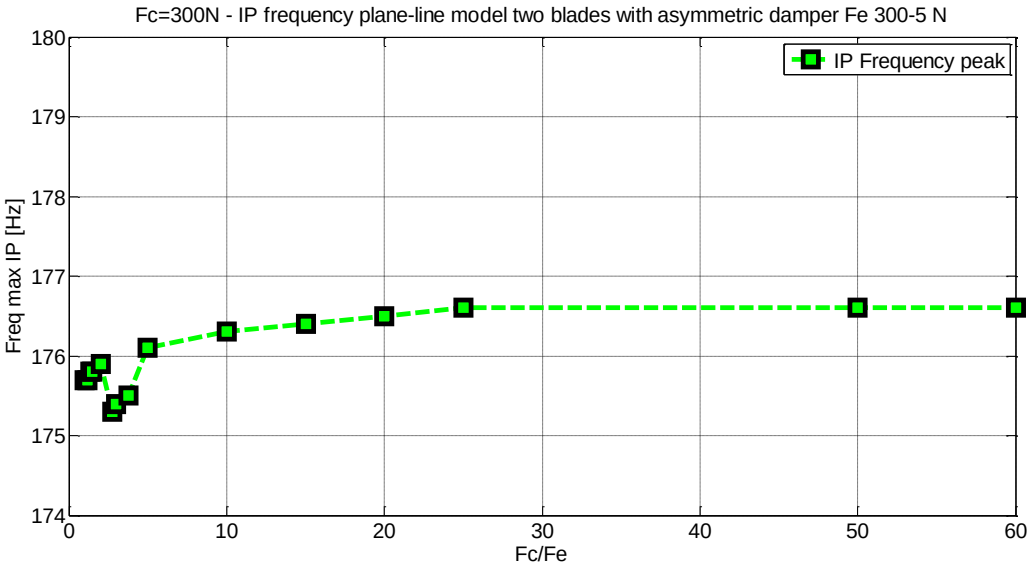

Figure 3.64 IP performance, resonance frequencies vs excitation force.

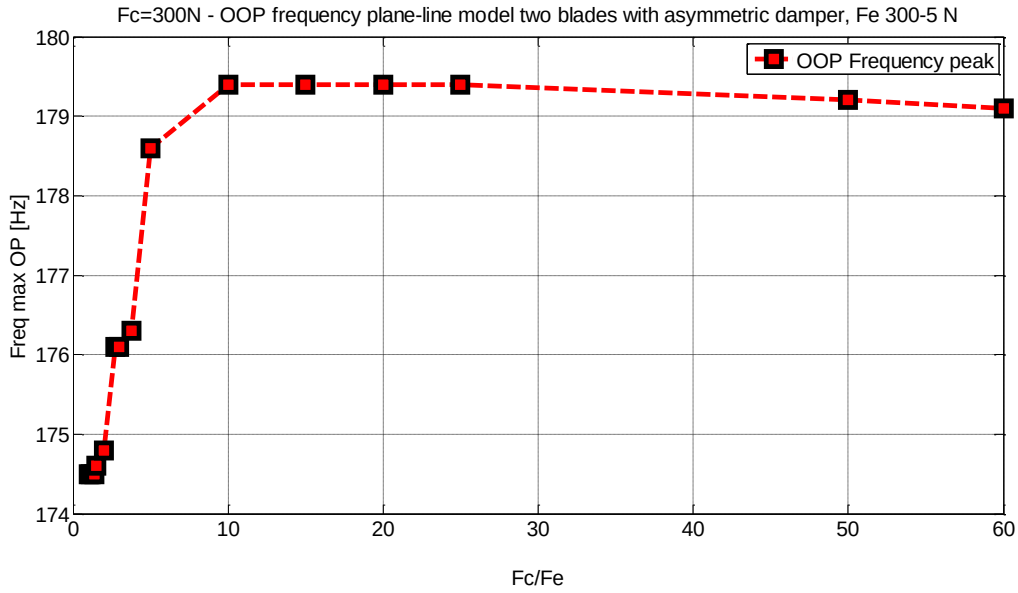

Figure 3.65 OOP performance, resonance frequencies vs excitation force.

The first couple of graphs shows what happens to the resonance frequencies of the IP and OOP peaks in terms of the excitation force. It is important to pay attention on the

fact that the abscissa reports the ratio between the centrifugal force, constant, and the external force, variable. The amount of change in the frequencies is very small with the IPs while it becomes more significant with the OOPs influenced by the non linearities introduced with the contact.

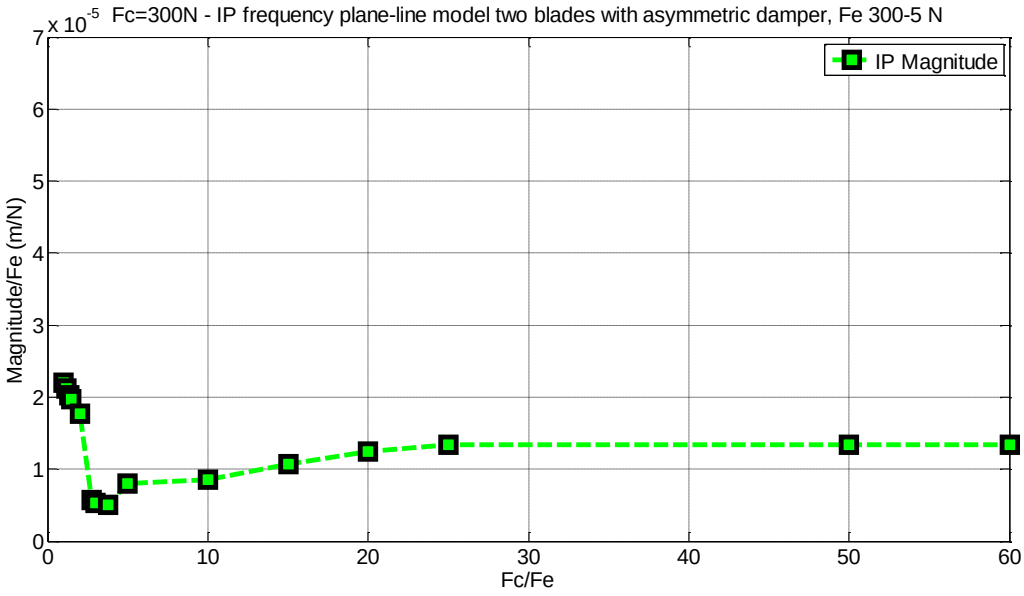

Figure 3.66 IP performance, resonance amplitude vs excitation force.

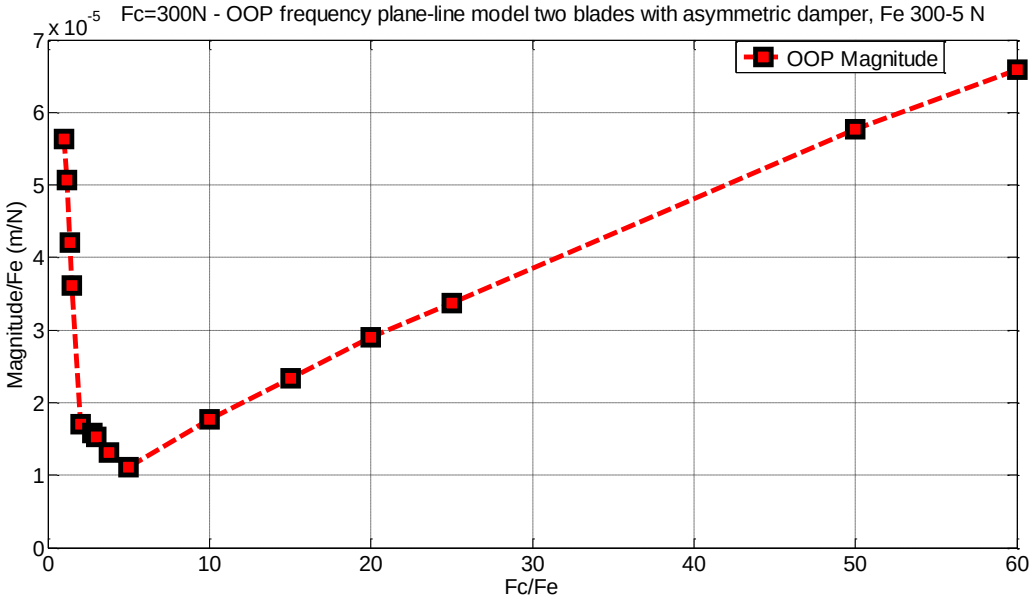

Figure 3.67 OOP performance, resonance amplitude vs excitation force.

Figure 3.66 and Figure 3.67 show the resonance amplitude normalized with respect to the external force vector plotted versus the ratio between centrifugal and external force for both the IP and OOP peaks. Also in this case, the OOPs' behavior is more interesting since the effect of the non-linearity and the change of the external force become more important on the resonance magnitude.

3.4. Forced response in time domain

The analysis of the forced response of the system of two blades and the damper in the frequency domain has been performed to give a brief introduction about the problem of the non-linearitiy due to the presence of a frictional contact between blades and damper paving the way to numerical analysis of the same system defined in time domain. Starting from the same physical parameters already introduced in the frequency domain, the system of two blades and the damper has been studied by the application of a numerical scheme, Newmark, used to apply direct time integration [16]. For sake of simplicity the damper introduced in the model is considered as a rigid body able to rotate and translate.

Direct time integration usually requires a very long computation time due to the dimension of the physical problem and to the need of satisfying a certain tolerance in order to make the iteration proceeding. In this chapter a numerical simulation of the linear and non-linear behavior of the system will be shown by the application of the iterative Newmark method, used to integrate the equation of motion of the system. Due to the complexity of the physical problem the same reduced element matrices already obtained in Ansys will be used in the computations.

3.4.1. Linear forced response

The linear forced response of the system is used to evaluate how the system reacts under the application of an external harmonic force. Since the linear response of the system has already been evaluated in two different ways in the frequency domain, it could be of great interest to reproduce the same physical environment in order to compare the results of the time integration method with the preceding one.

It follows that the same reduced model of the system of two blades is used in order to integrate the second order differential equation of motion of the system. Since the reduced model had considered 6 nodes and 10 modes, the reduced matrix have a size of 28x28.

$$M\ddot{U}(t) + C\dot{U}(t) + KU(t) = Fe(t) \qquad 3.36$$

Where M, C and K respectively represent the mass, the damping and the stiffness matrix of the system. The mass and the stiffness matrices have been obtained by the application the Craigh-Bampton method already explained in subsection 3.3.1.2.1, while the damping matrix of the system has been evaluated by the use of the definition of proportional damping [16], i.e. the damping matrix is calculated as a linear combination of the mass and the stiffness matrices with two premultiplying coefficients which depend on the modal damping the and the natural frequencies on which it is necessary to apply the damping.

$$C = a_0 \cdot M + a_1 \cdot K \quad (3.37)$$

$$a_0 = \frac{2\omega_1\omega_2}{\omega_1+\omega_2}\zeta \quad (3.38)$$

$$a_1 = \frac{2}{\omega_1+\omega_2}\zeta \quad (3.39)$$

With ω_1, ω_2 the first and the second natural frequencies and $\zeta = 0.001$ the modal damping already applied in the frequency domain. The application of the time integration becomes possible choosing a wright value of the time vector and the timestep. In order to consider the response of the system as a multiple of the period of its harmonic response, the total time of integration has been chosen as a multiple of the period of the external harmonic force, and the timestep as a certain percentage of it. In this way, with no dependence on the excitation frequency, the number of steps during which the integration is performed, remains constant.

$$\omega = 2\pi f \quad (3.40)$$

$$tmax = n \cdot \frac{1}{f} \quad (3.41)$$

$$dt = k \cdot \frac{1}{f} \quad (3.42)$$

Where f represents the excitation frequency of the harmonic external force, n the number of cycles used to perform the simulation and dt the length of the timestep, defined as a percentage of the period. As already anticipated in the introduction, Newmark

method is the numerical scheme used to perform the simulation; since the case of study is perfectly linear, the coefficient to solve the calculation are chosen to have the method unconditionally stable, i.e. the convergence of the method is not influenced by the length of the timestep. The only problem that arises in the numerical analysis is the presence of a transient state that takes a certain number of cycles before completing with the consequence of a longer time to perform the simulation in order to be sure to get to the steady state. The scheme used to perform the simulation is equal to the one already introduced in paragraph 3.3.1, with an external force of 5 N acting on the right blade.

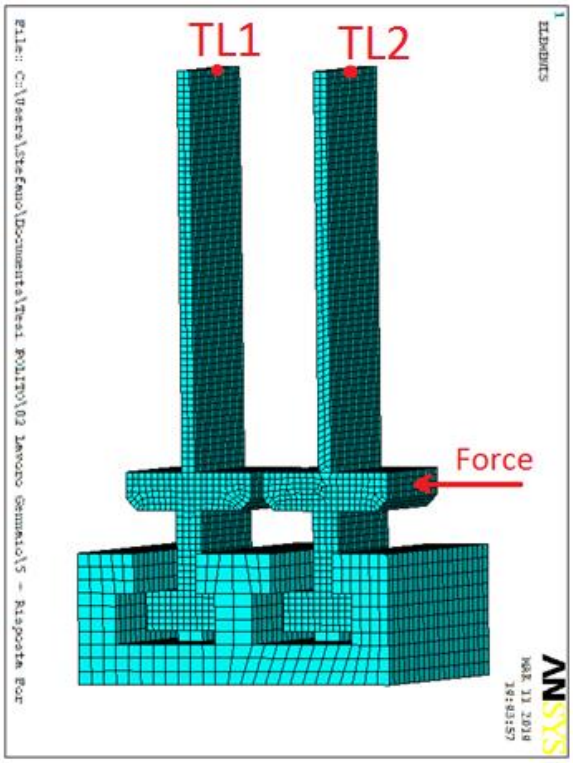

Figure 3.68 Linear forced response in time domain, FEM model.

Plotting the displacement along the x-axis of the right tip it is possible to see that the displacement is harmonic as the external excitation force, defined as a sinusoid.

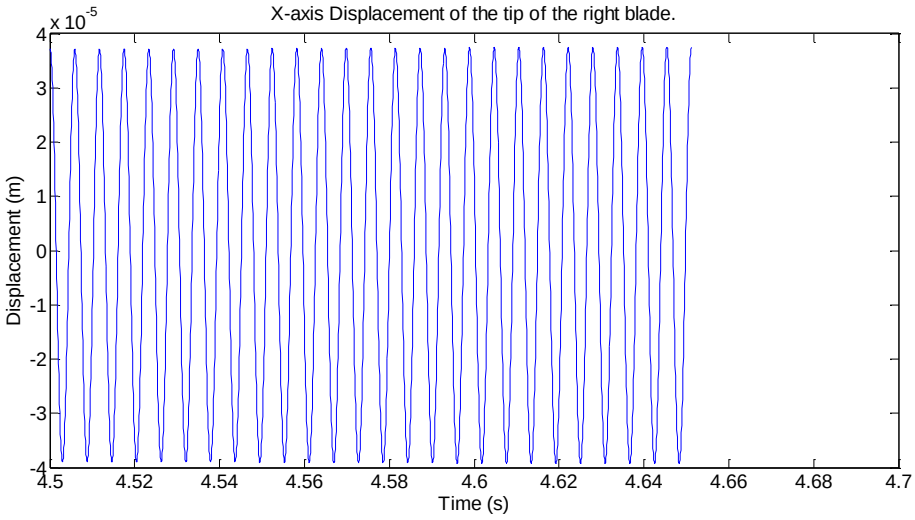

Figure 3.69 X-axis displacement, right tip

The only problem related with the time domain direct integration is related to the evaluation of the FRF, frequency response function used to compare the results with the one obtained through the commercial codes. Starting from a signal defined in time domain, i.e. the displacement of the tip, it is firstly necessary to evaluate its FFT, Fast Fourier transform, in order to know the amplitude of the response of the blade's tip, at a certain excitation frequency. It follows that, in order to build a complete FRF which ranges around the first resonance frequency of the blade, it is necessary to perform a very large number of simulation, varying the excitation frequency from the initial value of the interval of the FRF to the final one, i.e. from 170 to 190 Hz.

Choosing a frequency step of 0.1 Hz the simulation has been performed in exciting the blade with an external force of amplitude 5 N, as a harmonic wave with a frequency of 170 Hz. The displacement vector as well as the time vector has been saved, and a new time integration is performed increasing the frequency of the external force of the frequency step. Once the 100 time integrations have been completed, the FRF of the system is evaluated with the numerical procedure obtained in Matlab.

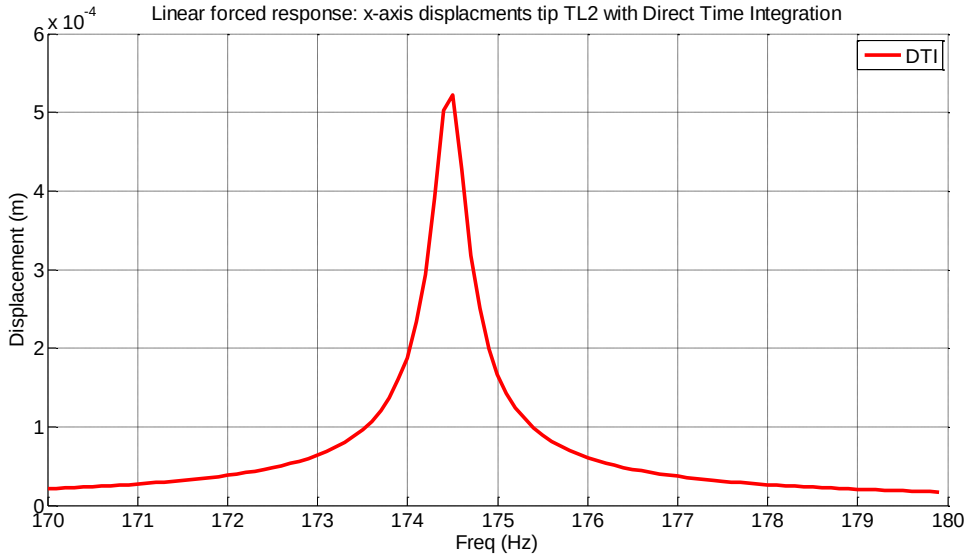

Figure 3.70 Linear forced response from time integration.

The results is verified comparing it with the solution obtained in Ansys and in the other Matlab code; the resonance frequency is exactly 174.5 Hz, equal to the one evaluated in the modal analysis.

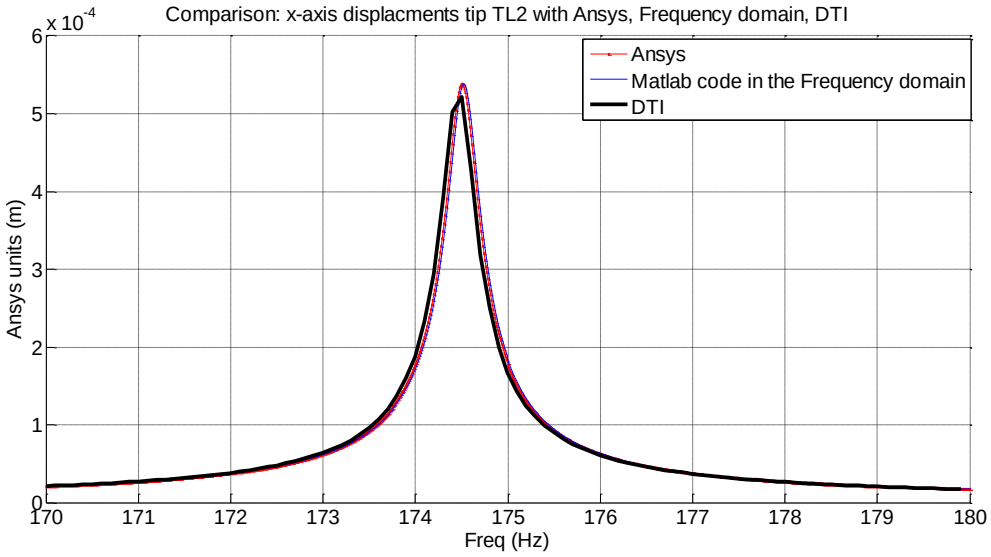

Figure 3.71 Linear forced response comparison.

Looking at Figure 3.71, the comparison shows that the forced response obtained through direct time integration is equivalent to the one calculated in the frequency domain; the amplitude of vibration of the blade shows a little difference in its value with respect to the ones previously calculated, but it can considered negligible. It is important to notice that the number of cycles chosen to run the simulation is the one immediately after the transient state, in order to speed up the calculations.

However the direct time integration method allows us to plot the behavior of the single point on the tip of the right blade in time domain and graphically represent the forced response of the system in time and in frequency, it is not immediately possible to get a sense of the main disadvantage of this way of proceeding, i.e. the very long time required for the computation. While in the case of the frequency domain, the solution of the linear problem requires only few minutes with dependence to the refinement of the discretization, in direct time integration, the solution of the linear problem takes more

than 4 hours. This deficiency is caused by the necessity of performing the integration for a certain set of frequency of excitation, in this case 100 sampling frequencies.

3.4.2. Non linear forced response

Once the implementation of the Newmark method has been completed in the case of the linear response, a very similar numerical scheme is introduced in order to solve the non-linear response of the system of two blades under the application of an external harmonic force. The aforementioned code is modified in order to introduce the non-linearity due to the presence of the contact forces; since the direct time integration works with the reduced order model obtained from Ansys, the degrees of freedom and consequently contact nodes used in the simulation remain unchanged. The equation of motion of the system has been modified in the following way:

$$M\ddot{U}(t) + C\dot{U}(t) + KU(t) = Fe(t) + B \cdot Fc \qquad 3.43$$

Where B represents the transformation matrix which allows rotating and translating the contact forces from the contact points to the damper center of mass. In this case all the matrices have a size of 31x31 due to the presence of the damper, modeled as a rigid body. Two contact points will be considered on the left contact and one the right one.

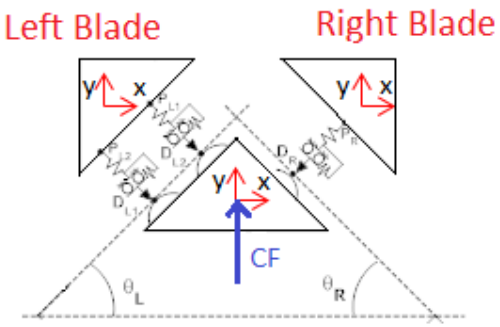

Figure 3.72 System model

In this simplified case, the damper is considered as a rigid body, with three degrees of freedom, two translations and one rotation about its center of mass. This assumption is a simplification of the previous problem in which the damper was considered deformable. In addition to this the axial displacement of the damper is considered negligible. As already mentioned in the state of the art, the damping effect generated by the presence of the damper is related to the damper mass and going deeply on the centrifugal force CF, which acts on the damper center of mass, due to the rotation of the system. The two triangles represent the blades' platforms on which the damper moves during the simulation.

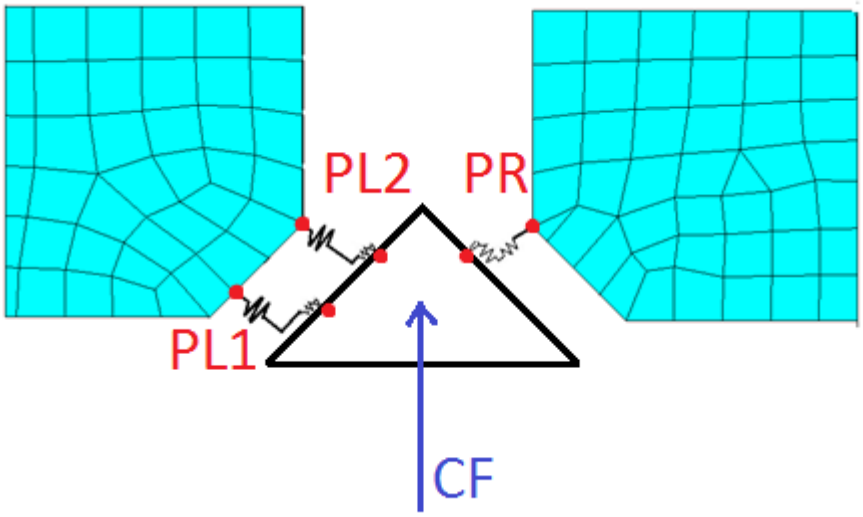

Figure 3.73 System representation.

3.4.2.1. Contact model

The contact model used to describe the system can be simplified to the case of a slider connected with a normal and a tangential spring. The contact is defined by a normal and a tangential stiffness, $k_n$and k_t, and by the relative displacements between the connected surfaces.

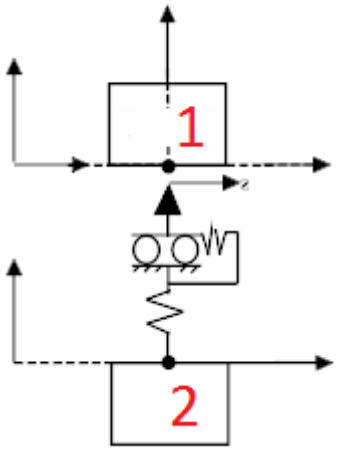

Looking at two consecutive timestep, 0 and 1, respectively, the contact status can be described by the use of a predictor corrector method as shown in TABLE XII according to the following assumption:

$$s^* = s - t_2 \qquad 3.44$$

With s displacement of the slider connected to body 1, t_2 tangential displacement of body 2 at the contact point.

TABLE XII CONTACT STATUS

CONTACT STATUS		
Stick		
Slider displacement: s	Tangential force on body 2	Normal force on body 2
$s^{(1)} = s^{(0)} + (t_2^{(1)} - t_2^{(0)})$	$T^{(1)} = k_t(t_1^{(1)} - s^{(1)})$	$N^{(1)} = k_n(n_2^{(1)} - n_1^{(1)})$
Positive slip		
Slider displacement: s	Tangential force on body 2	Normal force on body 2
$s^{(1)} = t_1^{(1)} - \frac{\mu N^{(1)}}{k_t}$	$T^{(1)} = \mu N^{(1)}$	$N^{(1)} = k_n(n_2^{(1)} - n_1^{(1)})$
Negative slip		
Slider displacement: s	Tangential force on body 2	Normal force on body 2
$s^{(1)} = t_1^{(1)} + \frac{\mu N^{(1)}}{k_t}$	$T^{(1)} = -\mu N^{(1)}$	$N^{(1)} = k_n(n_2^{(1)} - n_1^{(1)})$
Separation		
Slider displacement: s	Tangential force on body 2	Normal force on body 2
$s^{(1)} = t_1^{(1)}$	0	0

In the table, t represents the tangetial displacement of a body at the contact point, n the normal displacement at the contact and s is the displacement of the slider connected to body 1. T and N are respectively the tangential and normal contact forces. For sake of simplicity, it is possible to consider a stick state, the normal and the tangential contact forces can be computed in the following way:

$$N^{(1)} = \max(k_n \left(n_1^{(1)} - n_2^{(1)}\right), 0) \quad 3.45$$

$$T^{(1)} = k_t \left(t_1^{(1)} - t_2^{(1)} - s^{*(0)}\right) \quad 3.46$$

$$if\ N^{(1)} > 0\ \begin{cases} T^{(1)} \geq \mu N_1 \\ T^{(1)} \leq -\mu N_1 \end{cases} it\ follows \begin{cases} T^{(1)} = \mu N_1 \\ T^{(1)} = -\mu N_1 \end{cases} \quad 3.47$$

$$if \begin{cases} T^{(1)} = \mu N_1 \\ T^{(1)} = -\mu N_1 \end{cases} then \begin{cases} s^{*(1)} = t_1^{(1)} - t_2^{(1)} - \frac{\mu N^{(1)}}{k_t}\ \ positive\ slip \\ s^{*(1)} = t_1^{(1)} - t_2^{(1)} + \frac{\mu N^{(1)}}{k_t}\ \ negative\ slip \end{cases} \quad 3.48$$

Otherwise if $N^{(1)} \leq 0,\ T^{(1)} = 0$ due to separation.

3.4.2.2. Numerical solution

The coefficients chosen in the Newmark scheme should ensure unconditional stability, however this condition is not satisfied due to the presence of friction. It is necessary to consider a time step as low as possible to improve the convergence. Finally, in order to perform the simulation, an initial condition should be provided to the numerical solver: a static analysis in performed to get the initial displacement.

$$KU(t) = Fe(t) + B \cdot Fc \qquad 3.49$$

As already mentioned in the preceding paragraph, the main deficiency of the direct time integration is related to the time requested to complete the computation. In the case of the non-linear response, the computation time is much more longer with respect to the one required in the linear solution due to the problems of convergence of the Newmark scheme after the introduction of the contact forces. More than 2 days are necessary in order to obtain a FRF of the first natural frequency. In addition to this, the long time spent for calculation is also caused by the long transient state that the system has before reaching the steady state. The non-linearity that characterize the dynamics of the model can be directly shown by the response of the right tip under the application of the external force. The following figure shows only a portion of the transient state. This possibility represents a great advantage with respect to the preceding solutions which do not allow to plot the displacement of one node in time domain.

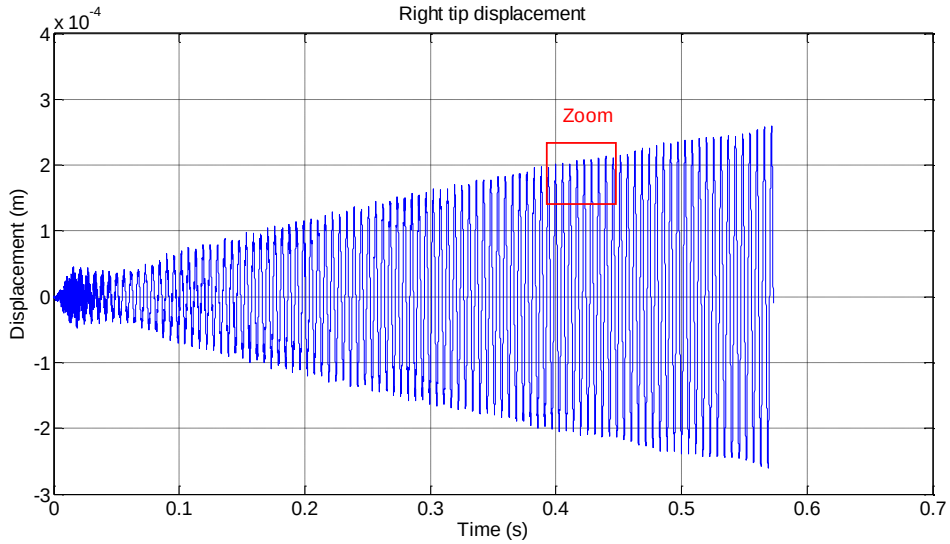

Figure 3.74 Non linear response, right tip in time domain.

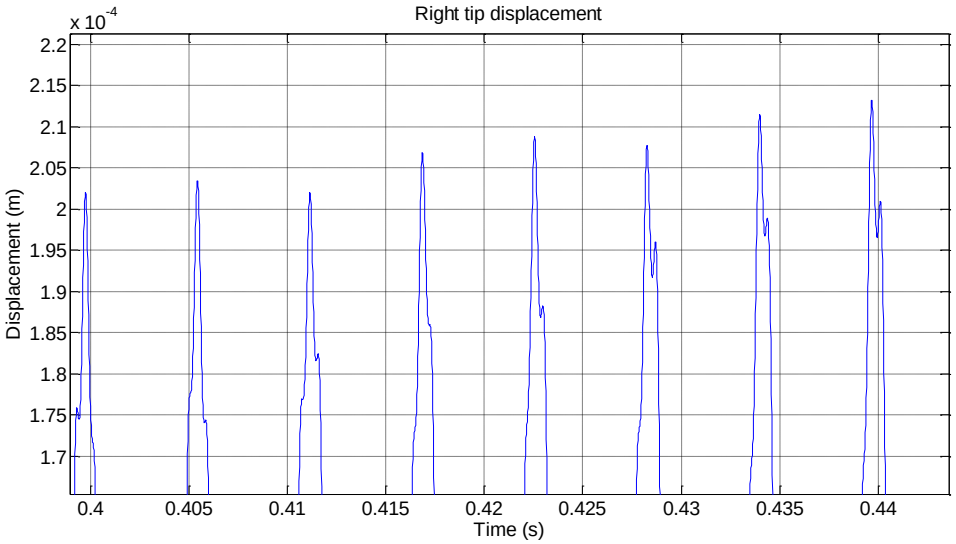

Figure 3.75 zoom.

Another important advantage of this kind of solution is the possibility to monitor the behavior of the contact forces and relative displacements of the contact point, enabling to plot the hysteresis cycles of the contact points.

The first test has been performed applying to the system of blades a harmonic force with amplitude of 5 N as in the case of the linear response. However the damper is present between the blades, it is supposed to be in stick with them, i.e. the whole model behaves as it is a unique solid body subjected to an external harmonic force with the consequence of a very low damping effect on the system in terms of natural frequency and vibration amplitude.

This situation becomes evident plotting the hysteresis cycles for the three contact points of the system. The right and the lower left contact points becomes in stick, i.e. the hysteresis cycle becomes a line with a slope equal to the tangential contact stiffness, while the upper left contact point separates from the blade's platform, i.e. zero tangential force. The hysteresis cycle has been plotted with the relative displacement between blade's platform and damper on the abscissa and the tangential contact force as ordinates. In this contact condition it is expected a growth in the resonance frequency of the system since the stick contact can be considered as an additional constraint applied to the model.

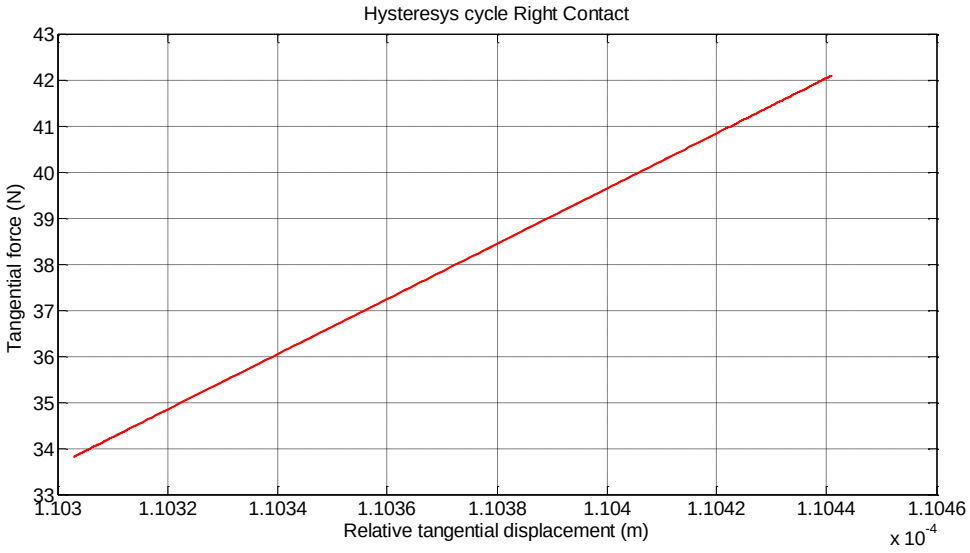

Figure 3.76 Hysteresis cycle right contact.

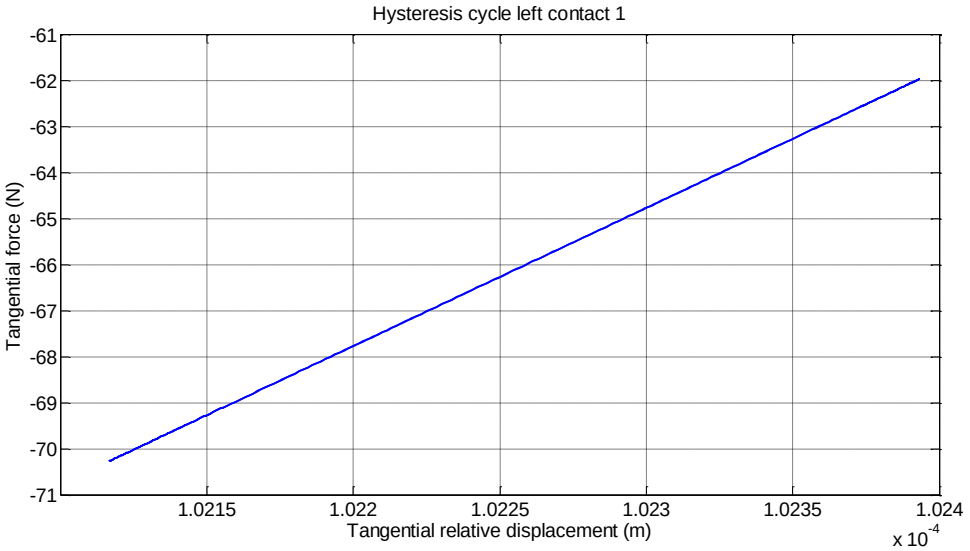

Figure 3.77 Hysteresis cycle left contact 1.

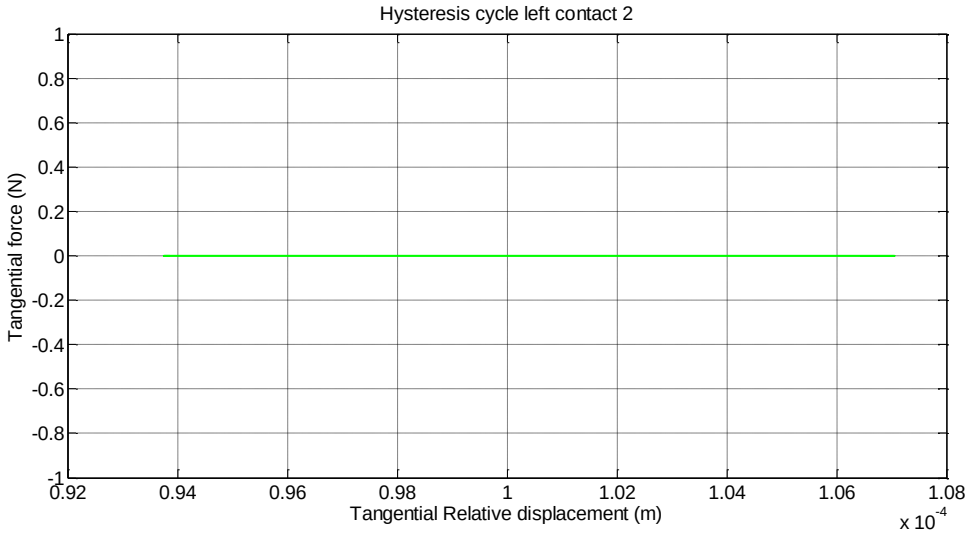

Figure 3.78 Hysteresis cycle left contact 2.

As shown in Figure 3.78 the damper separates from the blade's platform, eliminating the contact force on the upper left contact. For sake of simplicity, since in the stick condition, the damper behaves as if it is fixed against the blades' platforms on the right and the lower left contact, the same configuration can be reproduced avoiding the contact routine in the program and considering the vector of the contact forces obtained as the product of a stiffness matrix due to contact and the displacement vector. In this way, the numerical solution by Newmark method is improved in speed of calculation since the subroutine used to evaluate the contact force is avoided.

$$M\ddot{U}(t) + C\dot{U}(t) + KU(t) = Fe(t) + K_c U(t) \qquad 3.50$$

$$M\ddot{U}(t) + C\dot{U}(t) + (K - K_c)U(t) = Fe(t) \qquad 3.51$$

In addition to this there are no problems about convergence since the contribution of the normal stiffness of the contact points is directly included in the stiffness matrix of the system. All the contribution to the normal and tangential stiffness in the local references system can be rotated and translated in the global reference centered on the damper center of mass and added to the reduced stiffness matrix of the system. In this way the numerical calculation can be performed as in the linear case. As in the previous case, a larger enough number of cycles must be chosen in order to overtake the transient state and reach the steady one. Figure 3.79 Transient and steady state in stick conditions. Figure 3.79 shows that the transient state takes a quite long time before completing.

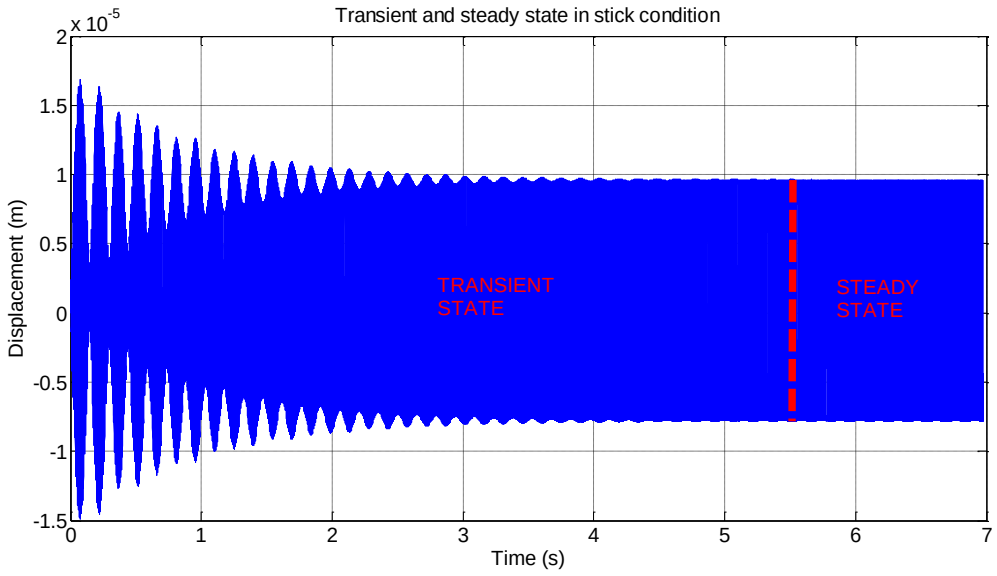

Figure 3.79 Transient and steady state in stick conditions.

The same considerations already formulated in the case of the linear response can be done for the non-linear case. The forced response of the system is evaluated in a frequency range around the first resonance frequency and compared with the result already

obtained through the commercial code. It is important to notice that the FRF of the system presents two peaks, the first one which in IP motion and the second one which is OOP. The distinction between in-phase and out-of-phase motion can be done looking at the direction of the displacements of the blades' tips.

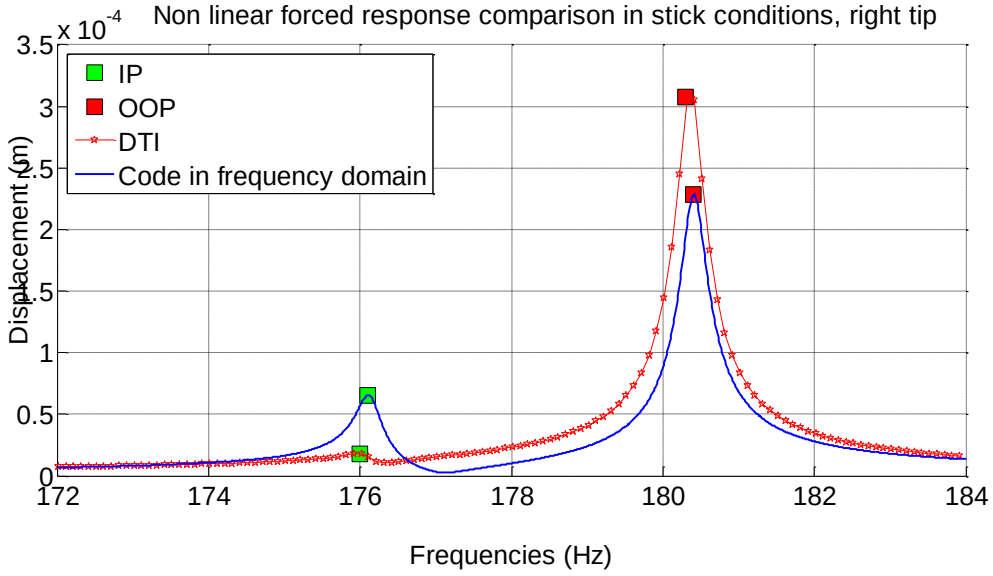

Figure 3.80 Non linear forced response comparison in stick conditions for the right tip, Fe=5N.

Figure 3.80 shows the behavior of the non-linear forced response obtained through direct time integration, since the results are carried out by an iterative numerical procedure, a certain error can be found with respect to the results obtained through the response evaluated in frequency domain. In addition to this, it is necessary to take into account that direct time integration usually takes a quite long time to get the solution and in order to speed up the calculations a low number of cycles is usually chosen. The presence of the end of the transient state can affect the results.

Once the non-linear forced response in stick condition has been performed, it could be of great interest focusing the attention on what happens in the slip state. Slip state occurs in presence of a higher excitation force applied to the model, forcing the damper to slide on the blades' platforms, dissipating energy through frictional contact. However the aim to plot the FRF of the system in slip condition, it is very import to highlight the capabilities of the code and of direct time integration to show what happens in terms of force and displacements on the contact points, displaying the non-linearity which arises due to the presence of the contact forces.

This is the reason why a plot of the hysteresis cycles of the contact points in slip conditions is shown in the following figures, illustrating what happens to the contact forces once the transient state has been surpassed.

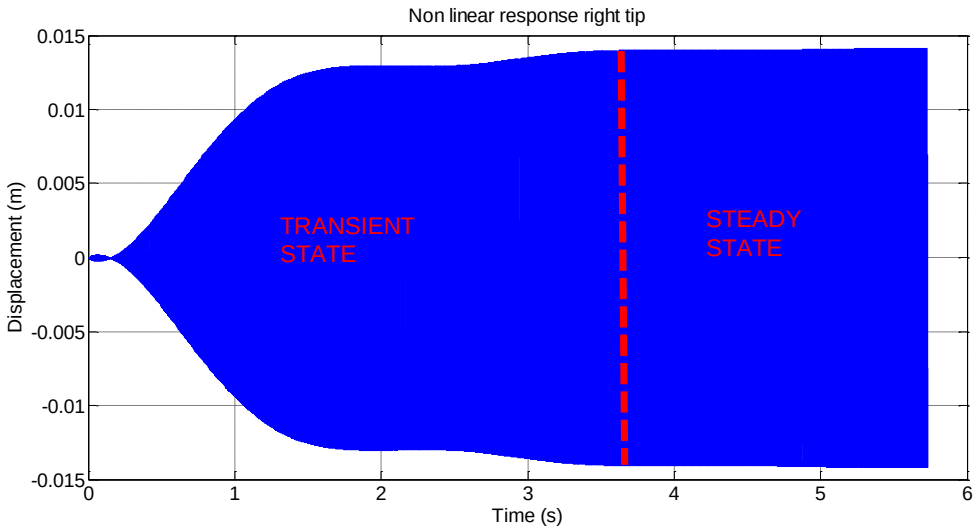

Figure 3.81 Displacement of the right tip: transient and steady state.

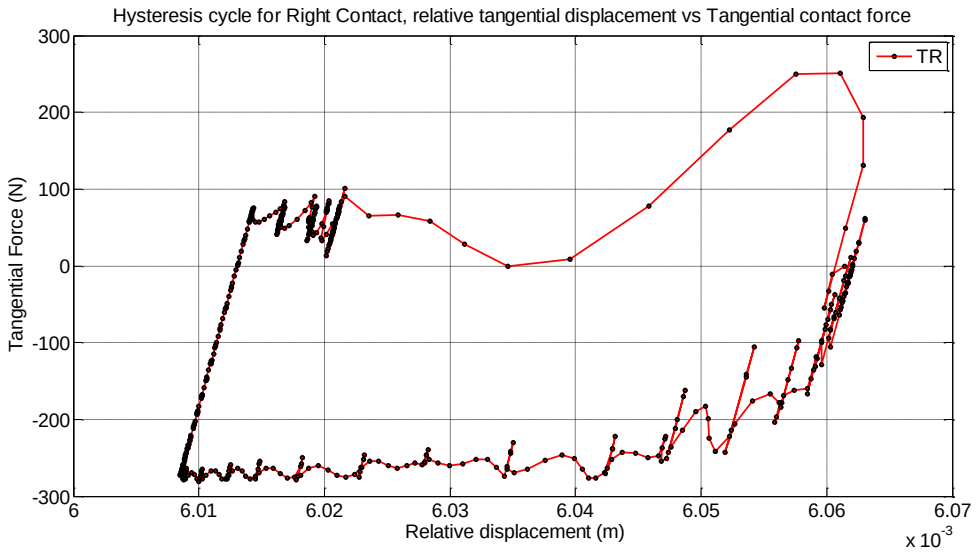

Figure 3.82 Hysteresis cycle for right contact in slip condition.

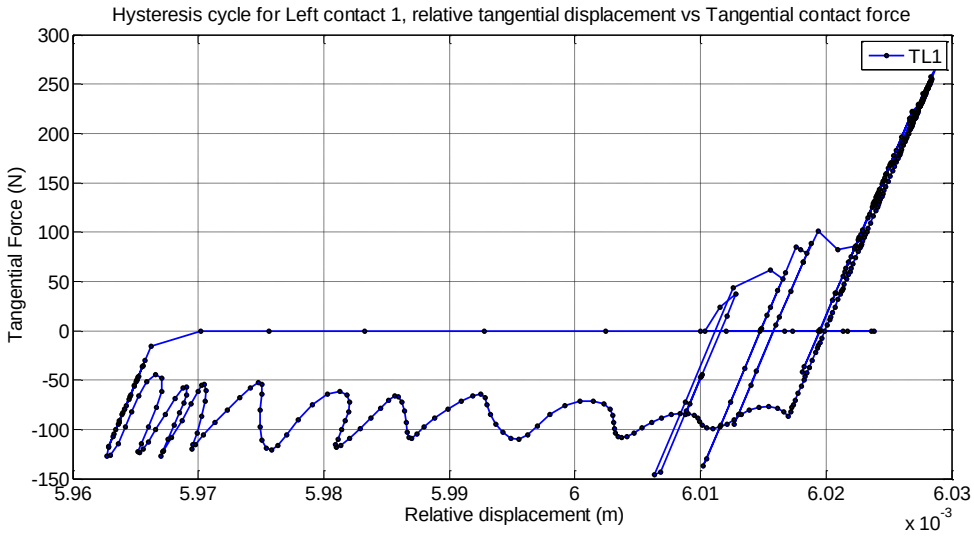

Figure 3.83 Hysteresis cycle left contact 1, slip condition.

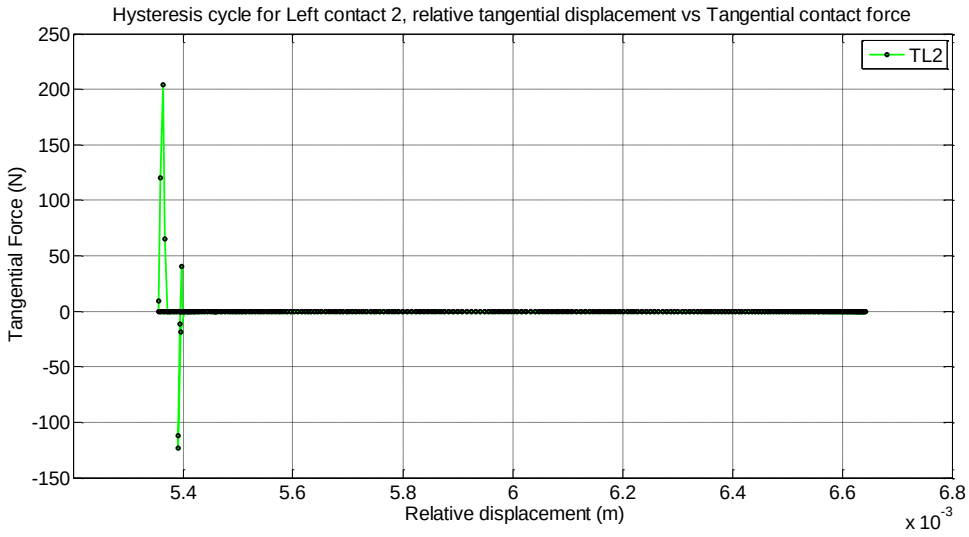

Figure 3.84 Hysteresis cycle left contact 2, lift off.

The three hysteresis cycles show the behavior of the tangential contact forces with respect to the relative displacement between damper and platforms. As in the stick case, it seems that the upper left contact point seems to lift off. Going deeply looking for the contact forces, a non-linear behavior can be found especially for the right contact and the lower left one.

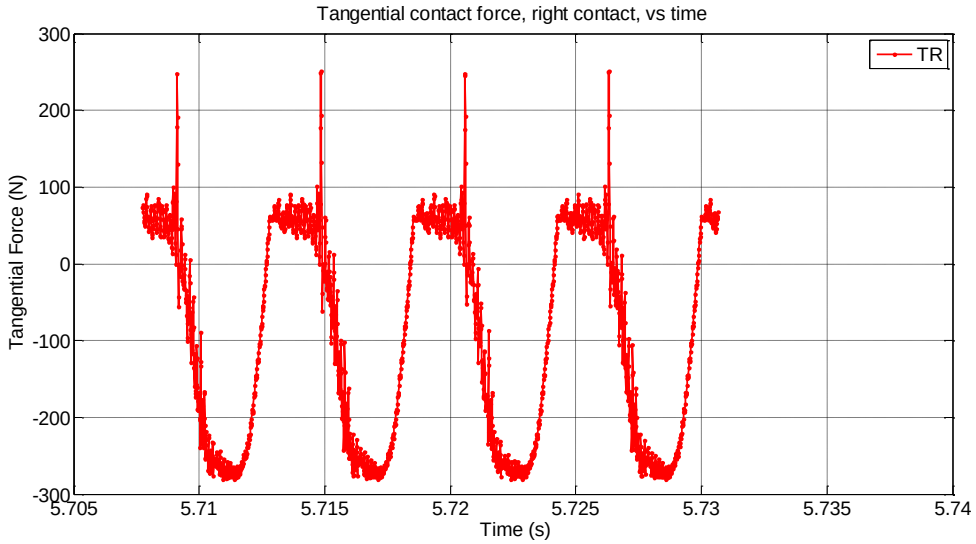

Figure 3.85 Tangential contact force on the right contact vs time, for 4 cycles.

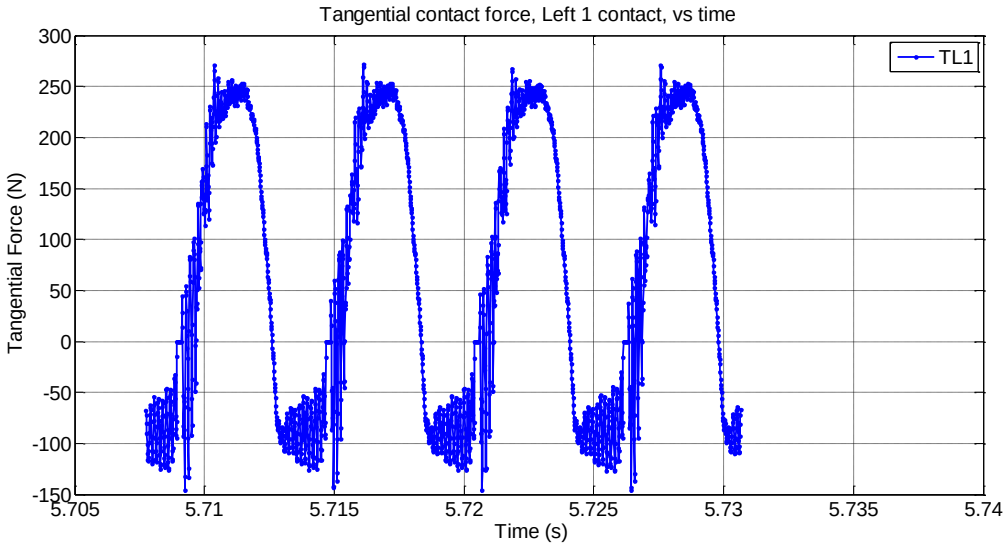

Figure 3.86 Tangential contact force on the left 1 contact vs time, for 4 cycles.

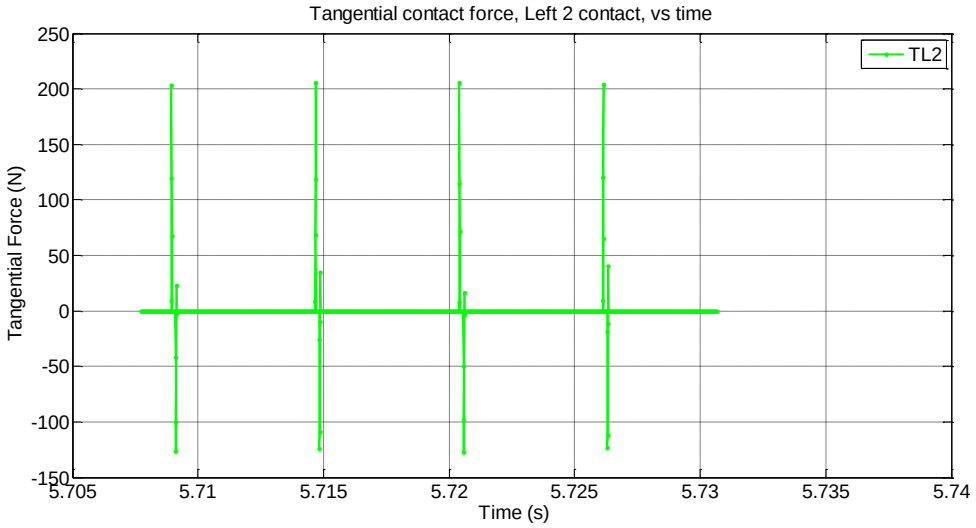

Figure 3.87 Tangential contact force on the left 2 contact vs time, for 4 cycles.

In the case of asymmetric underplatform damper, the lift off of the upper right contact frequently happens, as if the damper rotates with respect to its center on mass, and becoming constrained on the other two contact points.

4. CONCLUSIONS

In this thesis a complete dynamic analysis of a couple of turbine blades has been performed focusing the attention on the linear dynamics of the single blade, modeled through a multibody code called SAMS/2000 and on the non-linear dynamics of the system of two blades interconnected through an underplatform damper which dissipates energy through friction contact.

Fatigue failure frequently occurs in the case of turbine blades, due to the application of cyclic loads during working conditions; turbine blade are usually subjected to the presence of the centrifugal force which arises as a consequence of the disk rotation, and increase proportionally with the speed of rotation: alternating starting up and shutting down lead to very high bending loads on the blades increasing the possibility of initiation and propagation of a crack with consequential failure of the whole blade. Such failure would result in the destruction of the turbine having catastrophic consequences and a very large waste of money for the company owner. This situation becomes more critical when the blades reach their resonance condition during the rotation, with the consequence of an increase of the amplitude of vibration and of the possibility of failure.

This is the reason why a numerical simulation of the single blade has been carried out in the first part of the thesis thanks to the use of a multibody code called SAMS/2000 which allows to simulate the blade's rotation about a fixed axis and to monitor the displacement of a defined node on the blade. This test gives the possibility of understanding the blade deformation due to the rotation in working condition. However the numerical solution has been performed by the use of a simplified model of dummy blade, the way of proceeding adopted in this thesis opens the door to further application of the same methodology to more complex cases which can concern with simulation of the behavior of real systems of turbine blades eventually connected through different kind of joints

such a spring damper elements used to attenuate the vibration of the blades during rotation. The similarity of the problem with the dynamics of helicopter's blades can be the reason of the application of this solution to this kind of problem.

Going deeply with the problem of resonance of turbine blades in working conditions, the thesis shows an investigation on the effects of the presence of an underplatform damper connected with the blades' platforms through friction contacts. A numerical simulation on the effects of the damper on the aforementioned system has been investigated: the damper is used to dissipate energy through friction between its surfaces and the blades' platforms. Among all the possible solution presented in literature, the work analyses the case of an asymmetric underplatform damper with a flat and a semi-cylindrical contact surfaces. The damper behavior has been studied taking into account a constant value of the centrifugal force generated by the system rotation and exciting the model with an external force. The damper effects can be shown in a decrease of the amplitude of vibration of the blades, enhancing the fatigue life of the blades and slightly increasing the resonance frequency of the system. All these tests have been considered taking into account only the first flexural mode of the blades. The same general guideline has been used to develop the same numerical simulation using two different environments:

- Firstly all the calculations have been performed through a purposely developed code made specifically for a Company, working only in the frequency domain.
- Secondly, a very similar procedure has been developed using direct time integration to solve the non-linear problem caused by the presence of contact.

The main advantages and disadvantages of the two procedures immediately arise from the direct comparison between the two methods. The time required to solve the

numerical simulation is the essential difference which sticks out from the results: the numerical solution of the problem in frequency domain results much more efficient in terms of time, in less of one hour is possible to get the performance of the blade under the application of a set of external force, while in time domain more than two days are necessary to complete one FRF. The long time required to the direct time integration depends on the long transient state of the system and on the necessity of convergence of the numerical scheme adopted to solve the equation of motion. On the other hand, the direct time integration allows a better characterization of the damper behavior, such as the possibility of plotting the hysteresis cycles and the displacements of the blade tip during the excitation. As already mentioned in the preceding paragraphs, the comparison has been made possible by the use of the same physical model, through the use of the same reduced matrices of the system. The comparison of the results has been made taking into account both the linear forced response and the non-linear one, i.e. the case in presence of the damper.

The linear forced response has been performed in three different environments: Ansys mechanical, a commercial software developed in Matlab and through direct time integration. These set of test has been performed in order to make sure that the use of a condensed model enables to get the same results saving a large amount of time during computations. The greatest weakness of direct time integration appears studying the non-linear behavior of the system: the time required for computation; direct time integration takes about one hour to compute the integration for one excitation frequency. Due to the fact that more than 100 integrations must be performed in order to define the FRF around the first resonance frequency, it follows that the time of computation becomes overdone. This situation becomes worse in the case of the non-linear dynamics where, the non-linearity in the equation of motion introduced by the contact forces af

fects the convergence of the Newmark scheme which requires lower timestep in order to keep certain accuracy. It follows that obtaining a complete performance curve of the blade varying some physical parameters such as external force or centrifugal force becomes unattainable.

In conclusion it is possible to summarize that a frequency domain analysis of a system of blades and underplatform damper still represents the fastest and the most accurate way to investigate the effect of the damper on the system in improving the fatigue life of the blades, but the direct time integration can be kept as a reasonable alternative when it is interesting to focus only on what happens on the contact points in terms of displacements and contact forces. With regards to the damper, many different solutions can be adopted to enhance the dynamic behavior of turbine blades, with dependence on the damper mass and geometry, but what matters is how the damper behaves in dynamic conditions and going deeply how good it performs the task of reducing the amplitude of vibration without sticking.

APPENDICES

APPENDIX A: 2D RECTANGULAR ELEMENT MATLAB SCRIPT

This appendix contains the Matlab script used to evaluate analytically the closed solution for the stiffness and mass matrices of the 2D rectangular element which have been exported as subroutines for SAMS/2000.

```
%This subroutine is used to evaluate the 4-node 8DOFS plate element
clc
clear
syms x y a b c Rou
syms N1 N2 N3 N4
syms EEM EGM F V;

%% Natural coordinates
kesi = x/a;
yita = y/b;
N1 = 1/4*(1-kesi)*(1-yita);
N2 = 1/4*(1+kesi)*(1-yita);
N3 = 1/4*(1+kesi)*(1+yita);
N4 = 1/4*(1-kesi)*(1+yita);

Sx = [N1 0 N2 0 N3 0 N4 0];
Sy = [0 N1 0 N2 0 N3 0 N4];


S = [Sx;Sy];

%%Obtain the element Mass Matrix
S_T = transpose(S);
G = S_T*S;
for i= 1:8
    for j = 1:8
        M(i,j) = Rou*c*int(int(G(i,j),x,-a,a),y,-b,b);
    end
end
Mass = M/Rou/a/b/c;
PrinteleMass2D(Mass); % Mass need to premultiply Rou*a*b*c to get the
final results


%%Obtain the element Stiffness Matrix
DS(1,1:8) = diff(Sx,x);
DS(2,1:8) = diff(Sy,y);
DS(3,1:8) = diff(Sx,y)+diff(Sy,x);
```

APPENDIX A (CONTINUED)

```
% V = EEM/2/EGM-1;
% F = EEM/(1-V^2)
E = F*[1 V 0;V 1 0;0 0 (1-V)/2];

Dk = transpose(DS)*E*DS;

for i= 1:8
    for j = 1:8
        K(i,j) = c*int(int(Dk(i,j),x,-a,a),y,-b,b);
    end
end

Stiff = K/F;  %Stiffness need to premultiply F to get the final re-
sults
Printstiffness2D(Stiff);
```

APPENDIX B: 2D TRIANGULAR ELEMENT MATLAB SCRIPT

This appendix contains the Matlab script used to evaluate analytically the closed solution for the stiffness and mass matrices of the 2D triangular element which have been exported as subroutines for SAMS/2000.

```
%This subroutine is used to evaluate the 3-node 6DOFS triangular ele-
ment
clc
clear
syms x y x1 y1 x2 y2 x3 y3 a b c Rou
syms EEM EGM F V;
syms kesi yita

%%Shape functions
N1=kesi;
N2=yita;
N3=1-kesi-yita;


Sx = [N1 0 N2 0 N3 0];
Sy = [0 N1 0 N2 0 N3];
S = [Sx;Sy];


x=transpose([x1 x2 x3]);
y=transpose([y1 y2 y3]);
detJe=det([1 x1 y1;1 x2 y2;1 x3 y3]);
x13=x(1)-x(3);
x21=x(2)-x(1);
x32=x(3)-x(2);
y23=y(2)-y(3);
y31=y(3)-y(1);
y12=y(1)-y(2);

B1=[y23 0 y31 0 y12 0];
B2=[0 x32 0 x13 0 x21];
B3=[x32 y23 x13 y31 x21 y12];
B=(1/detJe)*[B1;B2;B3];


%% Stiffness matrix
% V = EEM/2/EGM-1;
% F = EEM/(1-V^2);
E = F*[1 V 0;V 1 0;0 0 (1-V)/2];
Dk = transpose(B)*E*B;
```

APPENDIX B (CONTINUED)

```
Stiff=detJe/2*Dk;
Printstiffness2D(Stiff);


%%Mass Matrix
%Obtain the element Mass Matrix
S_T = transpose(S);
G = S_T*S*detJe;
for i= 1:6
    for j = 1:6
        M(i,j) = Rou*c*int(int(G(i,j),kesi,0,1-yita),yita,0,1);
    end
end

% Mass = M/Rou/a/b/c;
Mass=M;
PrinteleMass2D(Mass);
```

CITED LITERATURE

[1]. Shabana, A. A.: Dynamics of Multibody Systems. Cambridge: *Cambridge University Press 2005*, 2005.

[2]. Moharos I., Oldal I., Szekrényes A.: Finite element methode. Budapest: *Typotex Publishing House*, 2012.

[3]. Kattan P.: Matlab Guide to Finite Elements an interactive approach. Heidelberg: *Springer-Verlag*, 2008.

[4]. Firrone, C. M.: Guida introduttiva agli elementi di contatto in Ansys. *Research Activity,* Torino, 2009.

[5]. Metrisin, J. T.: Guidelines for Obtaining Contact Convergence, 2008 International ANSYS Conference. *www.ansys.com.* 2008. Retrieved on January 20, 2014 from http://www.ansys.com/staticassets/ANSYS/staticassets/resourcelibrary/confpaper/2008-Int-ANSYS-Conf-guidelines-contact-convergence.pdf .

[6]. Zucca, S.: *LAQ AERMEC. Research Contract*, Torino, 2012.

[7]. Firrone C. M., Zucca S.: Modelling friction contacts in structural dynamics and its application to turbine blade disks. In: *Numerical Analysis Theory and Applications*, by Jan Awrejcewicz, 304-312. In Tech, 2011.

CITED LITERATURE (CONTINUED)

[8]. Sanliturk K. Y., Ewins D. J., Stanbridge A. B.: Underplatforms damper for turbine blades: Theoretical modeling, analysis and comparison with experimental data. In: *Journal of Engineering for Gas Turbines and Power Vol.123*, 2001: 919-929.

[9]. Yang B. D., Chu M. L., Menq C. H.: Stick-slip-separation analysis and non linear stiffness and damping characterization of friction contacts having variable normal load. In: *Journal of Sound and Vibration*, 1998: 461-481.

[10]. Zucca S., Botto D., Gola M. M.: Range of variability in the dynamics of semi-cylindrical frcition dampers for turbine blades. In: *Proceedings of ASME Turbo Expo 2008: Power for Land, Sea and Air GT2008*, 2008: 1-11.

[11]. Zucca S., Firrone C. M., Gola M. M.: Modeling underplatform dampers for turbine blades: a refined approach in the frequency domain. In: *Journal of Vibration and Control*, 2012: 1-16.

[12]. Kubin Z., Polreich V., Cerny V., Babkova P., Prchlik L.: Damping identification and its comparison for various types of blade couplings. In: *Proceedings of ASME Turbo Expo 2013: Turbine Technical Conference and Exposition GT2013*, 2013: 5-8.

CITED LITERATURE (CONTINUED)

[13]. Tatzko S., Scheidt L. P, Wallaschek J., Kayser A., Walz. G.: Investigation of alternate mistuned blades non linear coupled by underplatform dampers. In: *Proceedings of ASME Turbo Expo 2013: Turbine Technical Conference and Exposition GT2013*, 2013: 1-4, 9-11.

[14]. Ansys. *Ansys 14.0 Help.* 2011.

[15]. Gugliotta, A.: Elementi finiti parte IV: *www.polito.it.* Retrieved on March, 10, 2014 from http://www.mondovi.polito.it/ebook/doc/ag_p4.pdf

VITA

NAME:	Stefano Michelis
EDUCATION	B.A., Mechanical Engineering, Politecnico di Torino, Torino, Italy, 2012